Energy, Mines and Resources Canada
Énergie, Mines et Ressources Canada

CANMET

Canada Centre for Mineral and Energy Technology
Centre canadien de la technologie des minéraux et de l'énergie

Mining Research Laboratories
Laboratoires de recherche minière

ANISOTROPIC PROPERTIES STUDY OF LAC DU BONNET GRANITE SPECIMENS: REPORT #6

R. Jackson

MRL 91-007(TR)

January 1991

Canada

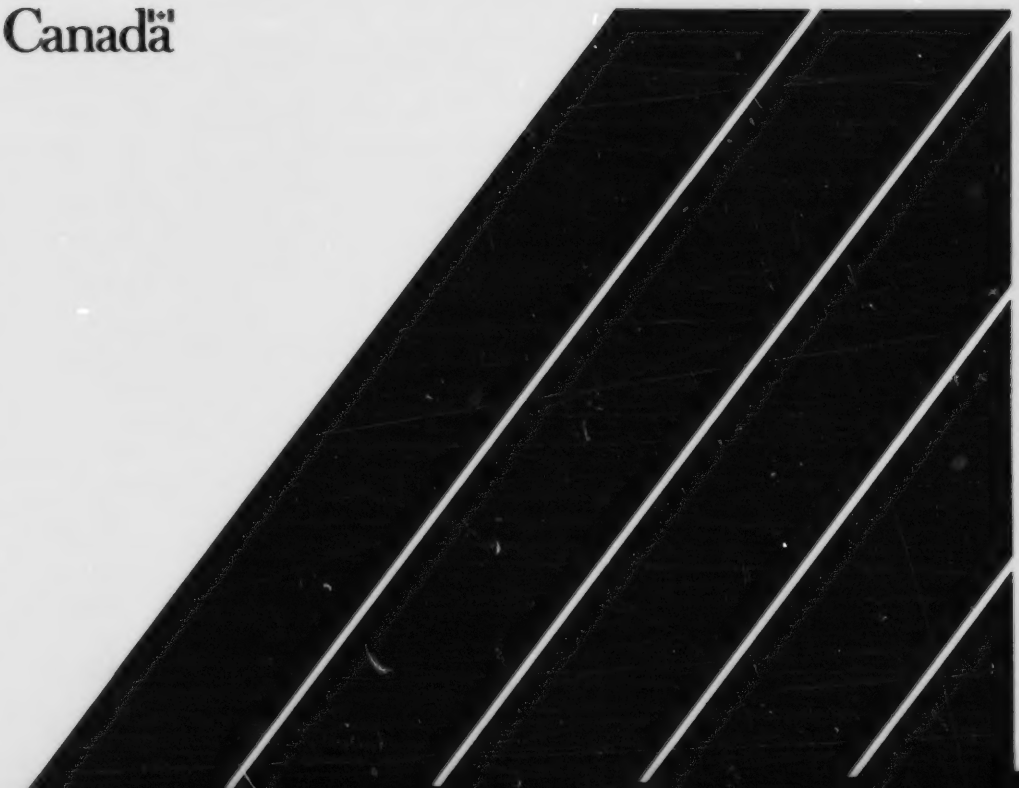

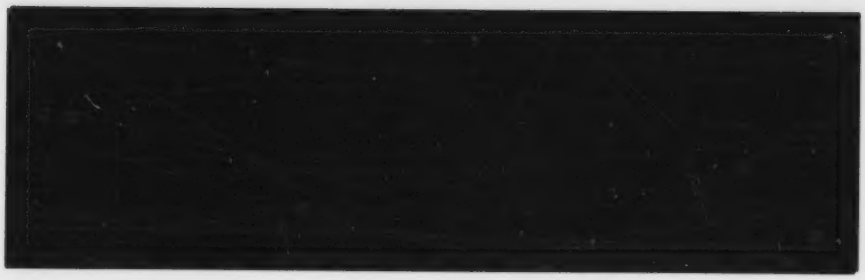

91-04541/

ANISOTROPIC PROPERTIES STUDY OF LAC DU BONNET GRANITE SPECIMENS: REPORT #6

R. Jackson

MRL 91-007(TR)

January 1991

MICROMEDIA

96 pp

ANISOTROPIC PROPERTIES STUDY OF LAC DU BONNET GRANITE SPECIMENS: REPORT #6

by

Rand Jackson*

ABSTRACT

Compressive and shear wave velocity measurements, as well as uniaxial compression testing, was conducted on samples obtained from borehole 403-018-S1 located in the Lac du Bonnet batholith near Pinawa, Manitoba. The purpose of the study is to ascertain if any anisotropy in terms of the uniaxial mechanical properties exists in the Lac du Bonnet samples and, if so, to what extent.

The uniaxial compressive strength, 50% tangent and secant moduli, 25 MPa secant modulus and Poisson's ratio exhibited maximum anisotropies of 1.25, 1.70, 1.75, 2.02 and 1.16, respectively. Deformation anisotropies are related largely to the existence of micro-cracks in the samples. Four twenty (420) level results indicated a higher degree of anisotropy in terms of the 50% tangent modulus of elasticity (1.70) than was indicated by a similar test series conducted on samples obtained from the 240 level (1.18). Samples from the higher in situ stress field of the 420 level appear to be more profoundly effected by stress relaxation.

---

*Research Officer, Canadian Mine Technology Laboratory, Mining Research Laboratories, CANMET, Energy,Mines and Resources Canada, Ottawa, Ontario.

Keywords:
Anisotropy, Rock Properties, Mechanical, Young's Modulus, Poisson's Ratio, Uniaxial Compressive Strength, Compressive Wave Velocity, Shear Wave Velocity, Lac du Bonnet

ÉTUDE DES PROPRIÉTÉS ANISOTROPES D'ÉCHANTILLONS TIRÉS DU GRANITE DU LAC DU BONNET

ÉTUDE #6

par
Rand Jackson*

RÉSUMÉ

Des mesures de la vitesse de l'onde de compression et de l'onde de cisaillement ainsi que des essais de compression uniaxiale ont été effectués sur des échantillons provenant du trou de forage 403-018-S1 creusé dans le batholite du Lac du Bonnet, près de Pinawa, au Manitoba. L'étude a pour but de voir si les échantillons sont anisotropes quant à leurs propriétés mécaniques uniaxiales et, dans l'affirmative, de déterminer jusqu'à quel point ils le sont.

La résistance à la compression uniaxiale, les modules tangent et sécant de 50%, le module sécant de 25 MPa et le coefficient de Poisson présentent des anisotropies maximales de 1,25, 1,70, 1,75, 2,02 et 1,16, respectivement. Les anisotropies de déformation sont largement reliées à l'existence de micro-fissures dans les échantillons. Certains provenant du niveau 420 présentent un degré d'anisotropie plus élevé (1,70), pour ce qui est du module tangent d'élasticité de 50%, qu'une série d'échantillons tirés du niveau 240 (1,18), qui ont été soumis à des essais semblables. Des échantillons tirés du champ de contrainte plus élevé du niveau 420 semblent être plus profondément touchés par la relaxation.

---

*Agent de recherche, Laboratoire canadien de technologie minière, Laboratoires de recherche minière, CANMET, Énergie, Mines et Ressources Canada, Ottawa (Ontario).

Mots clés:
Anistropie, propriétés de la roche, mécanique, module de Young, coefficient de Poisson, résistance à la compresson uniaxiale, vitesse de l'onde de compression, vitesse de l'onde de cisaillement, Lac du Bonnet

CONTENTS

	Page
ABSTRACT	i
RESUME	ii
INTRODUCTION	1
IDENTIFICATION OF SPECIMENS AND TESTS	1
DESCRIPTION OF TEST MEASUREMENTS	3
DATA TREATMENT	4
DATA SUMMARY	6
FAILURE CHARACTERISTICS	6
OBSERVATIONS	7
ACKNOWLEDGEMENTS	9
REFERENCES	9
Appendix A	30

TABLES

No.		
1.	Summary of Sample Depth, Dimensions, Density and Orientation	10
2.	Summary of Ultrasonic Velocity Properties	13
3.	Summary of Uniaxial Compression Properties	16
4.	Uniaxial Compressive Strength: Ellipsoidal Fit & Rotation into Standard Form	19
5.	50% Tangent Modulus of Elasticity: Ellipsoidal Fit & Rotation into Standard Form	21
6.	50% Secant Modulus of Elasticity: Ellipsoidal Fit & Rotation into Standard Form	23
7.	25 MPa Secant Modulus of Elasticity: Ellipsoidal Fit & Rotation into Standard Form	25
8.	Poisson's Ratio: Ellipsoidal Fit & Rotation into Standard Form	27
9.	Mean Maximum Anisotropies of Uniaxial Mechanical Properties	29

FIGURES

No. Page

1. Core Orientation for Anisotropy Specimens 2

INTRODUCTION

As part of the Canadian Nuclear Fuel Waste Management Project, Atomic Energy of Canada Limited is characterizing various rock formations to determine their suitability for long term disposal of high level wastes. The program also includes the construction of an underground research laboratory (URL) near Pinawa, Manitoba to provide an opportunity for extensive in situ investigations.

Biaxial testing conducted on core obtained during the construction and operating phases of the URL has indicated that the rock may be anisotropic in terms of modulus of elasticity (1). It was felt that further study in the form of acoustic velocity and uniaxial compression testing could provide additional insight into this behaviour.

Testing of sample suites from the 240 level has indicated that there is indeed some anisotropy in the mechanical properties of the Lac du Bonnet granite on that level largely related to the prevailing orientation of microcracks. This report presents results from a similar test program conducted on samples obtained from the 420 level.

IDENTIFICATION OF SPECIMENS AND TESTS

Five sections of 200-mm diameter core, previously labelled A through E on site, were obtained from borehole 403-018-S1 (trend = 337.11°, plunge = -0.205°). The rock can be described as a massive, grey, medium to coarse grained granite, composed of quartz, k-feldspar (oligoclase), plagioclase feldspar and biotite.

Each 200-mm diameter section was recored according to the configuration illustrated in Figure 1. The resulting 45-mm

diameter specimens were then identified according to their location and orientation as follows;

A: depth of the collar of the 45 mm hole from the collar of the 200 mm hole,

B: angle ß gives the location of the collar of the 45 mm hole around the circumference of the 200 mm core. The angle is measured clock-wise (looking down hole) from the orientation mark on the top of the core,

C: angle α is the angle between the core axis of the 45 mm core and the 200 mm core. The angle is measured clockwise (ie. dip) from the down hole direction of the 2080 mm core.

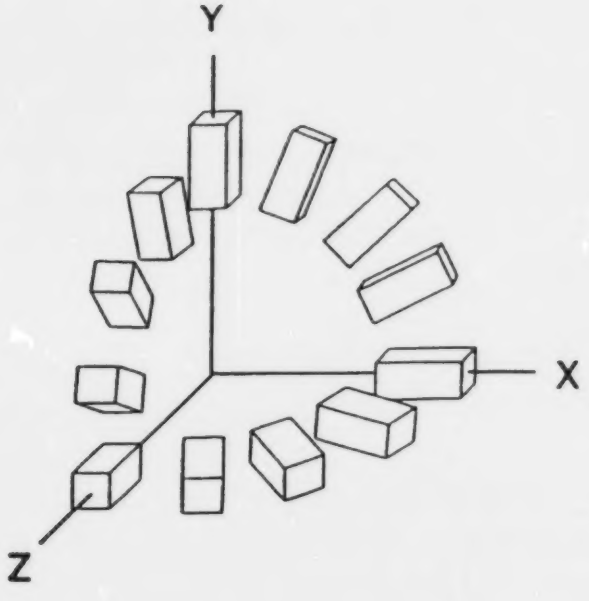

Figure 1: Core Orientation for Anisotropy Specimens
(after Peres-Rodrigues, 1967)

Table 1 provides a summary of the specimen identification number and its depth, dimensions, density and orientation. The following properties were determined for the samples listed;

1) compressive wave velocity, V_p
2) shear wave velocity, V_s
3) dynamic shear modulus, G_d
4) dynamic Young's modulus, E_d
5) dynamic Poisson's ratio, ν_d
6) uniaxial compressive strength
7) Poisson's ratio, ν
8) 50% tangent modulus of elasticity, E_t
9) 50% secant modulus of elasticity, $E_{s50\%}$
9) 25 MPa secant modulus of elasticity, E_{s25MPa}

DESCRIPTION OF TEST MEASUREMENTS

Compressive and shear wave velocity measurements were carried out on samples prior to being gauged for elastic deformation measurement. The testing equipment consisted of: transmitting and receiving platens utilizing piezoelectric transducers, a high voltage pulse generator, a signal amplifier and a Tektronix 2230 100 MHz digital storage oscilloscope equipped with delay sweep and a time base resolution of 0.01 micro-seconds.

For an outline of the uniaxial compression procedure, the reader is referred to Technical Data 303410-M01/78 (2). The two Phillips PR 9302 strain bridges and the Mosely Autograph 2FRA X-Y recorder referred to in that document were replaced, in the present study, by a Sciemetric Model 321 Electronic Measurement System equipped with a Model 84B Strain Gauge Adapter and a Hewlett Packard 7046B X-Y recorder. These equipment were used to measure and record the axial and transverse strains as a function of axial load.

DATA TREATMENT

The compressive and shear wave velocities were determined by dividing the specimen length by the wave travel time through the specimen. The dynamic properties were, then, calculated using the following equations (3);

Dynamic Young's Modulus

$$E_d = \frac{\rho V^2 (3V_p^2 - 4V_s^2)}{(V_p^2 - V_s^2)} \qquad (1)$$

where; E_d = dynamic Young's modulus
V_s = shear wave velocity
V_p = compressive wave velocity
ρ = density

Dynamic Shear Modulus

$$G_d = \rho V_s^2 \qquad (2)$$

where; G_d = dynamic shear modulus

Dynamic Poisson's Ratio

$$\mu_d = \frac{V_p^2 - 2V_s^2}{2(V_p^2 - V_s^2)} \qquad (3)$$

where; μ_d = dynamic Poisson's ratio

Analog outputs from the Sciemetric measurement system and press were recorded on a PC-based data acquisition system which was

subsequently used to generate the stress/strain curves contained in Appendix A. The tangent modulus of elasticity (E_t) was calculated for each sample by determining the slope of the tangent to the axial strain curve at 50% of the failure load. Secant moduli of elasticity (E_s) were calculated by determining the slopes of the lines joining the origin to points on the axial strain curve corresponding to stress levels of 25 MPa and 50% of the failure load. The ultimate compressive strength of each sample was calculated by dividing sample failure load by the sample's cross-sectional area. The ratio of the tangent to the axial strain curve to the tangent to the transverse strain curve at 50% failure load was used to determine the sample's Poisson's ratio (v).

As stated earlier, the samples were cored from 200-mm diameter sections along three orthogonal axes and at 22.5° intervals between those axes. (Please note that due to a measurement error, three additional samples were recored from section E at $\alpha = 90°$ and $\beta = 292.5°$, 315.0° and 337.5°). This configuration made it possible to resolve the mechanical properties of interest into x, y and z coordinates according to the cartesian system defined by the orthogonal axes. The points thus derived are then fitted to an ellipsoid-type quadratic equation which can be described as;

$$[x\ y\ z] \begin{bmatrix} \alpha_1 & \alpha_2 & \alpha_3 \\ \alpha_2 & \alpha_4 & \alpha_5 \\ \alpha_3 & \alpha_5 & \alpha_6 \end{bmatrix} \begin{bmatrix} x \\ y \\ z \end{bmatrix} = 10^5 \qquad (4)$$

The most probable values of the α_i coefficients were calculated using the method of least squares from the results determined for each specimen set. The standard form of each ellipsoid was subsequently obtained using a suitable rotation of the coordinate axes. The maximum degree of anisotropy could then be calculated by determining the ratio of the major to minor semi-

axes (Peres-Rodrigues, 1966). Because the samples were recored from the same borehole and were, therefore, oriented according to the same coordinate system, it was also possible to obtain an aggregate fit using the results from all 63 specimens.

DATA SUMMARY

Table 2 contains the results of the ultrasonic velocity measurements for each sample including the calculated values of the dynamic shear modulus, dynamic Young's modulus as well as Poisson's ratio estimated on the basis of velocity data. Table 3 summarizes the uniaxial compressive strength results. Both the secant and tangent moduli of elasticity and Poisson's ratio were determined for each sample at a stress level equal to 50% of the sample's failure load. The secant modulus was also determined at a stress level of 25 MPa. Tables 4 through 8 list the most probable ellipsoids, rotation matrices and normal equations for the uniaxial compressive strength, 50% tangent modulus, 50% secant modulus, 25 MPa secant modulus and Poisson's ratio, respectively for each core section as well as the aggregate results. Table 9 provides a summary of the maximum anisotropies determined for the properties listed above.

Individual stress/strain curves for the specimens are contained in Appendix A.

FAILURE CHARACTERISTICS

The predominant mode of failure was that of axial splitting and slabbing. Partially formed single diagonal failure planes were also apparent in some samples although the explosive nature of the failures made it impossible to measure failure angles.

OBSERVATIONS

As an earlier report in this test series mentioned(Jackson, 1988), anisotropies determined by performing an ellipsoidal fit on a limited number of test results often leads to misleading values due to existence of one or more anomalous specimens within the sample set. In fact, for this program, the number of tests conducted for each section of core was increased from nine to twelve in an attempt to minimize this effect. As Table 9 indicates, however, standard deviations associated with the mean anisotropies determined for the uniaxial mechanical properties still range from 8% to 47% of those means. Since all the core sections were obtained from the same borehole, it has been possible to perform the analysis on the aggregate sample population. These results are also listed in Table 9 and, while not listed, the standard deviations corresponding to the fitted coefficients were consistently less for the aggregate results than for the separate core sections.

Maximum anisotropies of 1.25 and 1.16 determined for the uniaxial compressive strength and Poisson's ratio, respectively indicate the samples obtained from the 420 level are very nearly isotropic in terms of these mechanical properties.

The results, however, indicated considerably higher maximum anisotropies for the sample suites' deformational properties. As Lama and Vutukuri (1978) point out, the orientation of such features as bedding planes (schistosity, gneissicity etc.), mineral content and voids (pores, microcracks etc.) can profoundly affect the anisotropy of observed mechanical properties including the modulus of elasticity.

The extent to which pores and microcracks affect the initial deformation modulus is often dependent upon their orientation with respect to the axis of loading. Cracks perpendicular to the loading axis tend to result in larger

deformations during initial loading than those which are parallel to it. It follows that if a preferred orientation of microcracks exists in an otherwise nearly homogeneous rock mass, the secant modulus will exhibit a greater degree of anisotropy than that observed for the tangent modulus. While the 50% secant modulus anisotropy determined here is larger than the 50% tangent modulus, the difference is nominal (1.75 vs. 1.70). The secant modulus was, therefore, determined for each sample at a stress level of 25 MPa under the supposition that the stress/strain behaviour during initial loading would be more profoundly effected by crack closure. As expected, this resulted in a considerably larger maximum anisotropy of 2.02.

In this type of analysis, the major semi-axis of the standard form will represent the largest predicted deformation modulus to be found at that stress level. If this is the case, the direction associated with the major semi-axis should coincide directly with the prevailing orientation of the microcracks if indeed one exists. Since the rotation matrices given in Tables 4 through 8 are comprised of direction cosines which transform the coordinate system defined by the trend and plunge of the borehole into ones containing the standard form, their orientation in space should be readily obtainable. This analysis is left to investigators at the URL.

In comparing results from the 420 level with those obtained from the 240 level, the most significant difference appears to be in the maximum anisotropies determined for the 50% tangent moduli. Two forty (240) level results indicate that the rock on this level is very nearly isotropic at this stress level with a mean maximum anisotropy of 1.18. Comparable values obtained from the 420 level, exhibit the much higher maximum anisotropy of 1.70. This is likely a result of the 420 level specimens being cored from a considerably higher in situ stress field ($\sigma_1 \approx 60$ MPa) compared to the 240 level ($\sigma_1 \approx 30$ MPa), (Martin, 1990). The resulting stress relaxation causes the 420 level samples to be increasingly effected by crack

closure even at stress levels equivalent to 50% of their failure strength.

ACKNOWLEDGEMENTS

The author would like to acknowledge the valuable assistance of Mr. Bernie Gorski, Ms. Catherine Mainguy and Ms. Kimberley Emde during this test program.

REFERENCES

1. Annor, A. and Geller, L., "Dilatational velocity, Young's modulus, Poisson's ratio, uniaxial compressive strength and Brazilian tensile strength for WN1 and WN2 samples", CANMET/MRL Technical Data 303410-M01/78, 1978.

2. Jackson, R., "Anisotropic properties study of Lac du Bonnet granite specimens: report #5", CANMET/MRL Technical Report 88-39(TR), 1988.

3. Lama, R.D., Saluja, S.S., Vutikuri, V.S., "Handbook on mechanical properties of rocks", Volume II, Chapter 7, Trans Tech Publications.

4. Lang, P., "Personal communication", 1985.

5. Martin, C.D., "Characterizing in situ stress domains at the AECL Underground Research Laboratory", Can. Geotech. J. 27, 1990.

Table 1 : Summary of sample depth, dimensions, density and orientation

Core Section	Sample Number	Sample Depth (m)	Length (mm)	Diameter (mm)	Density (gm/cc)	Orientation	
						α	β
A	A1	1.330	107.91	44.62	2.62	0.0	0.0
	A2	1.330	107.98	44.65	2.62	22.5	0.0
	A3	1.425	104.60	44.51	2.63	45.0	0.0
	A4	1.360	106.21	44.64	2.64	67.5	0.0
	A5	1.965	107.58	44.58	2.63	90.0	0.0
	A6	2.043	105.69	44.59	2.62	90.0	22.5
	A7	2.119	107.89	44.52	2.63	90.0	45.0
	A8	2.195	107.85	44.50	2.62	90.0	67.5
	A9	2.272	103.46	44.45	2.65	90.0	90.0
	A10	1.780	108.60	44.54	2.63	22.5	90.0
	A11	1.629	107.44	44.49	2.63	45.0	90.0
	A12	1.565	109.29	44.41	2.63	67.5	90.0
B	B1	2.352	108.78	44.60	2.67	0.0	0.0
	B2	2.352	109.65	44.41	2.67	22.5	0.0
	B3	2.452	109.75	44.50	2.66	45.0	0.0
	B4	2.382	108.90	44.56	2.66	67.5	0.0
	B5	2.983	103.56	44.43	2.61	90.0	0.0
	B6	3.048	105.44	44.44	2.64	90.0	22.5
	B7	3.126	106.52	44.43	2.64	90.0	45.0
	B8	3.202	105.06	44.48	2.63	90.0	67.5
	B9	3.279	107.35	44.42	2.63	90.0	90.0
	B10	2.810	105.01	44.56	2.61	22.5	90.0
	B11	2.647	108.88	44.52	2.65	45.0	90.0
	B12	2.579	108.86	44.41	2.67	67.5	90.0

Table 1 : cont'd

Core Section	Sample Number	Sample Depth (m)	Length (mm)	Diameter (mm)	Density (gm/cc)	Orientation	
						α	β
C	C1	5.430	102.16	44.64	2.62	0.0	0.0
	C2	5.530	106.31	44.31	2.63	22.5	0.0
	C3	5.607	110.76	44.49	2.63	45.0	0.0
	C4	5.460	101.94	44.63	2.63	67.5	0.0
	C5	6.072	103.17	44.44	2.64	90.0	0.0
	C6	6.410	104.19	44.64	2.62	90.0	22.5
	C7	6.209	101.13	44.43	2.61	90.0	45.0
	C8	6.284	103.85	44.48	2.60	90.0	67.5
	C9	6.362	103.27	44.55	2.60	90.0	90.0
	C10	5.430	105.14	44.56	2.62	22.5	90.0
	C11	5.718	104.82	44.53	2.63	45.0	90.0
	C12	5.654	109.45	44.40	2.62	67.5	90.0
D	D1	6.417	106. 36	44.57	2.63	0.0	0.0
	D2	6.500	102.95	44.39	2.62	22.5	0.0
	D3	6.507	109.33	44.57	2.62	45.0	0.0
	D4	6.440	105.95	44.62	2.62	67.5	0.0
	D5	7.050	106.54	44.24	2.63	90.0	0.0
	D6	7.125	101.37	44.14	2.63	90.0	22.5
	D7	7.203	101.69	44.33	2.63	90.0	45.0
	D8	7.277	99.84	44.23	2.63	90.0	67.5
	D9	7.356	104.84	44.27	2.63	90.0	90.0
	D10	6.860	111.07	44.49	2.63	22.5	90.0
	D11	6.717	107.70	44.42	2.65	45.0	90.0
	D12	6.650	108.78	44.44	2.64	67.5	90.0

Table 1 : cont'd

Core Section	Sample Number	Sample Depth (m)	Length (mm)	Diameter (mm)	Density (gm/cc)	Orientation	
						α	β
E	E1	0.360	106.37	44.60	2.63	0.0	0.0
	E2	0.360	91.34	44.42	2.63	22.5	0.0
	E3	0.460	107.94	44.46	2.64	45.0	0.0
	E4	0.390	110.39	44.62	2.64	67.5	0.0
	E5	0.942	103.99	44.28	2.63	90.0	0.0
	E6	0.874	111.19	44.66	2.61	90.0	22.5
	E7	1.020	102.95	44.28	2.63	90.0	337.5
	E8	0.820	108.04	44.62	2.63	90.0	45.0
	E9	1.098	104.15	44.27	2.63	90.0	315.0
	E10	1.295	106.82	44.58	2.63	90.0	67.5
	E11	1.174	105.05	44.27	2.63	90.0	292.5
	E12	1.250	103.58	44.30	2.63	90.0	90.0
	E13	0.771	108.78	44.49	2.63	22.5	90.0
	E14	0.450	108.25	44.46	2.63	45.0	90.0
	E15	0.587	109.60	44.42	2.63	67.5	90.0

Table 2 : Summary of ultrasonic velocity properties

Sample Number	P-wave (km/sec)	S-wave (km/sec)	Dynamic Shear Modulus (GPa)	Dynamic Young's Modulus (GPa)	Poisson's ratio
A1	2.66	1.29	4.37	11.76	0.35
A2	2.82	1.33	4.65	12.60	0.36
A3	3.21	1.54	6.21	16.77	0.35
A4	3.52	1.64	7.14	19.43	0.36
A5	3.76	1.91	9.64	25.54	0.33
A6	3.64	2.07	11.21	28.30	0.26
A7	3.54	1.97	10.19	26.01	0.28
A8	3.55	1.78	8.27	22.04	0.33
A9	3.76	1.81	8.64	23.33	0.35
A10	2.80	1.62	6.87	17.17	0.25
A11	3.11	1.79	8.38	21.04	0.26
A12	3.53	1.75	8.07	21.56	0.34
B1	2.82	1.54	6.36	16.35	0.29
B2	2.92	1.55	6.40	16.70	0.30
B3	3.23	1.77	8.33	21.42	0.29
B4	3.44	1.64	7.11	19.25	0.35
B5	3.70	1.79	8.35	22.50	0.35
B6	3.57	1.66	7.30	19.89	0.36
B7	3.39	1.55	6.37	17.41	0.37
B8	3.67	1.74	7.93	21.51	0.36
B9	3.83	1.87	9.23	24.79	0.34
B10	2.82	1.31	4.45	12.14	0.36
B11	3.15	1.62	6.96	18.36	0.32
B12	3.56	1.81	8.79	23.28	0.32

Table 2 : cont'd

Sample Number	P-wave (km/sec)	S-wave (km/sec)	Dynamic Shear Modulus (GPa)	Dynamic Young's Modulus (GPa)	Poisson's ratio
C1	2.65	0.97	2.48	7.05	0.42
C2	2.69	1.21	3.82	10.50	0.37
C3	3.27	1.43	5.40	14.91	0.38
C4	3.73	1.88	9.34	24.82	0.33
C5	3.35	1.91	9.67	24.33	0.26
C6	2.78	1.29	4.36	11.89	0.36
C7	3.58	1.37	4.91	13.89	0.41
C8	3.56	1.87	9.10	23.83	0.31
C9	3.31	1.48	5.71	15.69	0.38
C10	2.79	1.18	3.66	10.17	0.39
C11	3.26	1.61	6.84	18.29	0.34
C12	3.15	1.48	5.73	15.57	0.36
D1	3.50	2.08	11.33	27.79	0.23
D2	2.85	1.36	4.83	13.08	0.35
D3	3.32	1.58	6.58	17.80	0.35
D4	3.53	1.31	4.48	12.74	0.42
D5	3.99	1.92	9.66	26.08	0.35
D6	3.65	1.95	9.96	25.91	0.30
D7	3.56	1.52	6.10	16.92	0.39
D8	3.55	1.78	8.30	22.13	0.33
D9	3.52	1.76	8.14	21.70	0.33
D10	2.80	1.48	5.77	15.06	0.31
D11	3.29	1.64	7.17	19.15	0.33
D12	3.46	2.09	11.55	28.03	0.21

Table 2 : cont'd

Sample Number	P-wave (km/sec)	S-wave (km/sec)	Dynamic Shear Modulus (GPa)	Dynamic Young's Modulus (GPa)	Poisson's ratio
E1	2.76	1.43	5.38	14.15	0.32
E2	3.07	1.63	7.00	18.23	0.30
E3	3.30	1.56	6.39	17.34	0.36
E4	3.72	1.82	8.70	23.38	0.34
E5	3.78	1.89	9.37	25.00	0.33
E6	3.59	2.07	11.19	27.98	0.25
E7	3.93	1.73	7.87	21.73	0.38
E8	3.71	1.96	10.26	26.73	0.30
E9	3.83	1.87	9.23	24.78	0.34
E10	3.91	1.99	10.45	27.68	0.33
E11	3.64	1.83	8.81	23.44	0.33
E12	3.62	1.68	7.41	20.21	0.36
E13	3.09	1.78	8.36	20.92	0.25
E14	3.40	1.64	7.08	19.09	0.35
E15	3.57	1.76	8.13	21.75	0.34

Table 3 : Summary of uniaxial compression properties

Sample Number	Uniaxial Compressive Strength (MPa)	50% Tangent Modulus of Elasticity (GPa)	50% Secant Modulus of Elasticity (GPa)	25 MPa Secant Modulus of Elasticity (GPa)	Poisson's ratio
A1	135	48.01	26.00	17.32	0.30
A2	155	50.34	28.50	17.33	0.26
A3	152	49.25	32.81	22.15	0.32
A4	154	60.51	38.19	25.84	0.45
A5	145	62.05	49.70	38.78	0.37
A6	144	54.00	42.68	33.24	0.43
A7	153	83.31	47.27	27.16	0.46
A8	150	70.03	42.71	28.31	0.31
A9	145	56.13	36.02	25.43	0.29
A10	156	45.64	26.88	16.52	0.26
A11	128	43.20	24.35	17.12	0.21
A12	129	41.83	30.44	23.68	0.26
B1	130	49.13	24.89	16.25	0.27
B2	136	45.90	31.03	22.82	0.28
B3	132	44.75	28.97	20.76	0.32
B4	127	49.06	38.04	31.42	0.23
B5	143	54.42	42.48	33.09	0.31
B6	131	49.95	36.11	28.46	0.31
B7	159	47.99	36.30	26.94	0.26
B8	136	51.28	35.43	27.16	0.31
B9	140	56.97	37.72	27.59	0.31
B10	135	43.96	25.29	17.13	0.39
B11	116	43.41	27.42	20.99	0.27
B12	131	54.85	36.13	27.18	0.31

Table 3 : cont'd

Sample Number	Uniaxial Compressive Strength (MPa)	50% Tangent Modulus of Elasticity (GPa)	50% Secant Modulus of Elasticity (GPa)	25 MPa Secant Modulus of Elasticity (GPa)	Poisson's ratio
C1	132	42.61	21.61	14.71	0.40
C2	131	44.00	22.12	14.48	0.36
C3	146	45.05	30.59	20.84	0.33
C4	127	41.56	32.95	30.03	0.29
C5	121	48.27	29.49	21.65	0.20
C6	128	47.15	32.47	24.52	0.30
C7	132	61.64	38.85	27.90	0.38
C8	130	50.73	33.59	24.23	0.31
C9	126	53.08	33.01	24.58	0.33
C10	141	45.57	26.05	16.89	0.30
C11	134	46.60	25.78	17.96	0.35
C12	126	46.24	27.84	20.07	0.38
D1	143	50.22	25.97	16.43	0.21
D2	153	47.58	27.90	17.46	0.35
D3	147	42.79	27.71	18.68	0.31
D4	142	51.74	34.47	25.18	0.33
D5	145	58.95	41.50	30.49	0.31
D6	150	58.63	42.18	30.41	0.28
D7	142	61.00	37.20	25.19	0.28
D8	143	65.65	40.33	26.31	0.35
D9	142	65.09	40.70	27.34	0.38
D10	142	46.22	23.89	15.07	0.29
D11	143	46.16	nnnnn	20.14	0.27
D12	119	43.29	27.56	21.05	0.18

Table 3 : cont'd

Sample Number	Uniaxial Compressive Strength (MPa)	50% Tangent Modulus of Elasticity (GPa)	50% Secant Modulus of Elasticity (GPa)	25 MPa Secant Modulus of Elasticity (GPa)	Poisson's ratio
E1	180	50.14	27.20	15.18	0.24
E2	136	44.88	32.15	24.53	0.38
E3	135	44.83	32.11	24.49	0.38
E4	142	51.28	35.22	25.39	0.29
E5	151	50.36	40.63	32.54	0.22
E6	140	48.50	38.76	30.80	0.27
E7	142	49.32	39.41	31.33	0.31
E8	145	48.71	36.26	27.07	0.25
E9	141	54.10	37.76	29.40	0.25
E10	139	50.88	33.91	24.65	0.31
E11	143	65.65	46.24	32.99	0.38
E12	140	45.19	37.47	28.55	0.28
E13	131	43.83	25.29	17.50	0.27
E14	129	43.03	26.72	19.20	0.26
E15	141	49.09	32.62	24.11	0.19

Table 4 : Uniaxial Compressive Strength: Ellipsoidal Fit & Rotation into Standard Form

Core A

Most Probable Ellipsoid	Rotation Matrix	Normal Equation
$(X\ \ Y\ \ Z)\begin{pmatrix} +5.02 & -0.42 & +0.46 \\ -0.42 & +4.86 & -0.58 \\ +0.46 & -0.58 & +4.60 \end{pmatrix}\begin{pmatrix} X \\ Y \\ Z \end{pmatrix} = 10^5$	$\begin{pmatrix} +0.7709 & +0.5862 & -0.2492 \\ +0.1566 & -0.5537 & -0.8179 \\ +0.6174 & -0.5914 & +0.5186 \end{pmatrix}$	$\frac{x^2}{148^2} + \frac{y^2}{156^2} + \frac{z^2}{131^2} = 1$

Core B

Most Probable Ellipsoid	Rotation Matrix	Normal Equation
$(X\ \ Y\ \ Z)\begin{pmatrix} +5.26 & -0.76 & +1.09 \\ -0.76 & +5.35 & +0.48 \\ +1.09 & +0.48 & +5.34 \end{pmatrix}\begin{pmatrix} X \\ Y \\ Z \end{pmatrix} = 10^5$	$\begin{pmatrix} -0.1660 & +0.8437 & -0.5106 \\ +0.7389 & -0.2365 & +0.6310 \\ -0.6531 & -0.4820 & +0.5841 \end{pmatrix}$	$\frac{x^2}{131^2} + \frac{y^2}{125^2} + \frac{z^2}{163^2} = 1$

Core C

Most Probable Ellipsoid	Rotation Matrix	Normal Equation
$(X\ \ Y\ \ Z)\begin{pmatrix} +6.58 & -0.97 & -0.70 \\ -0.97 & +6.83 & -1.13 \\ -0.70 & -1.13 & +5.75 \end{pmatrix}\begin{pmatrix} X \\ Y \\ Z \end{pmatrix} = 10^5$	$\begin{pmatrix} +0.4883 & -0.8238 & +0.2878 \\ -0.7345 & -0.2099 & +0.6454 \\ +0.4713 & +0.5265 & +0.7076 \end{pmatrix}$	$\frac{x^2}{113^2} + \frac{y^2}{120^2} + \frac{z^2}{150^2} = 1$

Table 4 : Continued

Core D

Most Probable Ellipsoid	Rotation Matrix	Normal Equation
$(X\ \ Y\ \ Z)\begin{pmatrix}+5.33 & -0.38 & +0.46\\ -0.38 & +4.83 & -0.10\\ +0.46 & -0.10 & +4.53\end{pmatrix}\begin{pmatrix}X\\ Y\\ Z\end{pmatrix} = 10^5$	$\begin{pmatrix}+0.2945 & +0.9026 & +0.3141\\ -0.4535 & -0.1573 & +0.8773\\ -0.8412 & +0.4007 & -0.3629\end{pmatrix}$	$\frac{x^2}{146^2} + \frac{y^2}{152^2} + \frac{z^2}{132^2} = 1$

Core E

Most Probable Ellipsoid	Rotation Matrix	Normal Equation
$(X\ \ Y\ \ Z)\begin{pmatrix}+4.58 & +0.67 & +1.93\\ +0.67 & +4.25 & +1.76\\ +1.93 & +1.76 & +3.40\end{pmatrix}\begin{pmatrix}X\\ Y\\ Z\end{pmatrix} = 10^5$	$\begin{pmatrix}+0.6697 & -0.7418 & -0.0356\\ -0.4169 & -0.4152 & +0.8086\\ +0.6146 & +0.5267 & +0.5873\end{pmatrix}$	$\frac{x^2}{163^2} + \frac{y^2}{258^2} + \frac{z^2}{119^2} = 1$

Aggregate Results

Most Probable Ellipsoid	Rotation Matrix	Normal Equation
$(X\ \ Y\ \ Z)\begin{pmatrix}+5.23 & -0.20 & +0.90\\ -0.20 & +4.08 & +0.28\\ +0.90 & +0.28 & +4.38\end{pmatrix}\begin{pmatrix}X\\ Y\\ Z\end{pmatrix} = 10^5$	$\begin{pmatrix}+0.4883 & -0.8238 & +0.2878\\ -0.7345 & -0.2099 & +0.6454\\ +0.4713 & +0.5265 & +0.7076\end{pmatrix}$	$\frac{x^2}{140^2} + \frac{y^2}{131^2} + \frac{z^2}{164^2} = 1$

Table 5: 50% Tangent Modulus of Elasticity: Ellipsoidal Fit & Rotation into Standard Form

Core A

Most Probable Ellipsoid

$$(X\ \ Y\ \ Z)\begin{pmatrix} +28.09 & -5.94 & +21.16 \\ -5.94 & +28.50 & +0.64 \\ +21.16 & +0.64 & +41.10 \end{pmatrix}\begin{pmatrix} X \\ Y \\ Z \end{pmatrix} = 10^5$$

Rotation Matrix

$$\begin{pmatrix} +0.1658 & -0.9527 & -0.2548 \\ -0.7821 & -0.2844 & +0.5545 \\ +0.6007 & -0.1073 & +0.7922 \end{pmatrix}$$

Normal Equation

$$\frac{x^2}{58.02^2} + \frac{y^2}{95.68^2} + \frac{z^2}{41.87^2} = 1$$

Core B

Most Probable Ellipsoid

$$(X\ \ Y\ \ Z)\begin{pmatrix} +28.68 & +11.82 & +10.37 \\ +11.82 & +33.42 & +9.91 \\ +10.37 & +9.91 & +43.49 \end{pmatrix}\begin{pmatrix} X \\ Y \\ Z \end{pmatrix} = 10^5$$

Rotation Matrix

$$\begin{pmatrix} +0.8068 & -0.5813 & -0.1056 \\ -0.3591 & -0.6244 & +0.6937 \\ +0.4692 & +0.5217 & +0.7125 \end{pmatrix}$$

Normal Equation

$$\frac{x^2}{72.92^2} + \frac{y^2}{58.52^2} + \frac{z^2}{41.68^2} = 1$$

Core C

Most Probable Ellipsoid

$$(X\ \ Y\ \ Z)\begin{pmatrix} +39.03 & -12.33 & +2.69 \\ -12.33 & +46.91 & +3.97 \\ +2.69 & +3.97 & +50.31 \end{pmatrix}\begin{pmatrix} X \\ Y \\ Z \end{pmatrix} = 10^5$$

Rotation Matrix

$$\begin{pmatrix} +0.5234 & -0.8011 & -0.2905 \\ -0.3377 & +0.1180 & -0.9338 \\ -0.7824 & -0.5868 & +0.2087 \end{pmatrix}$$

Normal Equation

$$\frac{x^2}{42.10^2} + \frac{y^2}{44.83^2} + \frac{z^2}{58.66^2} = 1$$

Table 5: Continued

Core D

Most Probable Ellipsoid	Rotation Matrix	Normal Equation
$(X\ \ Y\ \ Z)\begin{pmatrix} +24.13 & -0.35 & +20.97 \\ -0.35 & +28.98 & +14.65 \\ +20.97 & +14.65 & +37.01 \end{pmatrix}\begin{pmatrix} X \\ Y \\ Z \end{pmatrix} = 10^5$	$\begin{pmatrix} +0.5465 & -0.8335 & +0.0813 \\ -0.6820 & -0.3867 & +0.6207 \\ +0.4859 & +0.3947 & +0.7798 \end{pmatrix}$	$\frac{x^2}{59.99^2}+\frac{y^2}{143.69^2}+\frac{z^2}{41.70^2}=1$

Core E

Most Probable Ellipsoid	Rotation Matrix	Normal Equation
$(X\ \ Y\ \ Z)\begin{pmatrix} +41.24 & +1.49 & +7.50 \\ +1.49 & +38.35 & +5.10 \\ +7.450 & +5.10 & +43.82 \end{pmatrix}\begin{pmatrix} X \\ Y \\ Z \end{pmatrix} = 10^5$	$\begin{pmatrix} +0.6204 & -0.7752 & -0.1191 \\ +0.5370 & +0.5305 & -0.6559 \\ -0.5716 & -0.3429 & -0.7454 \end{pmatrix}$	$\frac{x^2}{51.34^2}+\frac{y^2}{54.59^2}+\frac{z^2}{43.89^2}=1$

Aggregate Results

Most Probable Ellipsoid	Rotation Matrix	Normal Equation
$(X\ \ Y\ \ Z)\begin{pmatrix} +29.07 & -0.13 & +14.69 \\ -0.13 & +32.98 & +6.69 \\ +14.69 & +6.69 & +42.45 \end{pmatrix}\begin{pmatrix} X \\ Y \\ Z \end{pmatrix} = 10^5$	$\begin{pmatrix} +0.3694 & -0.9260 & +0.0776 \\ +0.7856 & +0.2667 & -0.5582 \\ -0.4963 & -0.2672 & -0.8260 \end{pmatrix}$	$\frac{x^2}{55.49^2}+\frac{y^2}{73.35^2}+\frac{z^2}{43.26^2}=1$

Table 6: 50% Secant Modulus of Elasticity, Ellipsoidal Fit & Rotation into Standard Form

Core A

Most Probable Ellipsoid

$$(X \quad Y \quad Z)\begin{pmatrix} +66.68 & -0.98 & +47.46 \\ -0.98 & +44.40 & +9.49 \\ +47.46 & +9.49 & +132.08 \end{pmatrix}\begin{pmatrix} X \\ Y \\ Z \end{pmatrix} = 10^5$$

Rotation Matrix

$$\begin{pmatrix} +0.5877 & -0.7711 & -0.2451 \\ -6648 & -0.6329 & +0.3968 \\ +0.4611 & +0.0702 & +0.8846 \end{pmatrix}$$

Normal Equation

$$\frac{x^2}{45.57^2}+\frac{y^2}{51.69^2}+\frac{z^2}{25.19^2} = 1$$

Core B

Most Probable Ellipsoid

$$(X \quad Y \quad Z)\begin{pmatrix} +65.60 & +18.39 & +13.14 \\ +18.39 & +58.22 & -4.24 \\ +13.14 & -4.24 & +145.35 \end{pmatrix}\begin{pmatrix} X \\ Y \\ Z \end{pmatrix} = 10^5$$

Rotation Matrix

$$\begin{pmatrix} +0.7471 & +0.6560 & -0.1074 \\ +0.6464 & -0.7546 & -0.1129 \\ +0.1551 & -0.0149 & +0.9878 \end{pmatrix}$$

Normal Equation

$$\frac{x^2}{35.39^2}+\frac{y^2}{48.89^2}+\frac{z^2}{26.04^2} = 1$$

Core C

Most Probable Ellipsoid

$$(X \quad Y \quad Z)\begin{pmatrix} +102.24 & -34.52 & -7.26 \\ -34.52 & +112.42 & -42.53 \\ -7.26 & -42.53 & +199.27 \end{pmatrix}\begin{pmatrix} X \\ Y \\ Z \end{pmatrix} = 10^5$$

Rotation Matrix

$$\begin{pmatrix} +0.7391 & -0.6003 & -0.3055 \\ -0.6709 & -0.6966 & -0.2544 \\ +0.0601 & -0.3930 & +0.9176 \end{pmatrix}$$

Normal Equation

$$\frac{x^2}{27.39^2}+\frac{y^2}{39.64^2}+\frac{z^2}{21.47^2} = 1$$

Table 6 : Continued

Core D

Most Probable Ellipsoid

$$(X \quad Y \quad Z)\begin{pmatrix} +60.80 & +5.54 & +79.33 \\ +5.54 & +56.42 & +23.35 \\ +79.33 & +23.35 & +136.69 \end{pmatrix}\begin{pmatrix} X \\ Y \\ Z \end{pmatrix} = 10^5$$

Rotation Matrix

$$\begin{pmatrix} +0.2363 & -0.9705 & +0.0473 \\ -0.8211 & -0.1735 & +0.5437 \\ +0.5195 & +0.1674 & +0.8379 \end{pmatrix}$$

Normal Equation

$$\frac{x^2}{43.06^2}+\frac{y^2}{102.92^2}+\frac{z^2}{22.91^2} = 1$$

Core E

Most Probable Ellipsoid

$$(X \quad Y \quad Z)\begin{pmatrix} +71.68 & +10.45 & +35.58 \\ +10.45 & +61.91 & +1.12 \\ +35.58 & +1.12 & +122.79 \end{pmatrix}\begin{pmatrix} X \\ Y \\ Z \end{pmatrix} = 10^5$$

Rotation Matrix

$$\begin{pmatrix} +0.7643 & -0.5386 & -0.3546 \\ -0.4502 & -0.8394 & +0.3045 \\ +0.4617 & +0.0731 & +0.8840 \end{pmatrix}$$

Normal Equation

$$\frac{x^2}{45.73^2}+\frac{y^2}{38.60^2}+\frac{z^2}{26.59^2} = 1$$

Aggregate Results

Most Probable Ellipsoid

$$(X \quad Y \quad Z)\begin{pmatrix} +68.54 & +7.57 & +34.11 \\ +7.57 & +56.51 & +5.40 \\ +34.11 & +5.40 & +139.59 \end{pmatrix}\begin{pmatrix} X \\ Y \\ Z \end{pmatrix} = 10^5$$

Rotation Matrix

$$\begin{pmatrix} -0.7090 & -0.6665 & -0.2306 \\ -0.5968 & -0.7412 & +0.3075 \\ +0.3758 & +0.0803 & +0.9232 \end{pmatrix}$$

Normal Equation

$$\frac{x^2}{44.58^2}+\frac{y^2}{40.70^2}+\frac{z^2}{25.49^2} = 1$$

Table 7: 25 MPa Secant Modulus of Elasticity: Ellipsoidal Fit & Rotation into Standard Form

Core A

Most Probable Ellipsoid	Rotation Matrix	Normal Equation
$(X\ \ Y\ \ Z)\begin{pmatrix} +136.11 & +9.17 & +50.85 \\ +9.17 & +70.06 & +27.25 \\ +50.85 & +27.25 & +342.63 \end{pmatrix}\begin{pmatrix} X \\ Y \\ Z \end{pmatrix} = 10^5$	$\begin{pmatrix} +0.0690 & -0.9939 & +0.0856 \\ -0.9715 & -0.0475 & +0.2323 \\ +0.2268 & +0.0992 & +0.9689 \end{pmatrix}$	$\frac{x^2}{38.61^2} + \frac{y^2}{28.35^2} + \frac{z^2}{16.73^2} = 1$

Core B

Most Probable Ellipsoid	Rotation Matrix	Normal Equation
$(X\ \ Y\ \ Z)\begin{pmatrix} +121.04 & +30.06 & +0.06 \\ +30.06 & +95.42 & -36.86 \\ +0.06 & -36.86 & +312.92 \end{pmatrix}\begin{pmatrix} X \\ Y \\ Z \end{pmatrix} = 10^5$	$\begin{pmatrix} +0.8570 & +0.5042 & +0.1064 \\ +0.5147 & -0.8475 & -0.1295 \\ -0.0249 & -0.1658 & +0.9859 \end{pmatrix}$	$\frac{x^2}{26.85^2} + \frac{y^2}{37.39^2} + \frac{z^2}{17.70^2} = 1$

Core C

Most Probable Ellipsoid	Rotation Matrix	Normal Equation
$(X\ \ Y\ \ Z)\begin{pmatrix} +182.81 & -40.98 & -26.58 \\ -40.98 & +181.23 & -138.72 \\ -26.58 & -138.72 & +491.45 \end{pmatrix}\begin{pmatrix} X \\ Y \\ Z \end{pmatrix} = 10^5$	$\begin{pmatrix} +0.8639 & -0.4792 & -0.1548 \\ -0.5147 & -0.8475 & -0.1295 \\ -0.0286 & -0.3536 & +0.9350 \end{pmatrix}$	$\frac{x^2}{21.81^2} + \frac{y^2}{31.55^2} + \frac{z^2}{13.55^2} = 1$

Table 7: Continued

Core D

Most Probable Ellipsoid	Rotation Matrix	Normal Equation
$(X\ \ Y\ \ Z)\begin{pmatrix} +139.11 & +17.42 & +32.66 \\ +17.42 & +101.79 & +28.42 \\ +32.66 & +28.42 & +371.47 \end{pmatrix}\begin{pmatrix} X \\ Y \\ Z \end{pmatrix} = 10^5$	$\begin{pmatrix} +0.3172 & -0.9465 & +0.0596 \\ -0.9376 & -0.3036 & +0.1694 \\ +0.1422 & +0.1097 & +0.9837 \end{pmatrix}$	$\frac{x^2}{32.59^2} + \frac{y^2}{26.75^2} + \frac{z^2}{16.24^2} = 1$

Core E

Most Probable Ellipsoid	Rotation Matrix	Normal Equation
$(X\ \ Y\ \ Z)\begin{pmatrix} +126.95 & +21.36 & +67.98 \\ +21.36 & +98.95 & -11.73 \\ +67.98 & -11.73 & +250.48 \end{pmatrix}\begin{pmatrix} X \\ Y \\ Z \end{pmatrix} = 10^5$	$\begin{pmatrix} -0.6574 & +0.6919 & +0.2985 \\ +0.6366 & +0.7219 & -0.2714 \\ +0.4033 & -0.0117 & +0.9150 \end{pmatrix}$	$\frac{x^2}{36.86^2} + \frac{y^2}{28.61^2} + \frac{z^2}{18.88^2} = 1$

Aggregate Results

Most Probable Ellipsoid	Rotation Matrix	Normal Equation
$(X\ \ Y\ \ Z)\begin{pmatrix} +134.06 & +20.12 & +33.87 \\ +20.12 & +92.49 & -13.73 \\ +33.87 & -13.73 & +326.19 \end{pmatrix}\begin{pmatrix} X \\ Y \\ Z \end{pmatrix} = 10^5$	$\begin{pmatrix} -0.4160 & +0.9029 & +0.1083 \\ +0.8945 & +0.4278 & -0.1303 \\ +0.1639 & -0.0426 & +0.9855 \end{pmatrix}$	$\frac{x^2}{35.12^2} + \frac{y^2}{26.71^2} + \frac{z^2}{17.35^2} = 1$

Table 8: Poisson's Ratio: Ellipsoidal Fit & Rotation into Standard Form

Core A

Most Probable Ellipsoid	Rotation Matrix	Normal Equation
$(X\ Y\ Z)\begin{pmatrix} +11.80 & -1.98 & +5.50 \\ -1.98 & +5.96 & -1.39 \\ +5.50 & -1.39 & 12.91 \end{pmatrix}\begin{pmatrix} X \\ Y \\ Z \end{pmatrix} = 1$	$\begin{pmatrix} +0.3632 & +0.9270 & -0.0935 \\ +0.6526 & -0.3247 & -0.6846 \\ +0.6650 & -0.1876 & +0.7229 \end{pmatrix}$	$\frac{x^2}{0.43^2} + \frac{y^2}{0.38^2} + \frac{z^2}{0.23^2} = 1$

Core B

Most Probable Ellipsoid	Rotation Matrix	Normal Equation
$(X\ Y\ Z)\begin{pmatrix} +11.45 & +0.17 & -1.95 \\ +0.17 & +10.76 & +1.68 \\ -1.95 & +1.68 & +9.60 \end{pmatrix}\begin{pmatrix} X \\ Y \\ Z \end{pmatrix} = 1$	$\begin{pmatrix} +0.5714 & +0.8072 & +0.1478 \\ +0.7036 & -0.3892 & -0.5945 \\ +0.4224 & -0.4437 & +0.7904 \end{pmatrix}$	$\frac{x^2}{0.30^2} + \frac{y^2}{0.28^2} + \frac{z^2}{0.36^2} = 1$

Core C

Most Probable Ellipsoid	Rotation Matrix	Normal Equation
$(X\ Y\ Z)\begin{pmatrix} +8.65 & -4.76 & -0.03 \\ -4.76 & +18.37 & -3.62 \\ -0.03 & -3.62 & +7.55 \end{pmatrix}\begin{pmatrix} X \\ Y \\ Z \end{pmatrix} = 1$	$\begin{pmatrix} -0.6103 & -0.4108 & -0.6773 \\ -0.7139 & -0.0853 & +0.6950 \\ +0.3433 & -0.9077 & +0.2412 \end{pmatrix}$	$\frac{x^2}{0.43^2} + \frac{y^2}{0.35^2} + \frac{z^2}{0.22^2} = 1$

Table 8: Continued

Core D

Most Probable Ellipsoid

$$(X\ \ Y\ \ Z)\begin{pmatrix} +7.07 & +2.38 & +6.47 \\ +2.38 & +10.85 & -1.11 \\ +6.47 & -1.11 & +9.42 \end{pmatrix}\begin{pmatrix} X \\ Y \\ Z \end{pmatrix} = 1$$

Rotation Matrix

$$\begin{pmatrix} +0.0714 & +0.9505 & -0.3025 \\ -0.6565 & +0.1835 & -0.7317 \\ +0.7510 & -0.2508 & -0.6109 \end{pmatrix}$$

Normal Equation

$$\frac{x^2}{0.30^2} + \frac{y^2}{0.26^2} + \frac{z^2}{0.99^2} = 1$$

Core E

Most Probable Ellipsoid

$$(X\ \ Y\ \ Z)\begin{pmatrix} +13.91 & -4.74 & +2.19 \\ -4.74 & +20.04 & -10.25 \\ +2.19 & -10.25 & +13.69 \end{pmatrix}\begin{pmatrix} X \\ Y \\ Z \end{pmatrix} = 1$$

Rotation Matrix

$$\begin{pmatrix} +0.9361 & +0.1593 & -0.3135 \\ -0.1542 & -0.6153 & -0.7731 \\ +0.3160 & -0.7721 & +0.5514 \end{pmatrix}$$

Normal Equation

$$\frac{x^2}{0.28^2} + \frac{y^2}{0.41^2} + \frac{z^2}{0.19^2} = 1$$

Aggregate Results

Most Probable Ellipsoid

$$(X\ \ Y\ \ Z)\begin{pmatrix} +9.56 & +0.07 & +1.44 \\ +0.07 & +8.93 & -0.89 \\ +1.44 & -0.89 & +9.27 \end{pmatrix}\begin{pmatrix} X \\ Y \\ Z \end{pmatrix} = 1$$

Rotation Matrix

$$\begin{pmatrix} +0.5244 & +0.8320 & -0.1811 \\ +0.5253 & -0.4835 & -0.7002 \\ +0.6701 & -0.2721 & +0.6906 \end{pmatrix}$$

Normal Equation

$$\frac{x^2}{0.33^2} + \frac{y^2}{0.36^2} + \frac{z^2}{0.31^2} = 1$$

Table 9: Mean Maximum Anisotropies of Uniaxial Mechanical Properties

Core Section	Uniaxial Compressive Strength	50% Tangent Modulus of Elasticity	50% Secant Modulus of Elasticity	25 MPa Secant Modulus of Elasticity	Poisson's Ratio
A	1.19	2.29	2.05	2.31	1.87
B	1.30	1.75	1.88	2.11	1.29
C	1.33	1.39	1.85	2.32	1.95
D	1.15	3.44	4.49	2.01	3.81
E	2.17	1.24	1.92	1.95	2.16
Mean	1.43	2.02	2.44	2.14	2.21
Standard Deviation	0.42	0.89	1.15	0.17	0.95
Aggregate Results	1.25	1.70	1.75	2.02	1.16

Appendix A

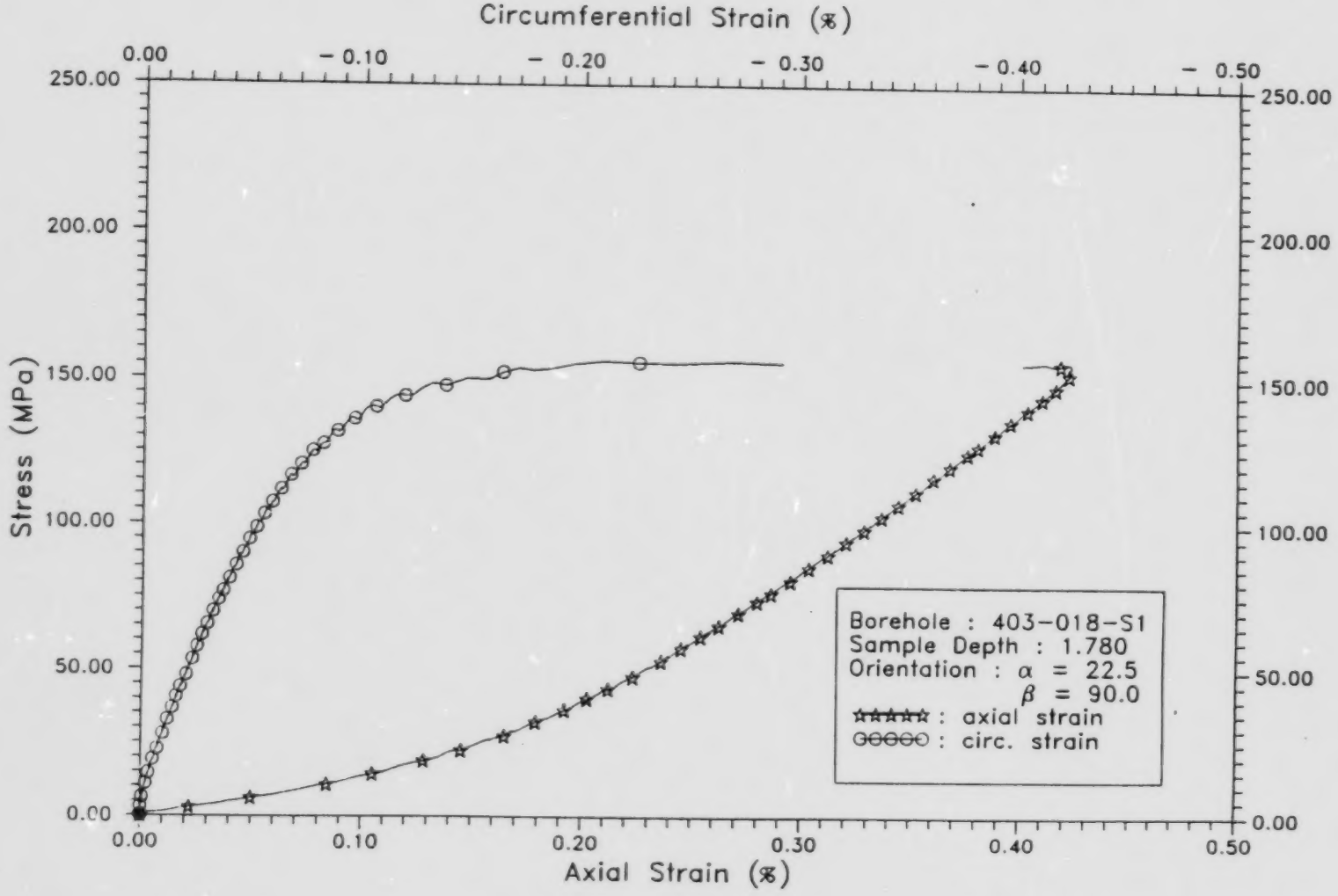

Fig. A1: Axial and Circumferential stress/strain curves for anisotropy test specimens

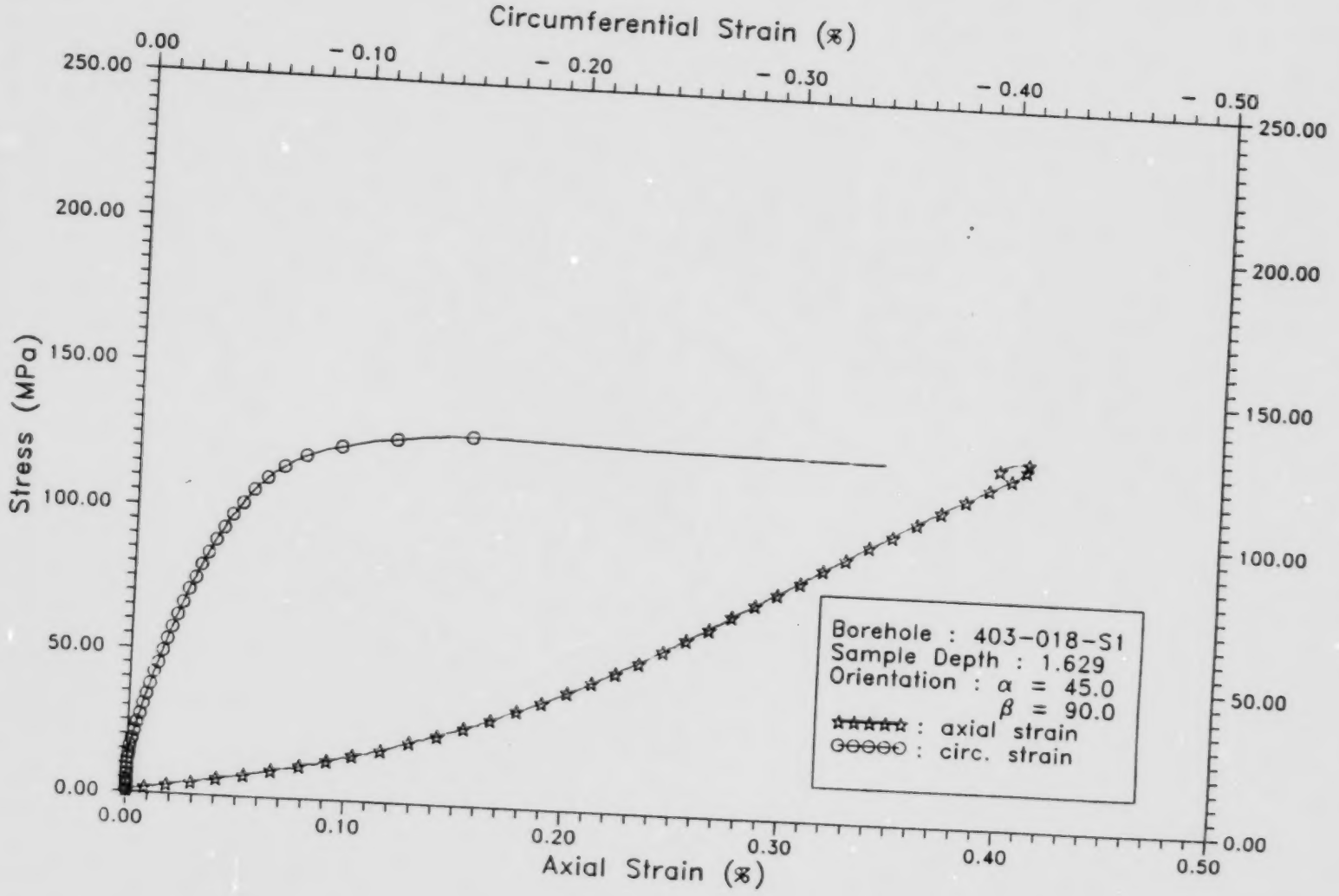

Fig. A2: Axial and Circumferential stress/strain curves for anisotropy test specimens

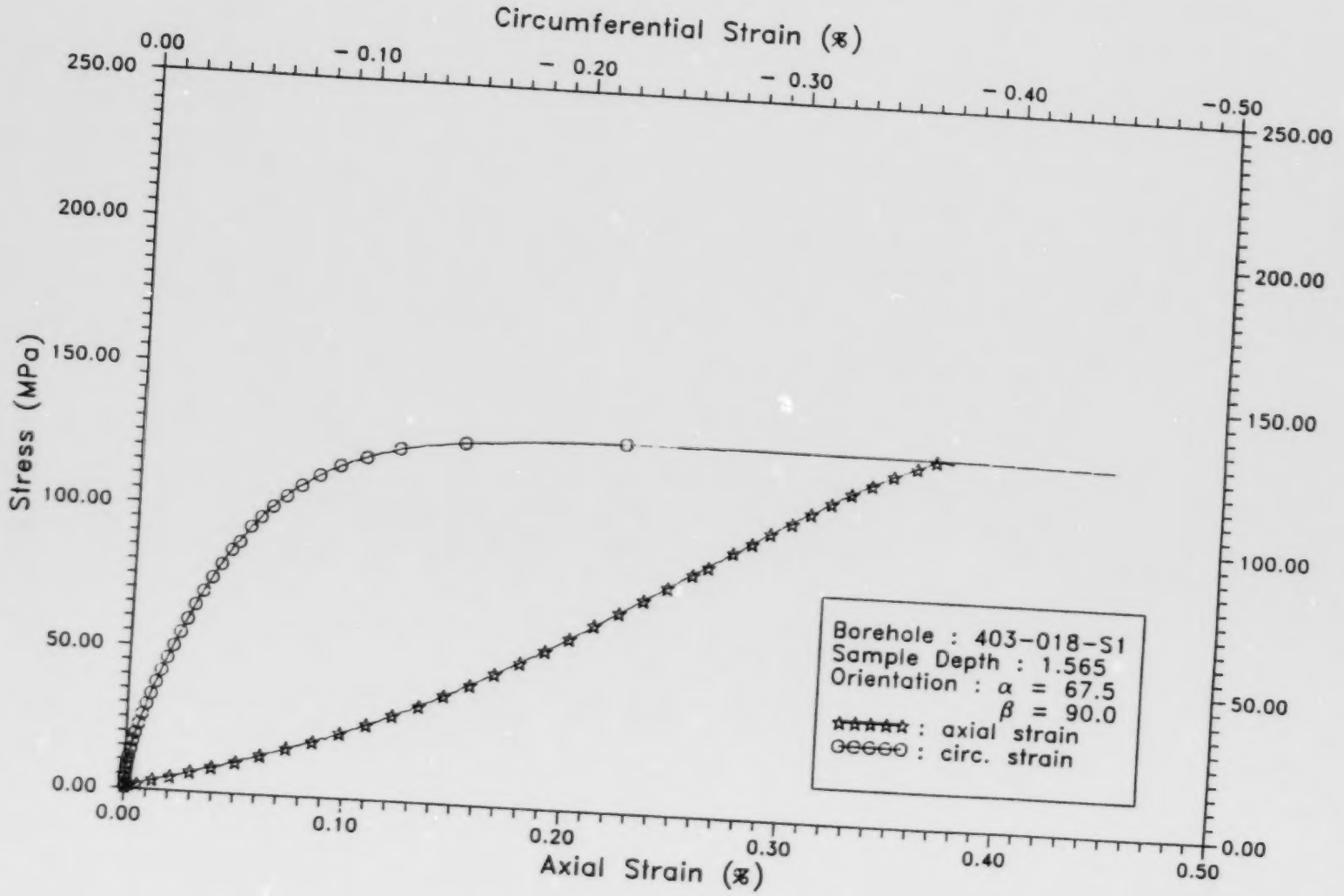

Fig. A3: Axial and Circumferential stress/strain curves for anisotropy test specimens

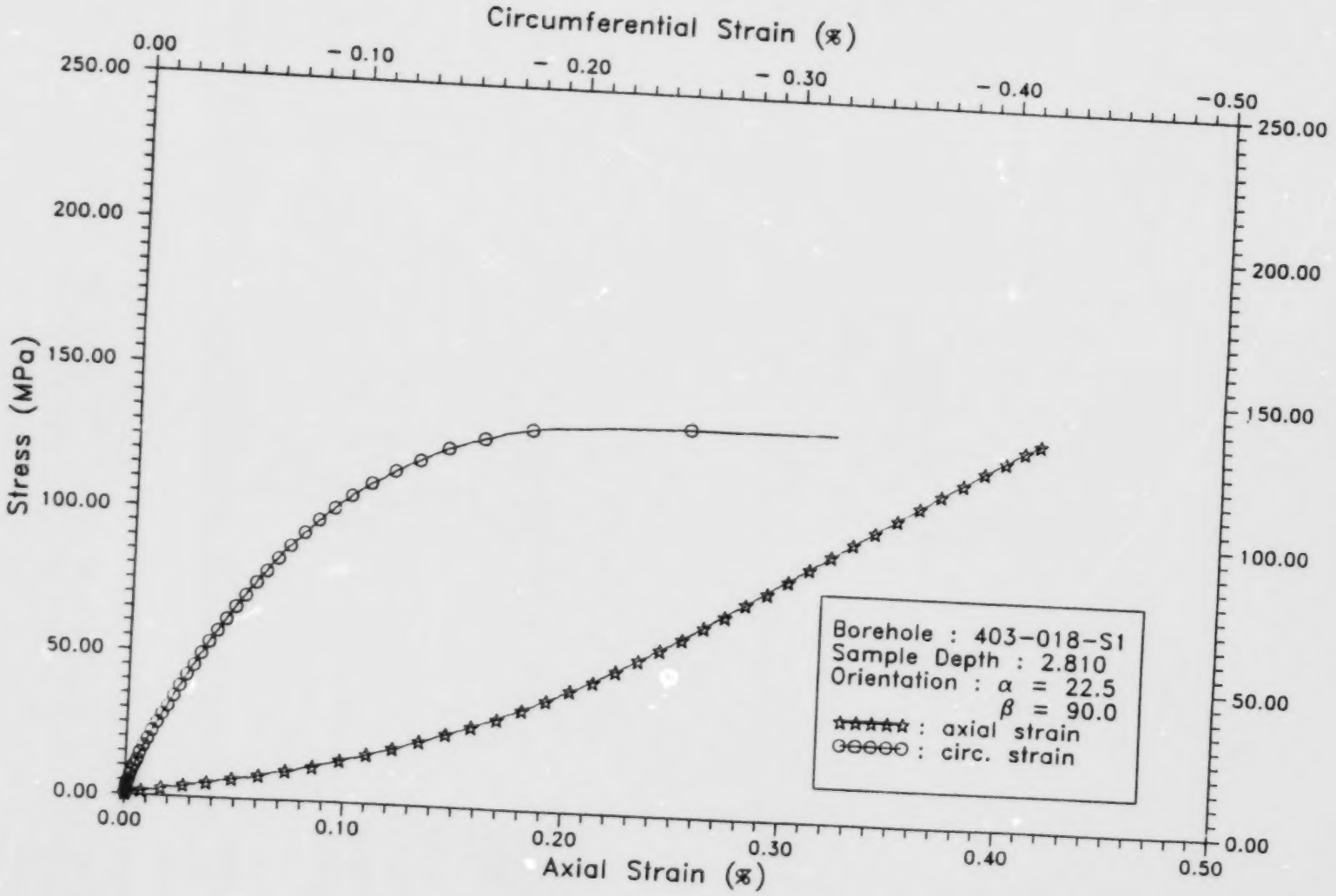

Fig. A4: Axial and Circumferential stress/strain curves for anisotropy test specimens

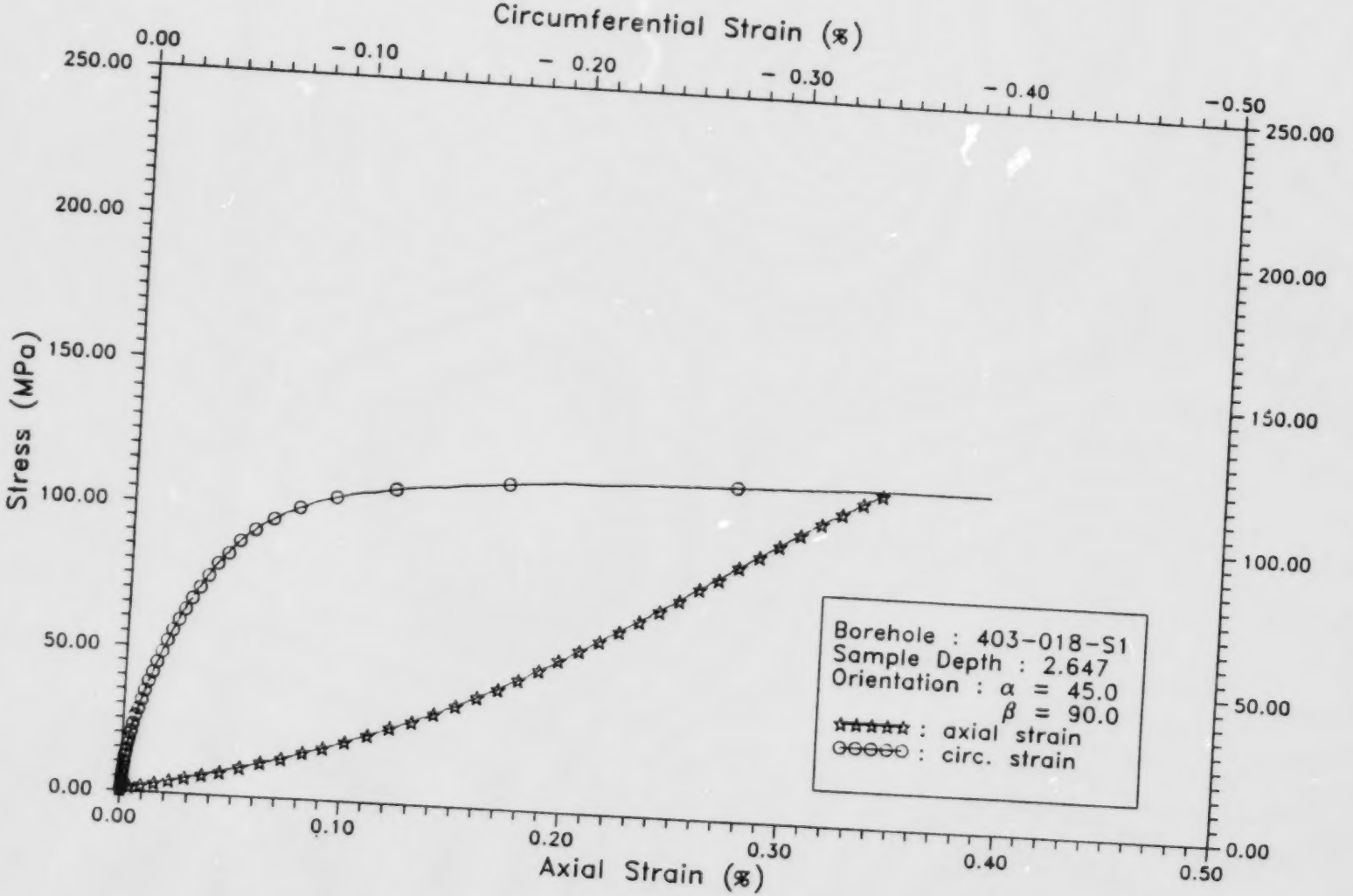

Fig. A5: Axial and Circumferential stress/strain curves for anisotropy test specimens

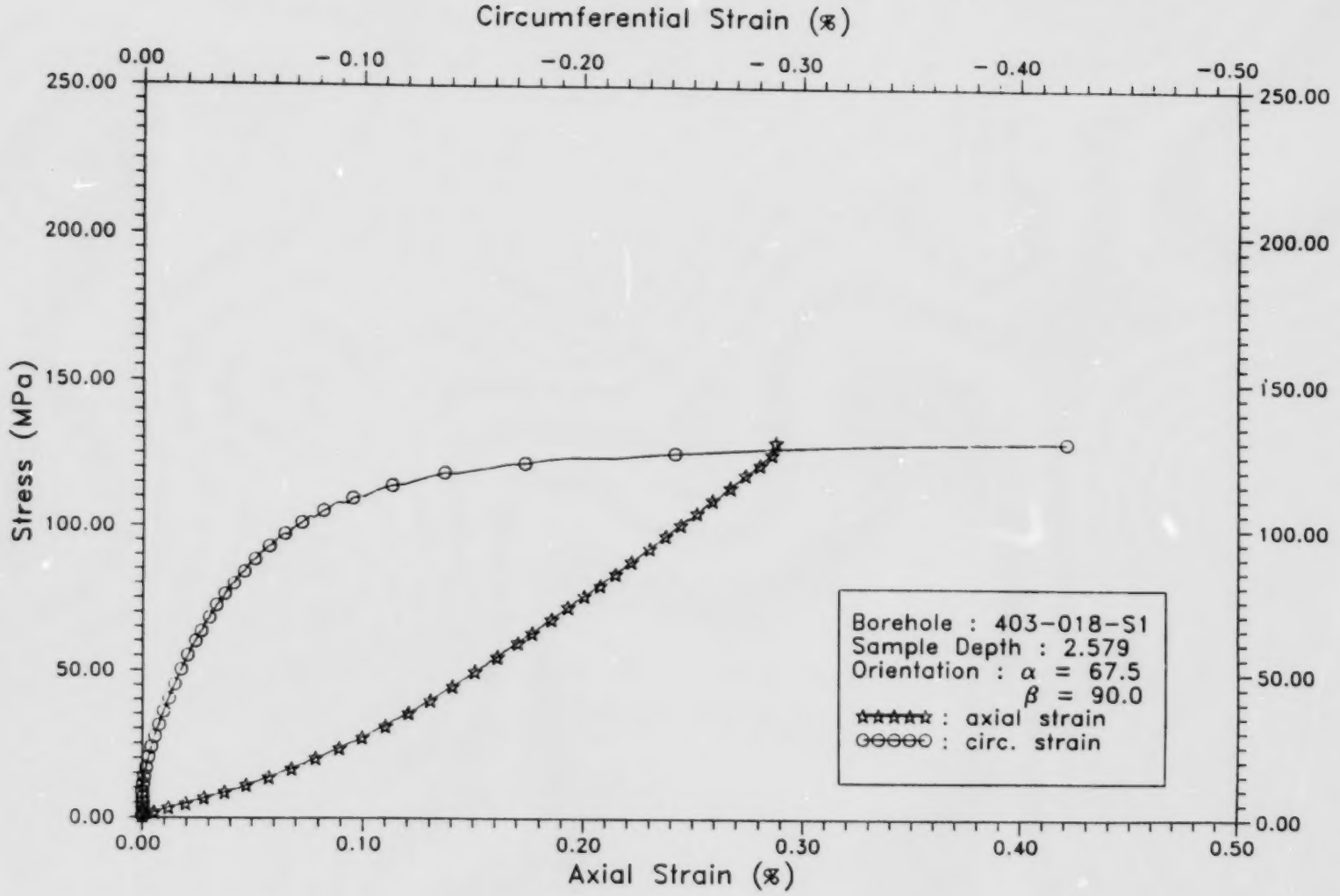

Fig. A6: Axial and Circumferential stress/strain curves for anisotropy test specimens

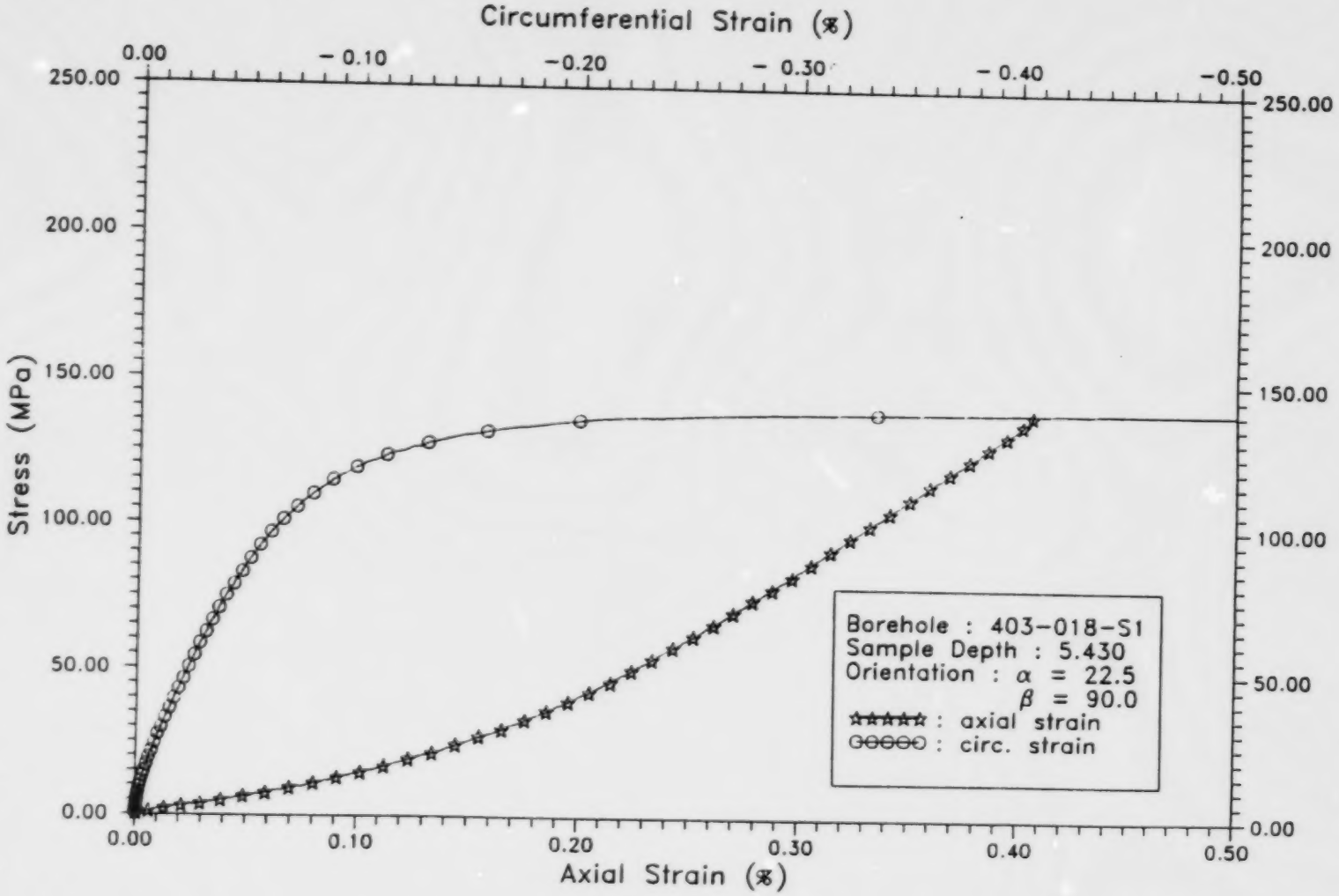

Fig. A7: Axial and Circumferential stress/strain curves for anisotropy test specimens

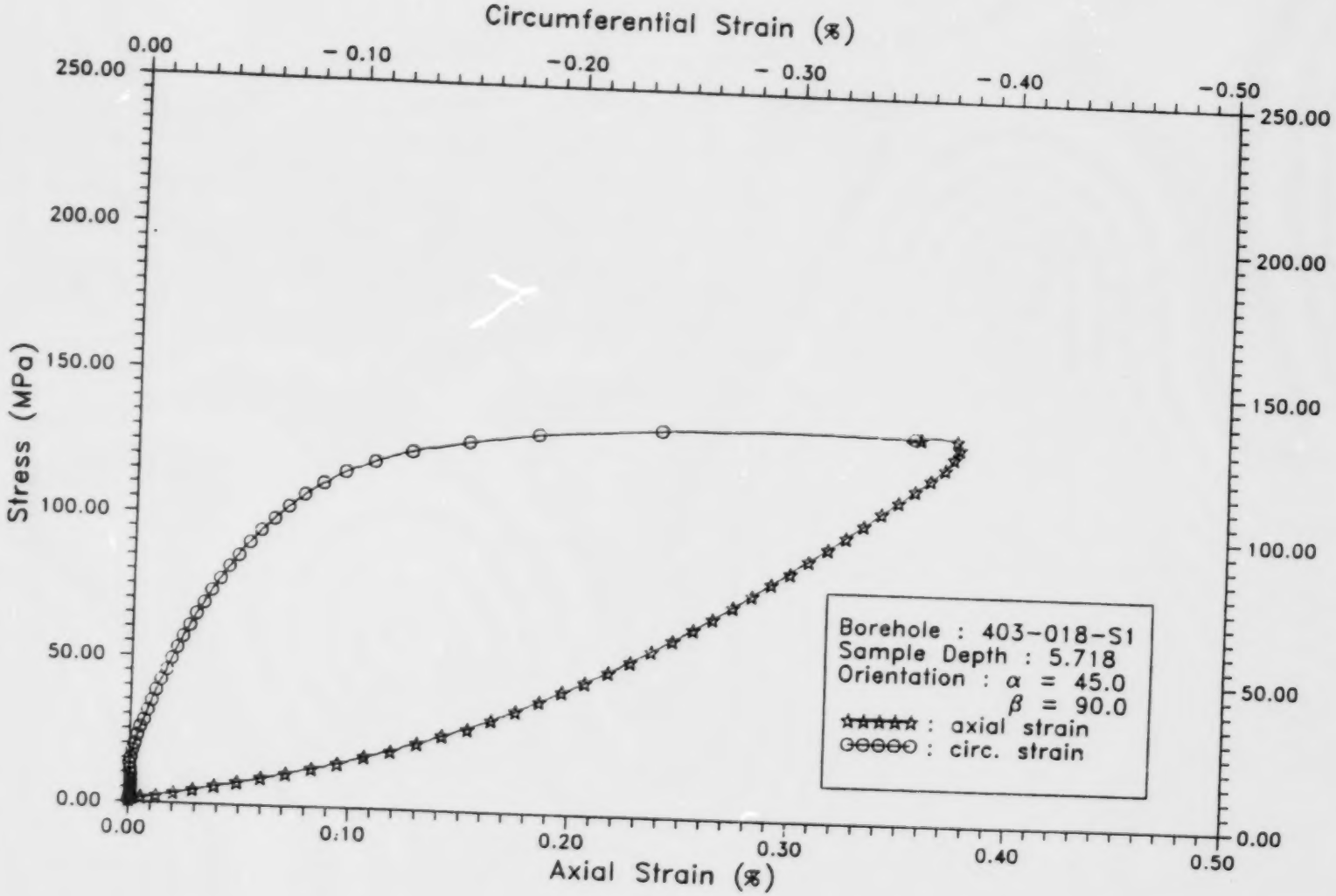

Fig. A8: Axial and Circumferential stress/strain curves for anisotropy test specimens

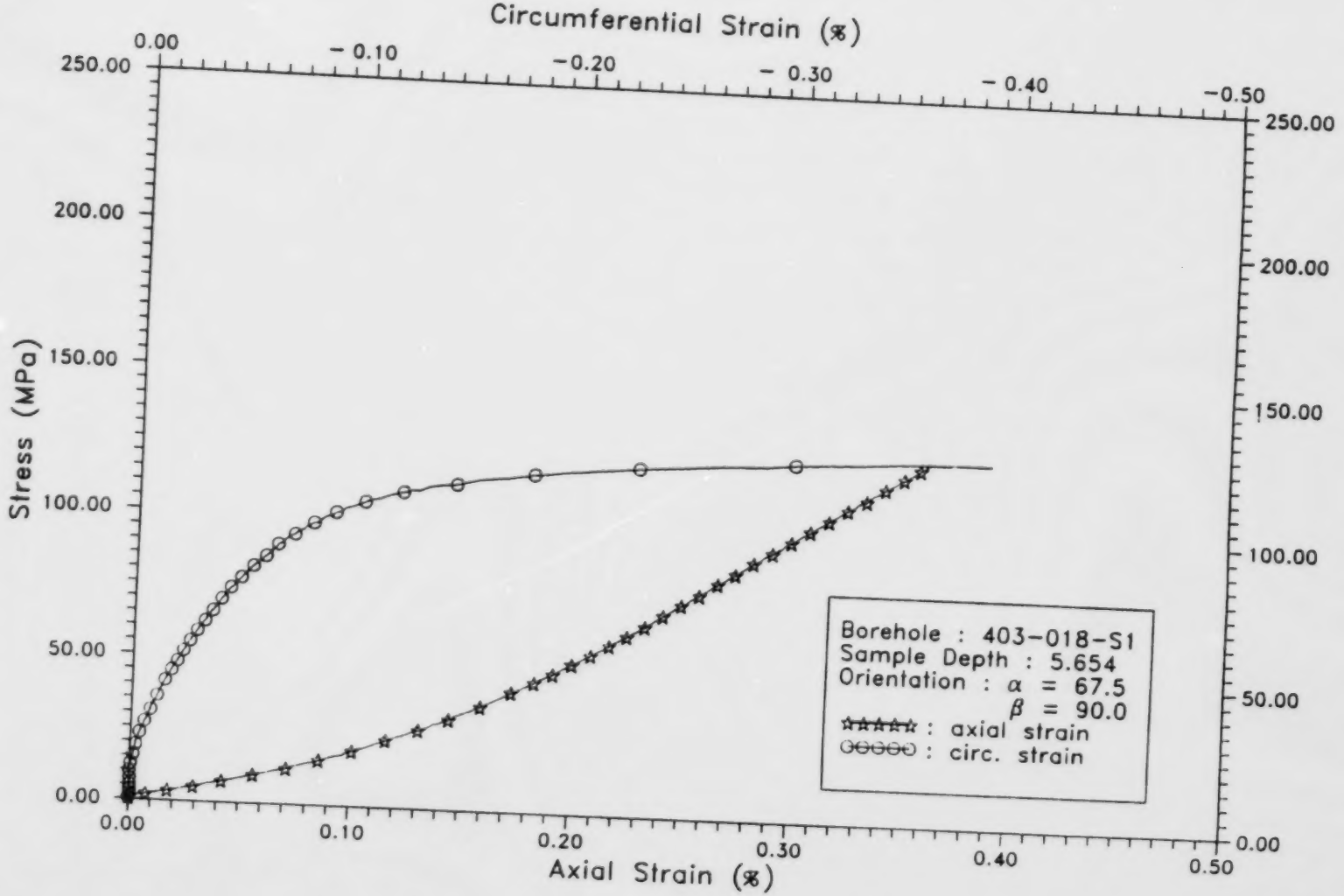

Fig. A9: Axial and Circumferential stress/strain curves for anisotropy test specimens

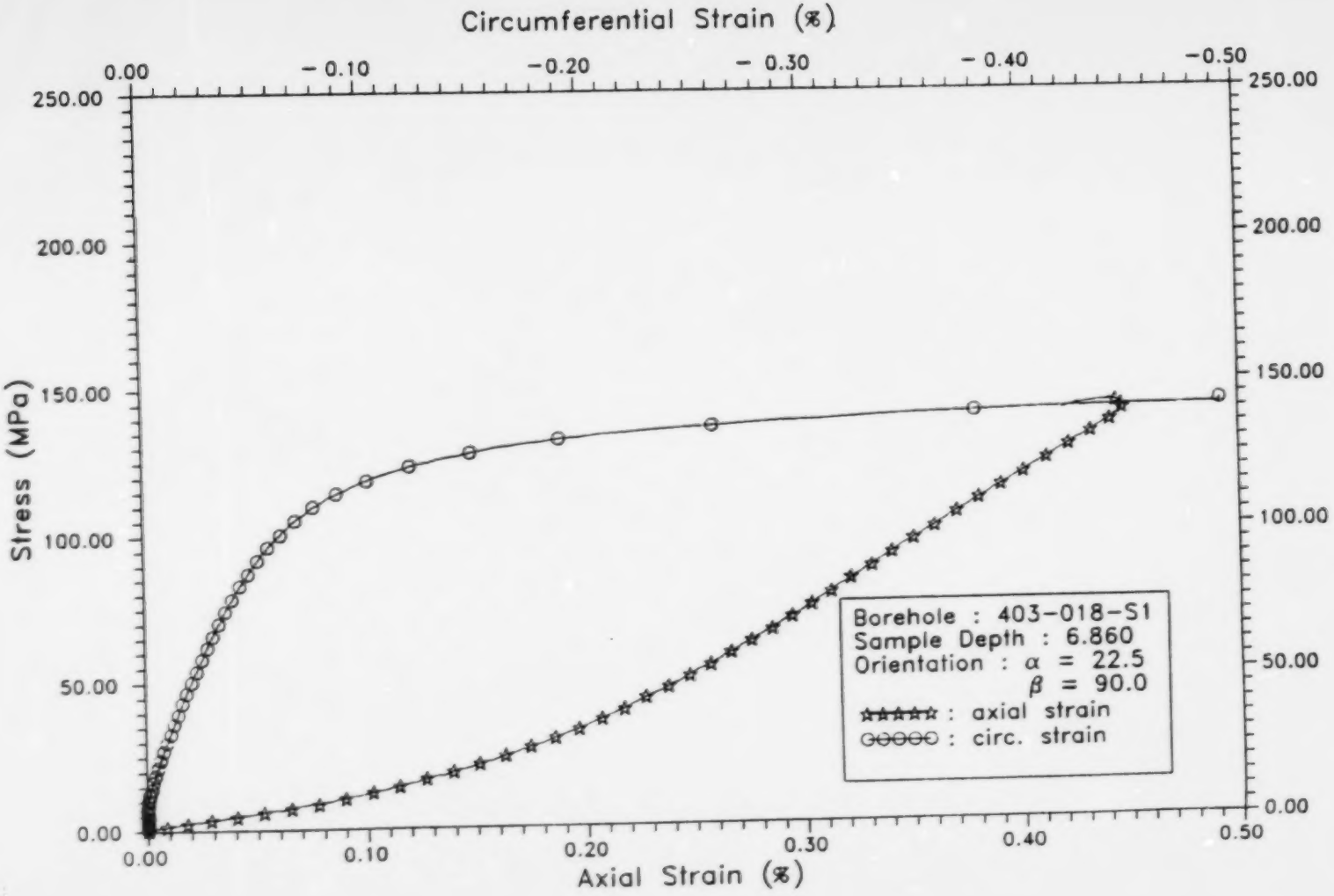

Fig. A10: Axial and Circumferential stress/strain curves for anisotropy test specimens

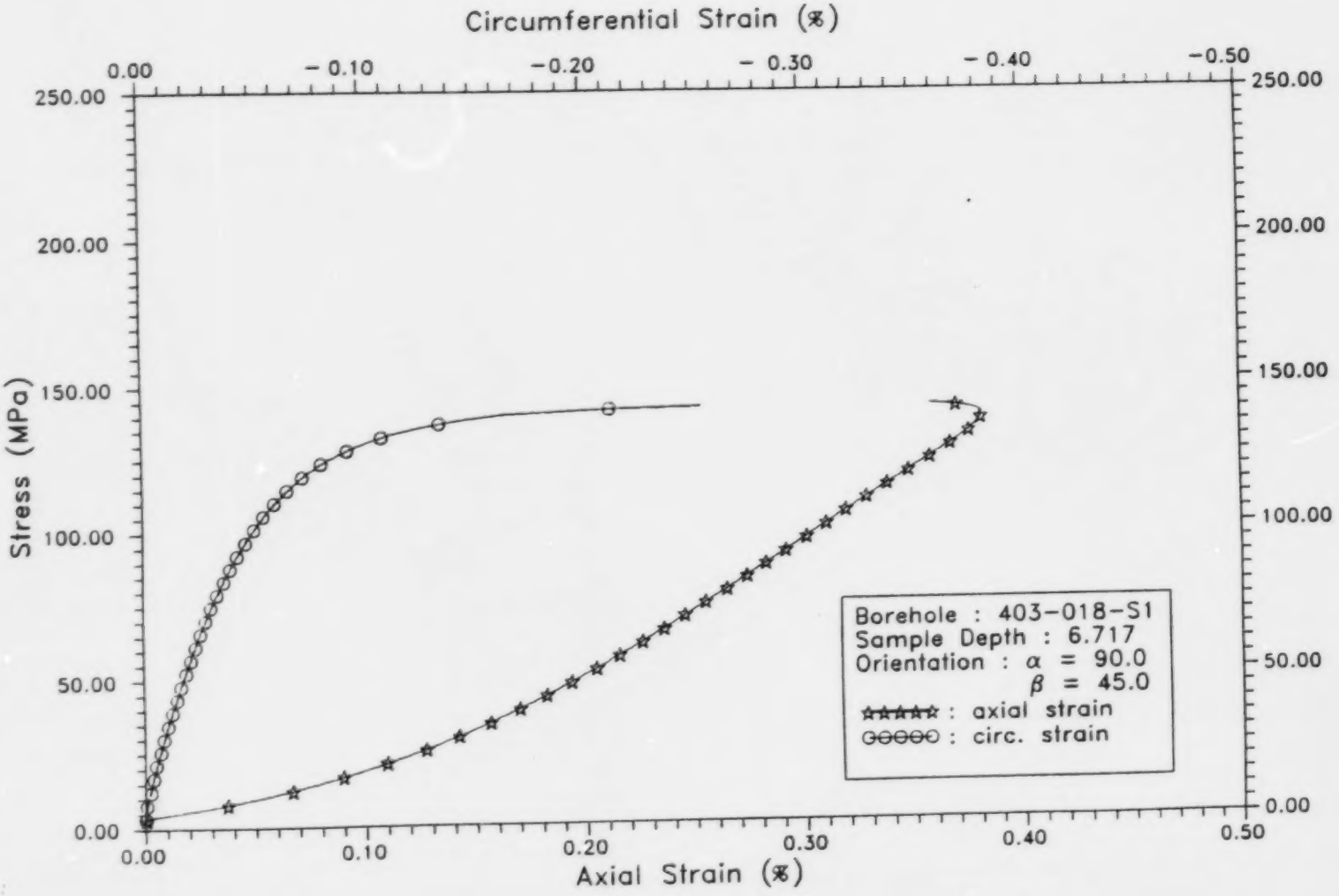

Fig. A11: Axial and Circumferential stress/strain curves for anisotropy test specimens

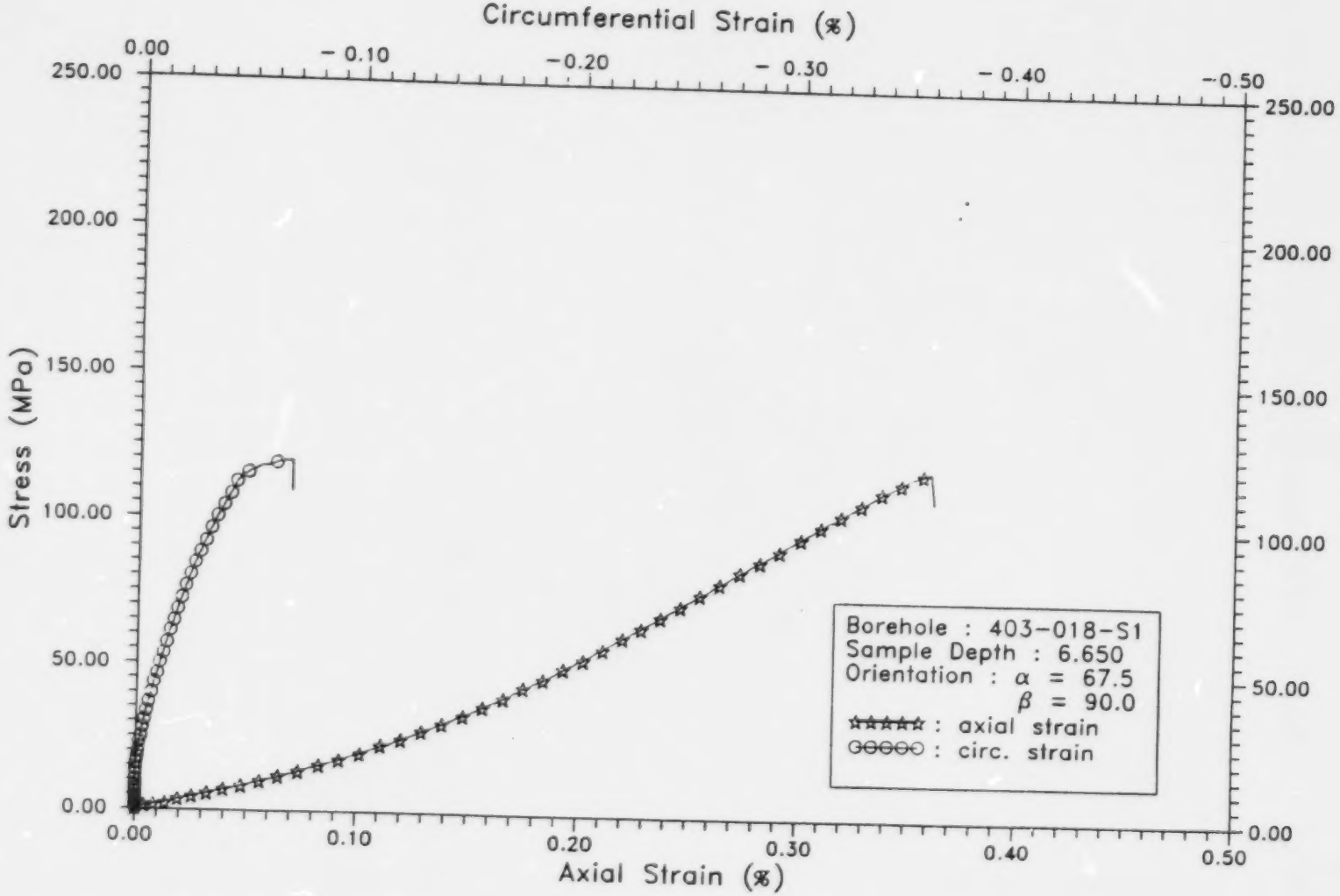

Fig. A12: Axial and Circumferential stress/strain curves for anisotropy test specimens

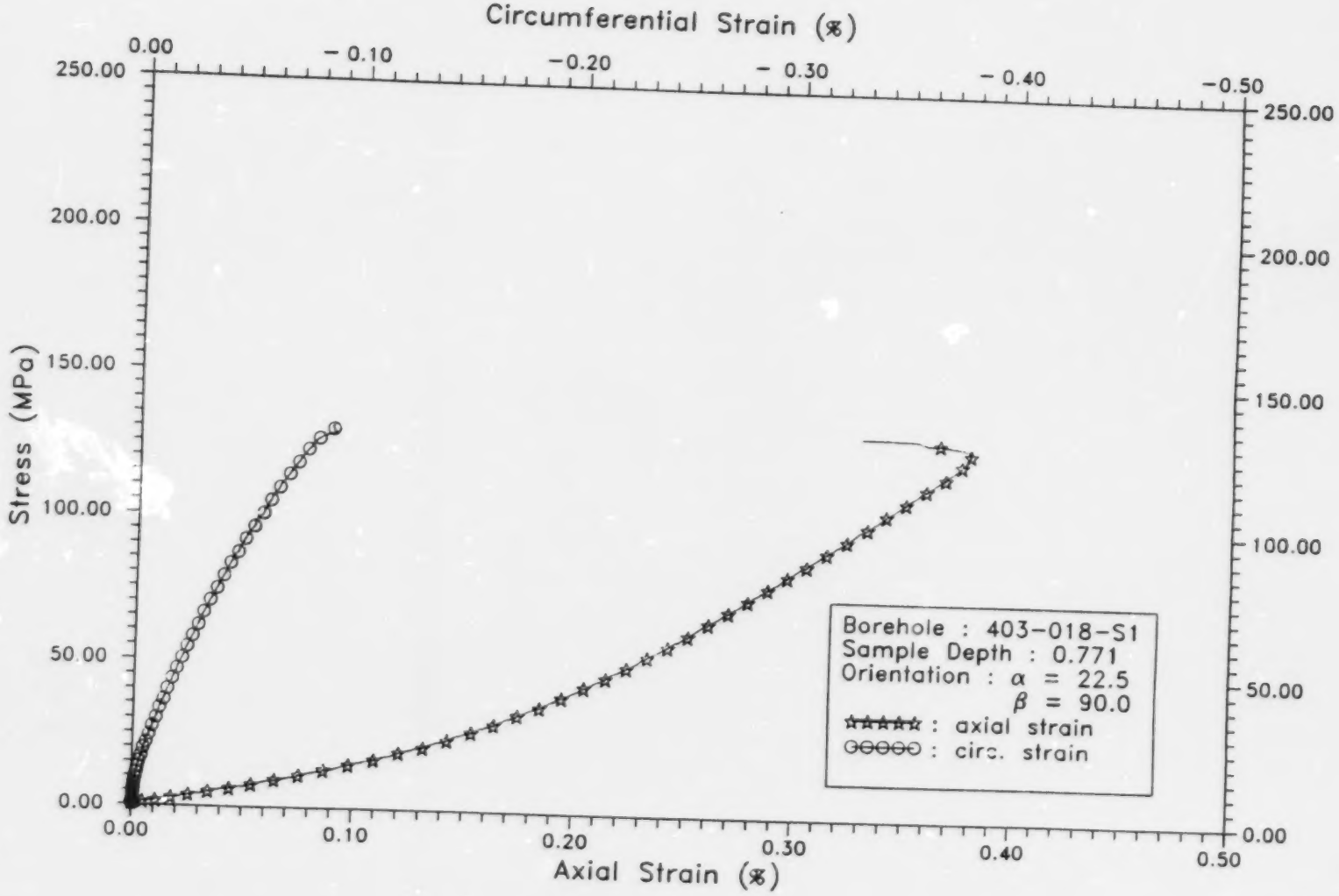

Fig. A13: Axial and Circumferential stress/strain curves for anisotropy test specimens

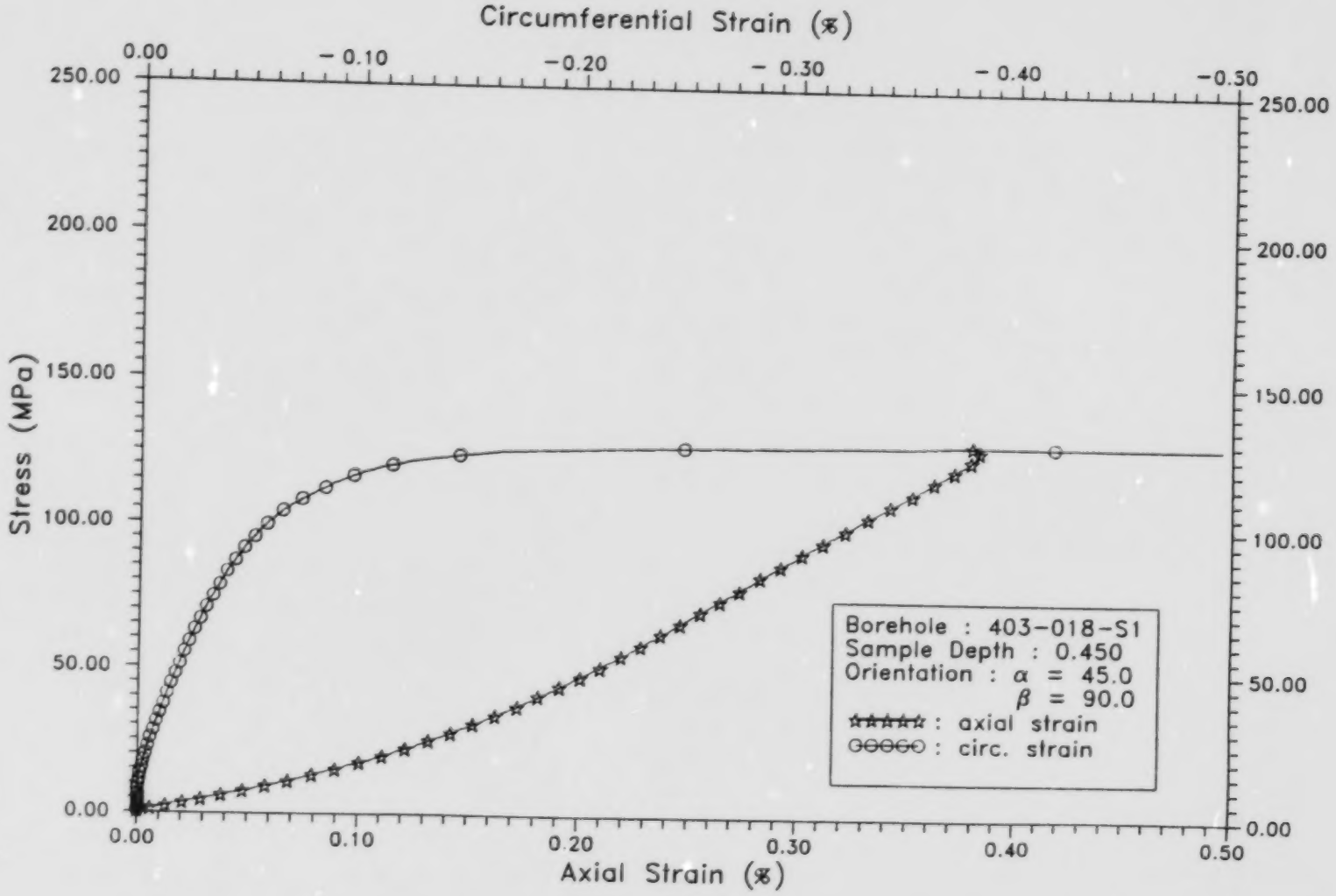

Fig. A14: Axial and Circumferential stress/strain curves for anisotropy test specimens

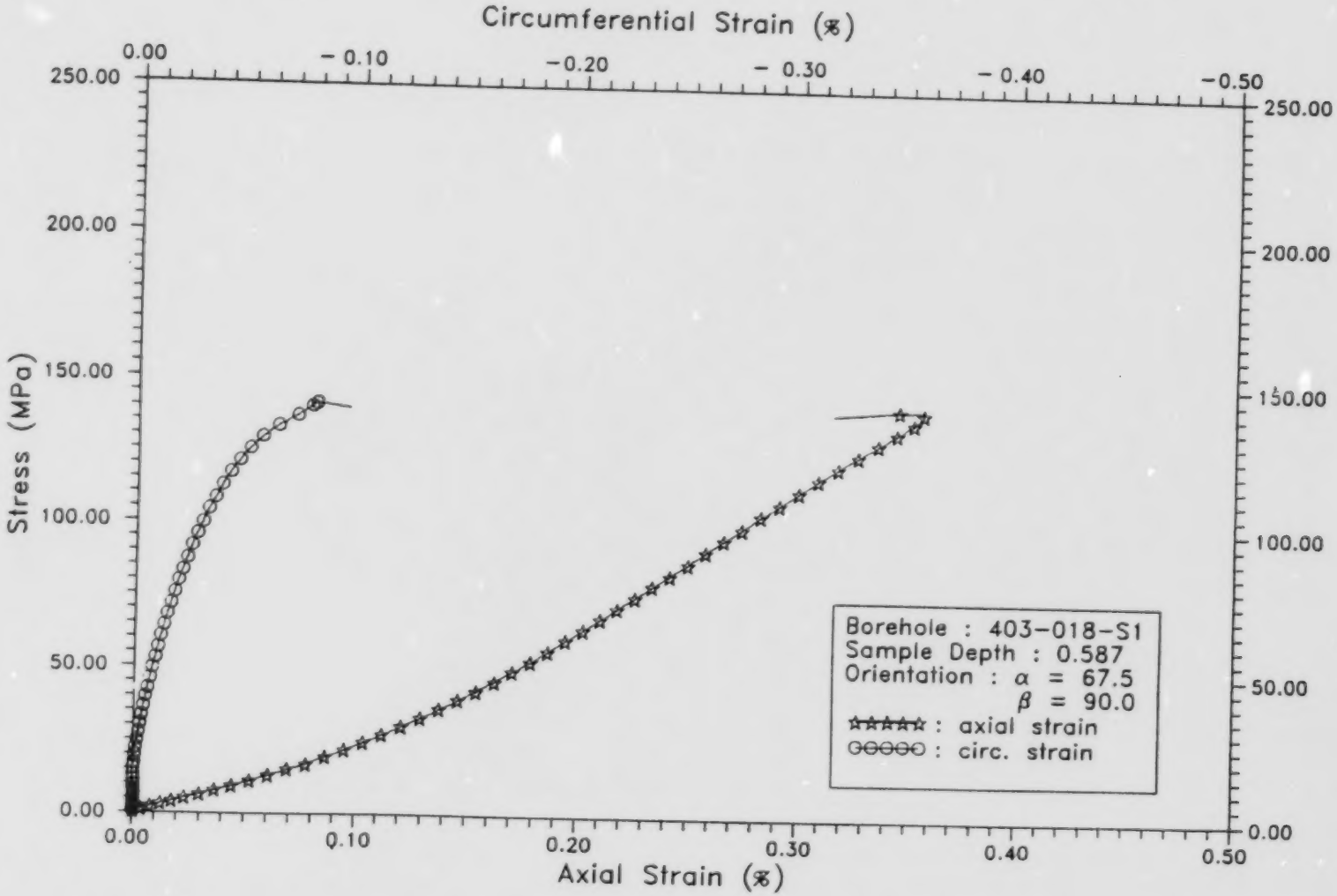

Fig. A15: Axial and Circumferential stress/strain curves for anisotropy test specimens

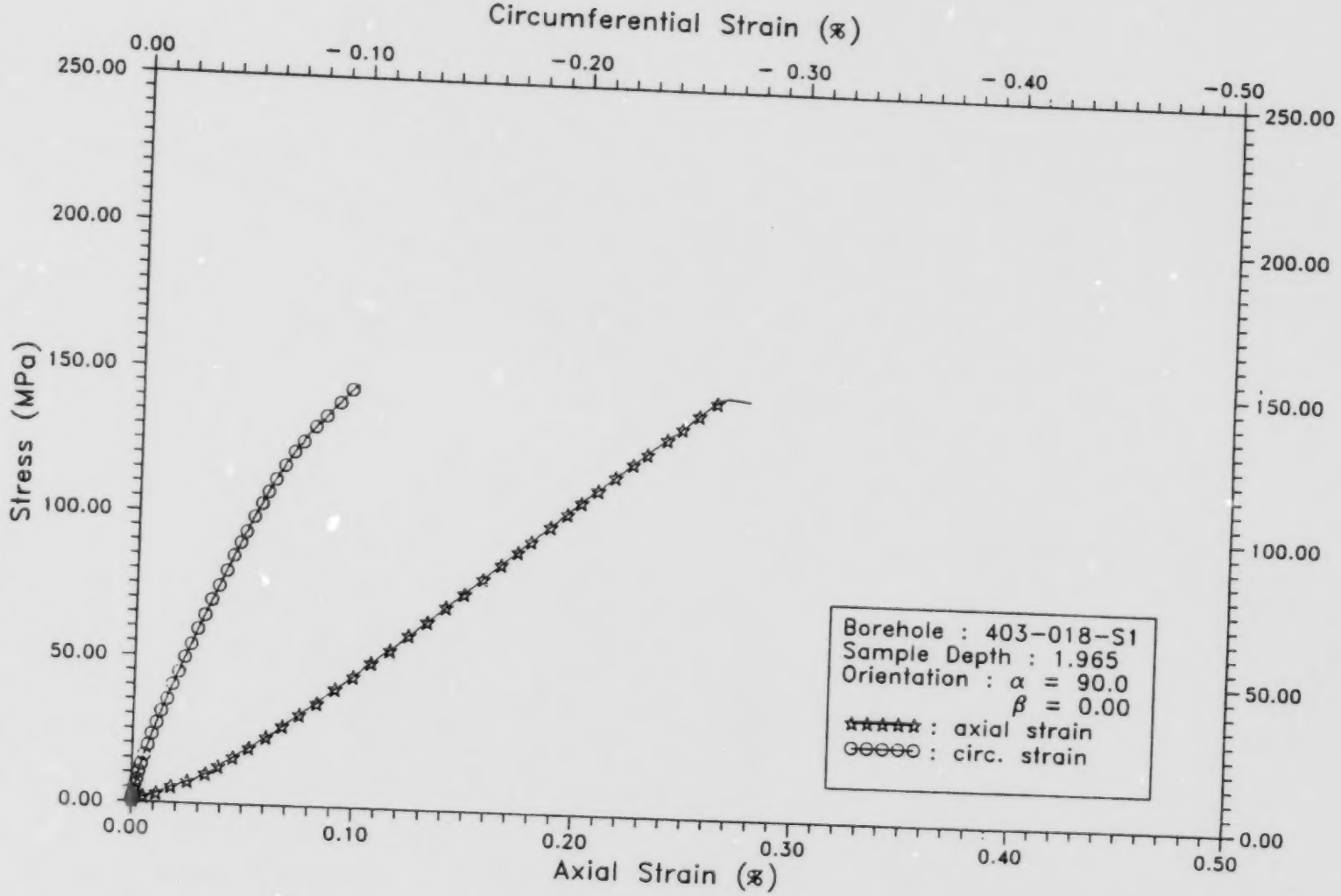

Fig. A16: Axial and Circumferential stress/strain curves for anisotropy test specimens

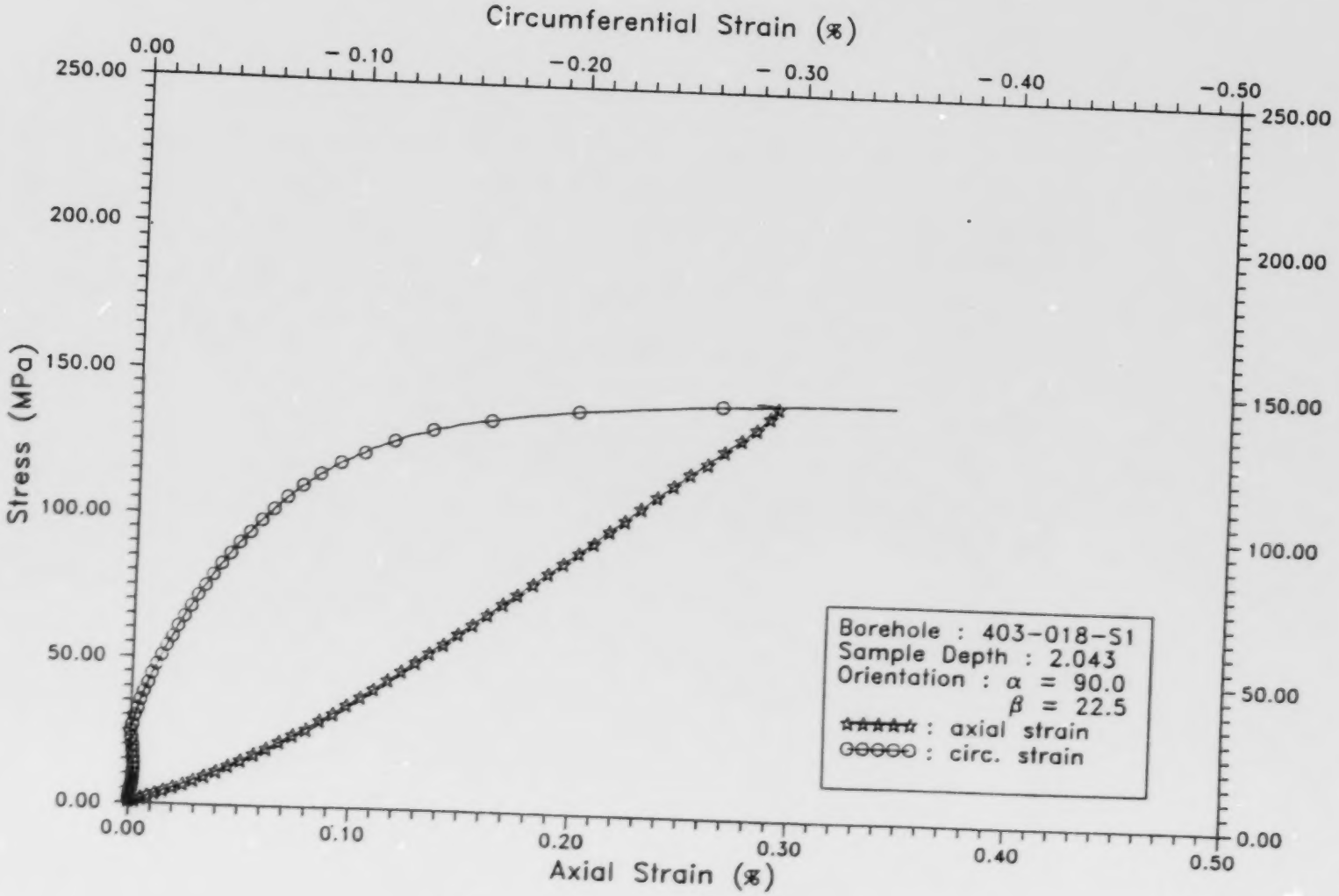

Fig. A17: Axial and Circumferential stress/strain curves for anisotropy test specimens

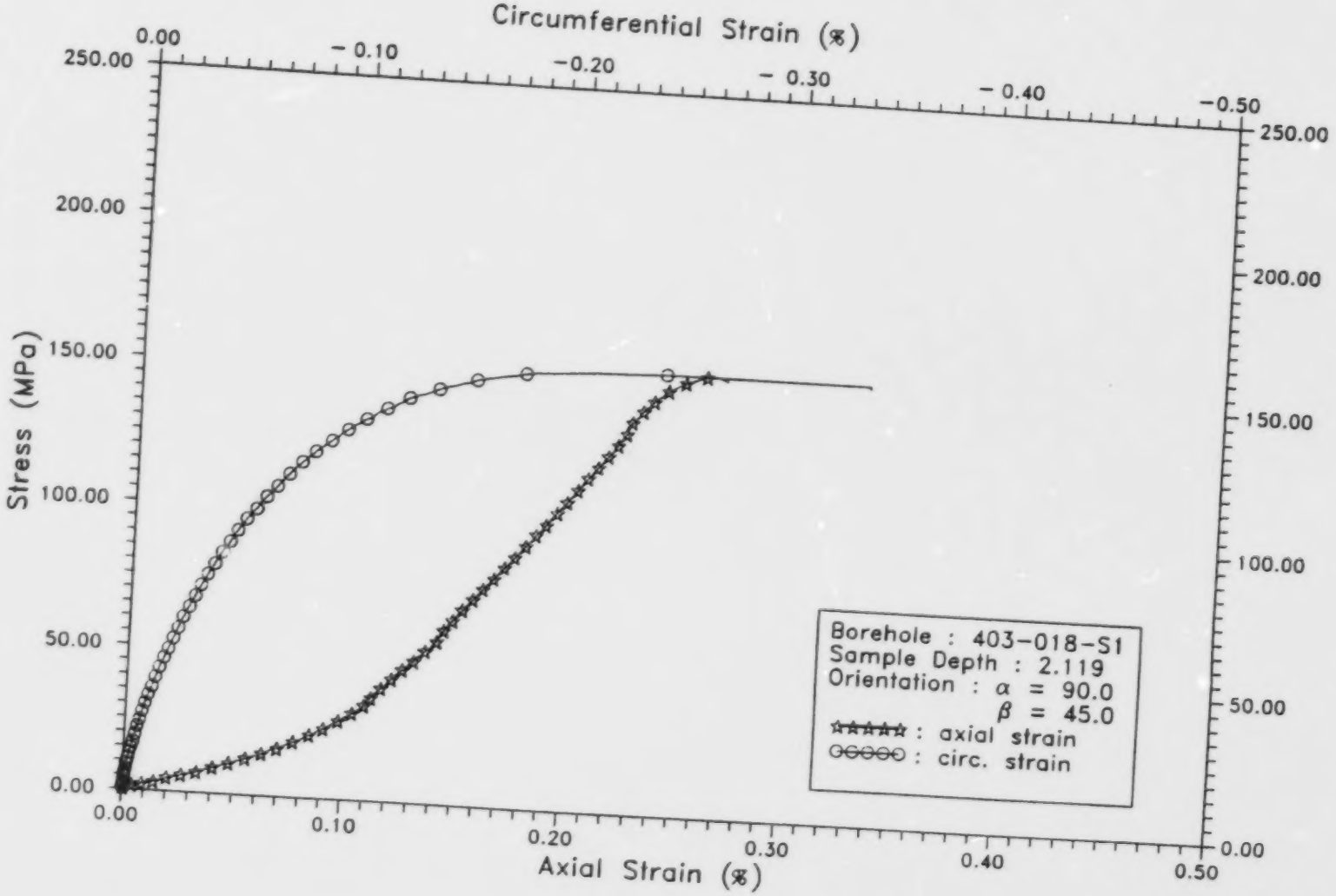

Fig. A18: Axial and Circumferential stress/strain curves for anisotropy test specimens

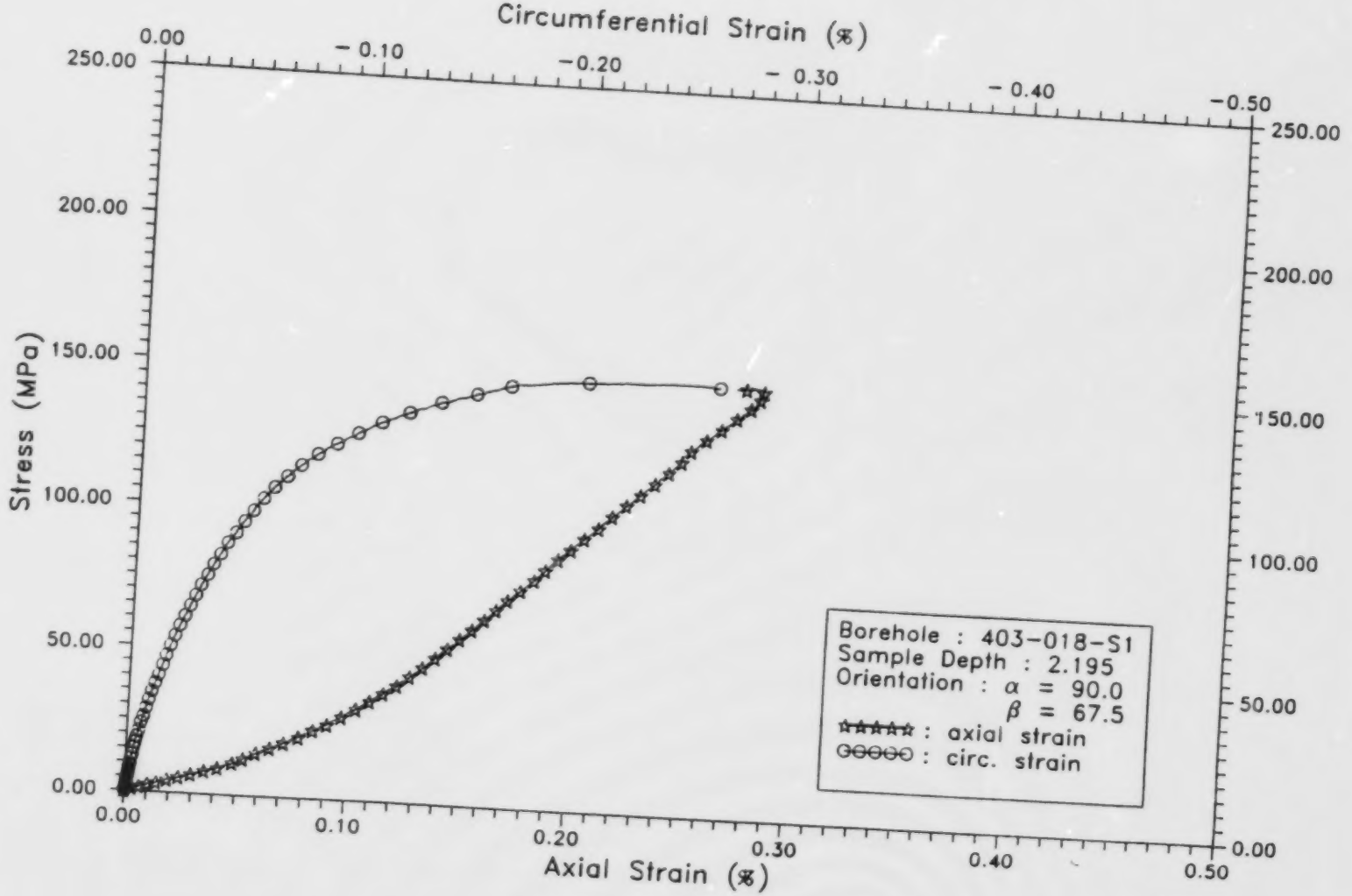

Fig. A19: Axial and Circumferential stress/strain curves for anisotropy test specimens

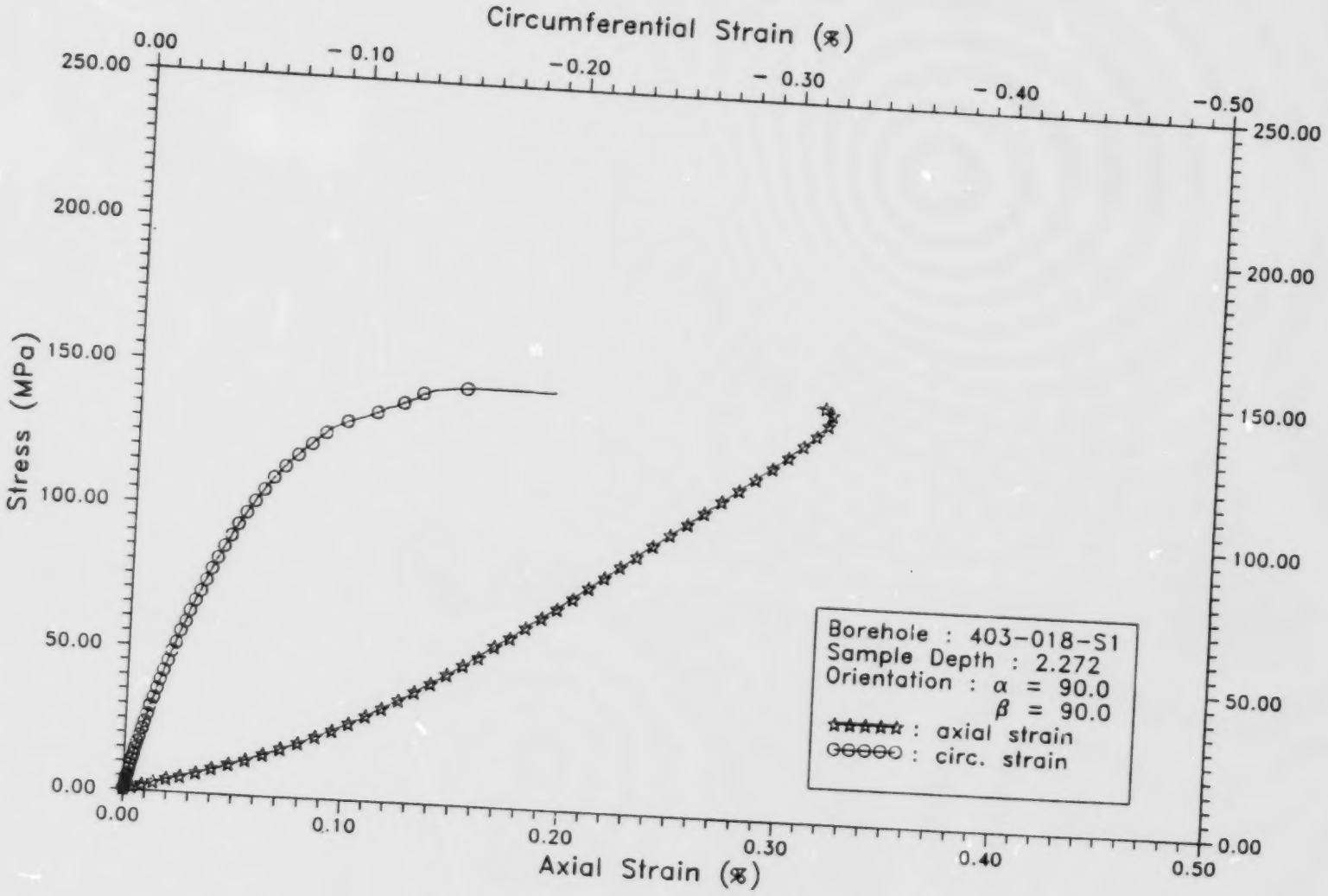

Fig. A20: Axial and Circumferential stress/strain curves for anisotropy test specimens

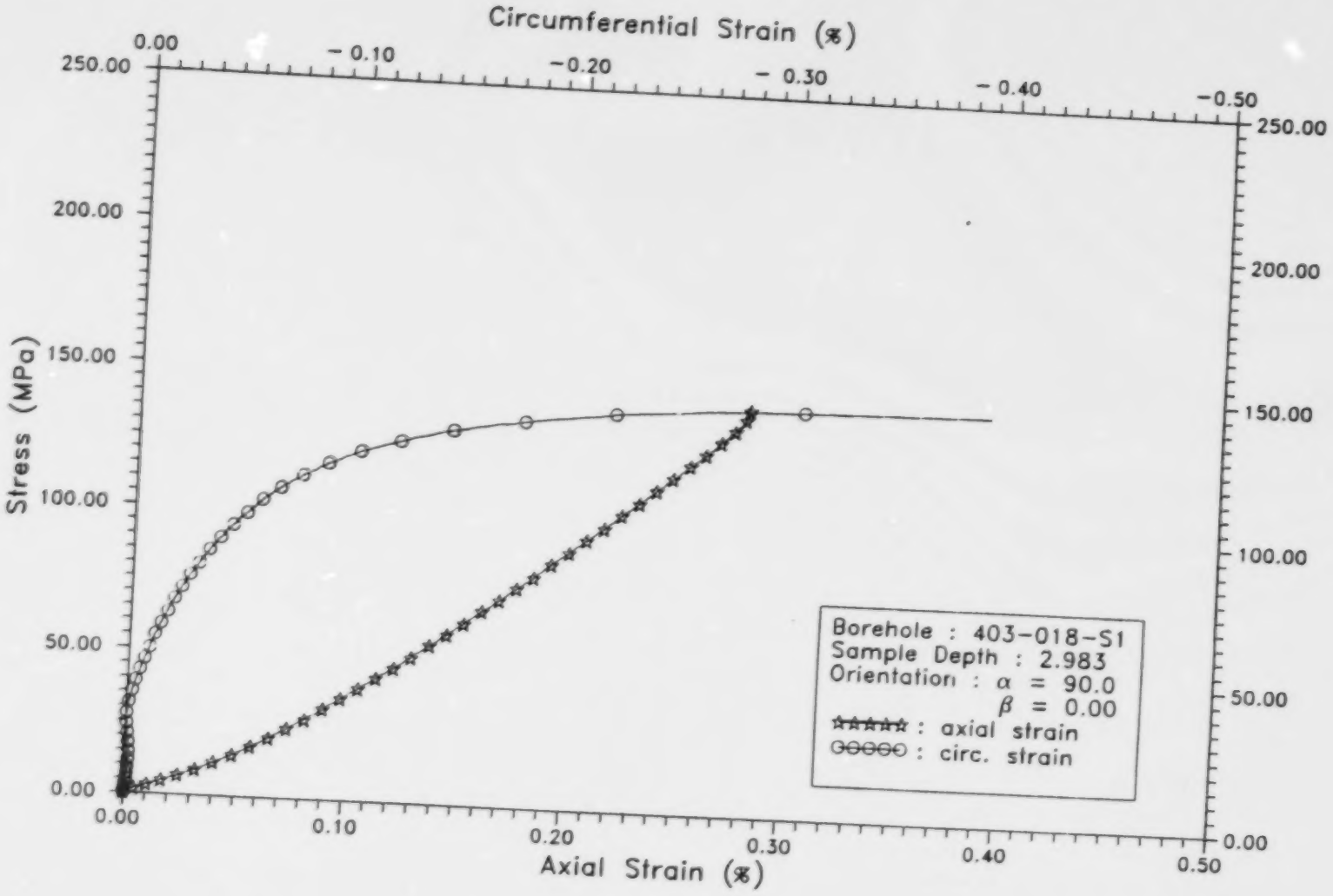

Fig. A21: Axial and Circumferential stress/strain curves for anisotropy test specimens

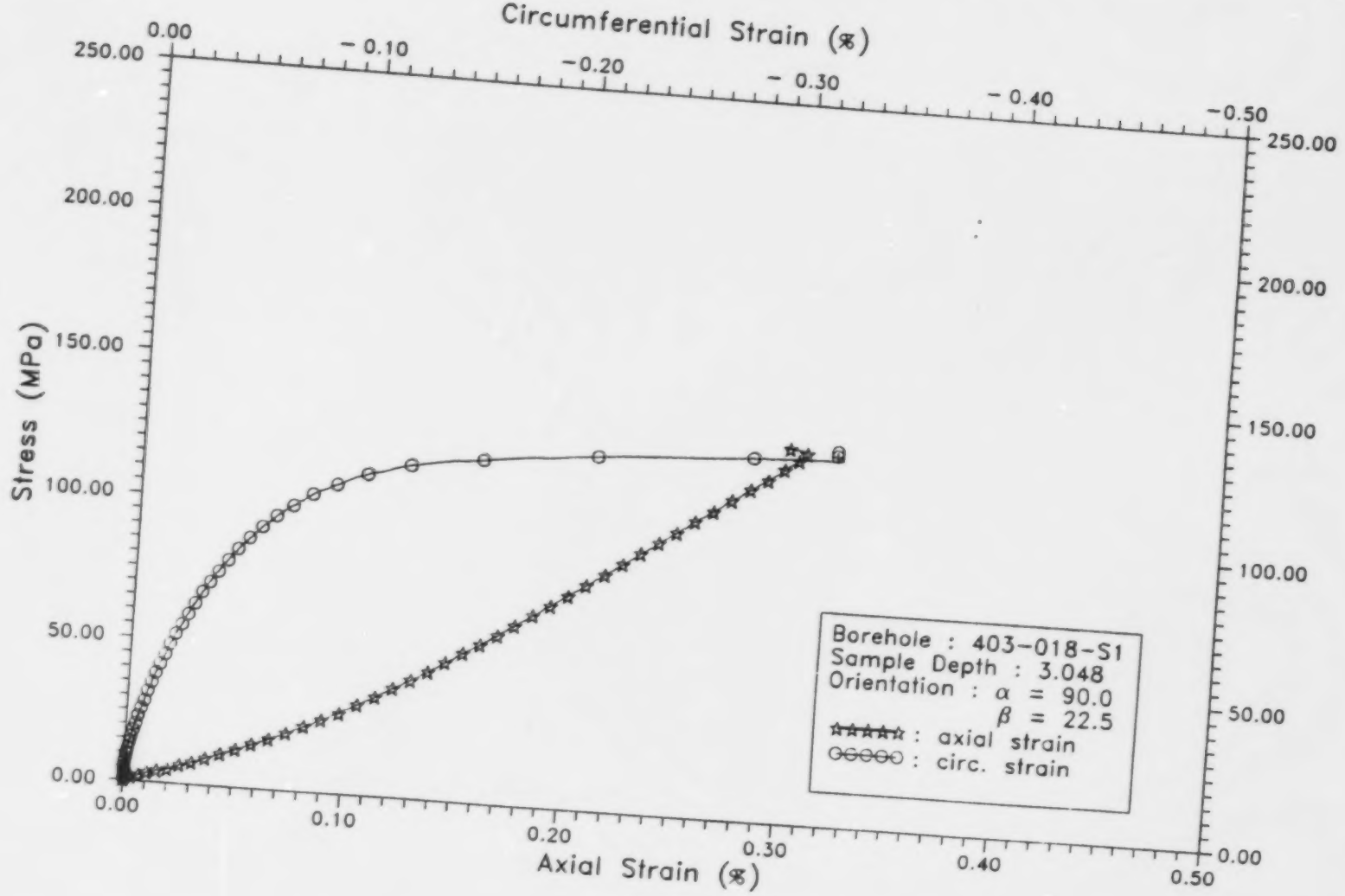

Fig. A22: Axial and Circumferential stress/strain curves for anisotropy test specimens

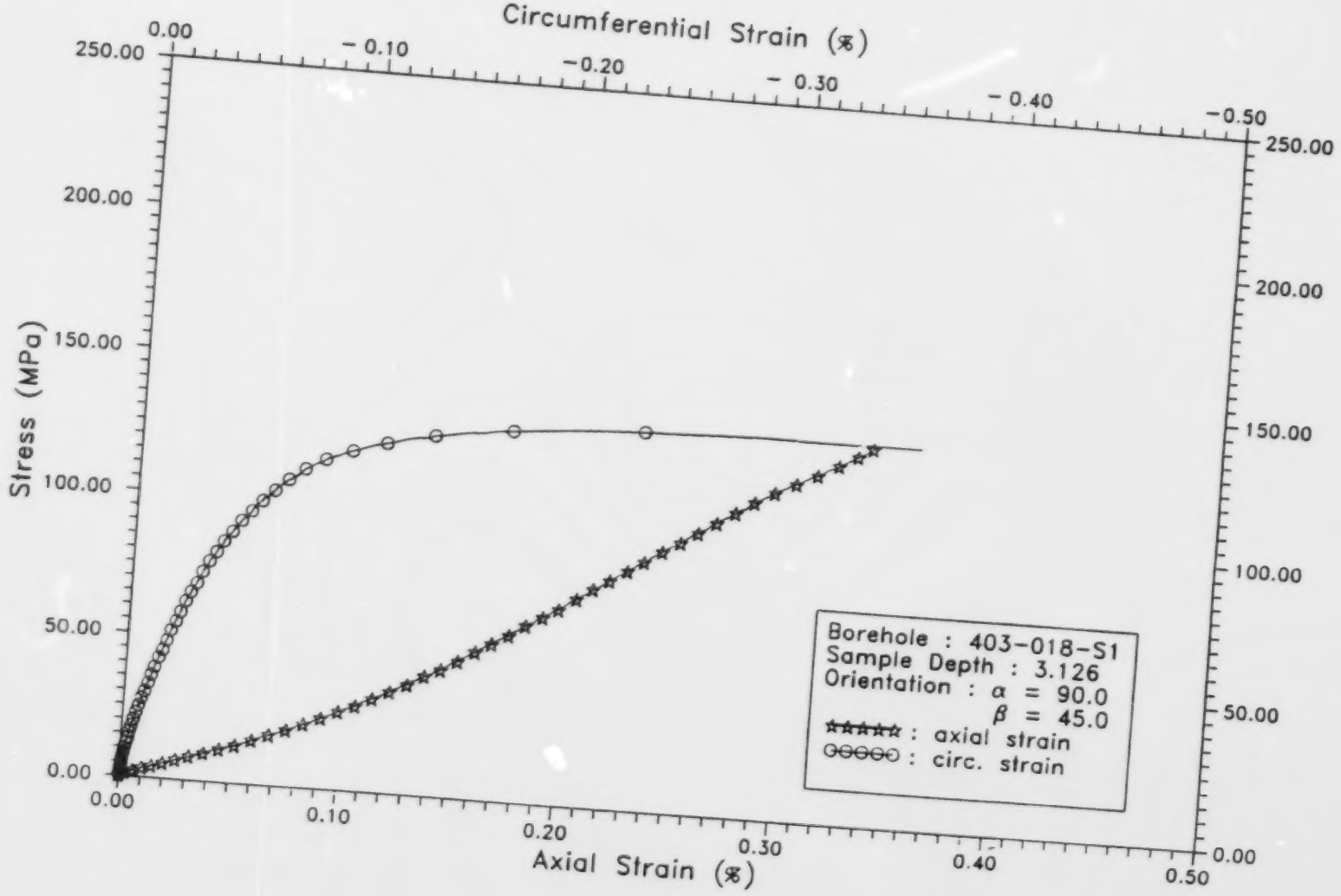

Fig. A23: Axial and Circumferential stress/strain curves for anisotropy test specimens

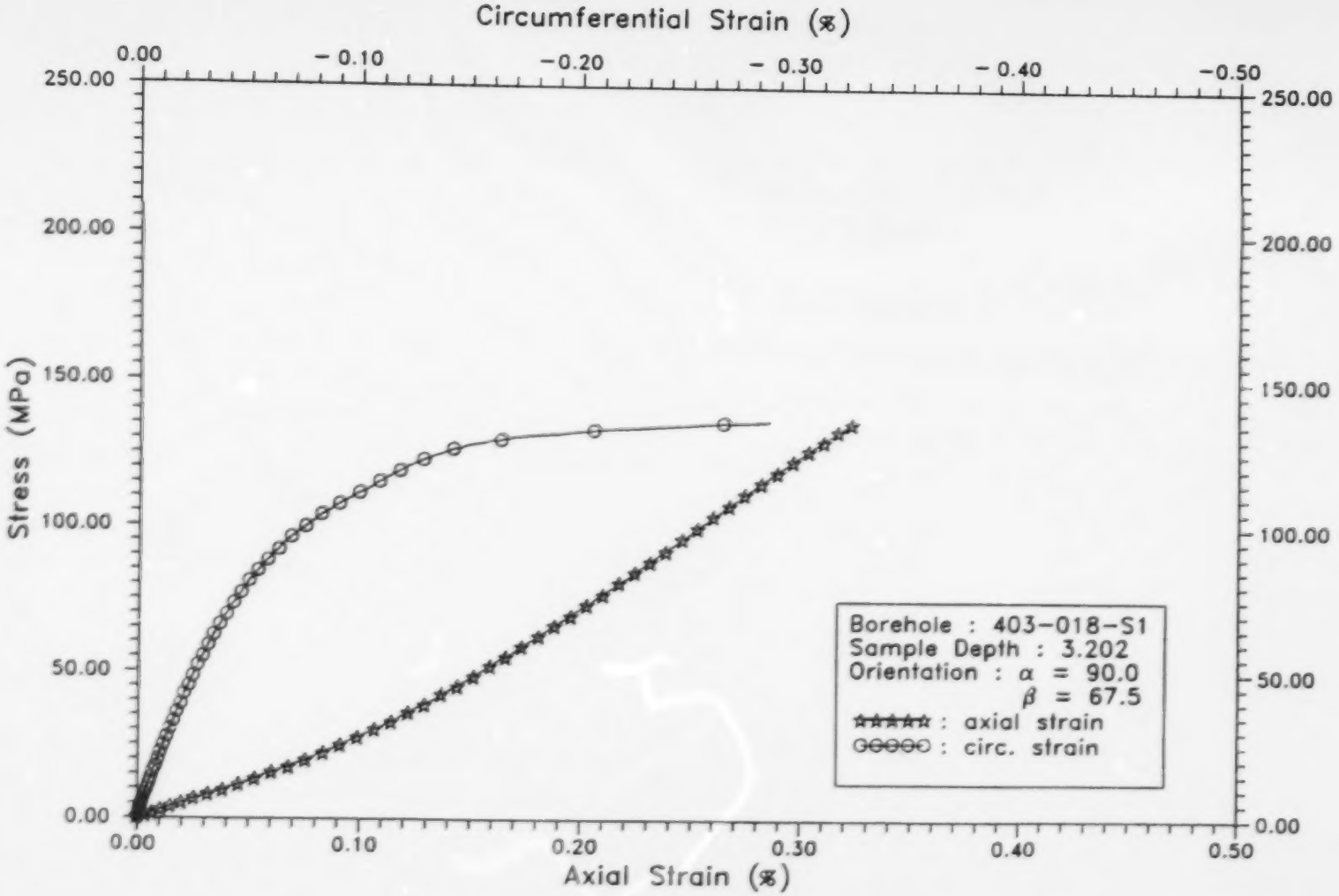

Fig. A24: Axial and Circumferential stress/strain curves for anisotropy test specimens

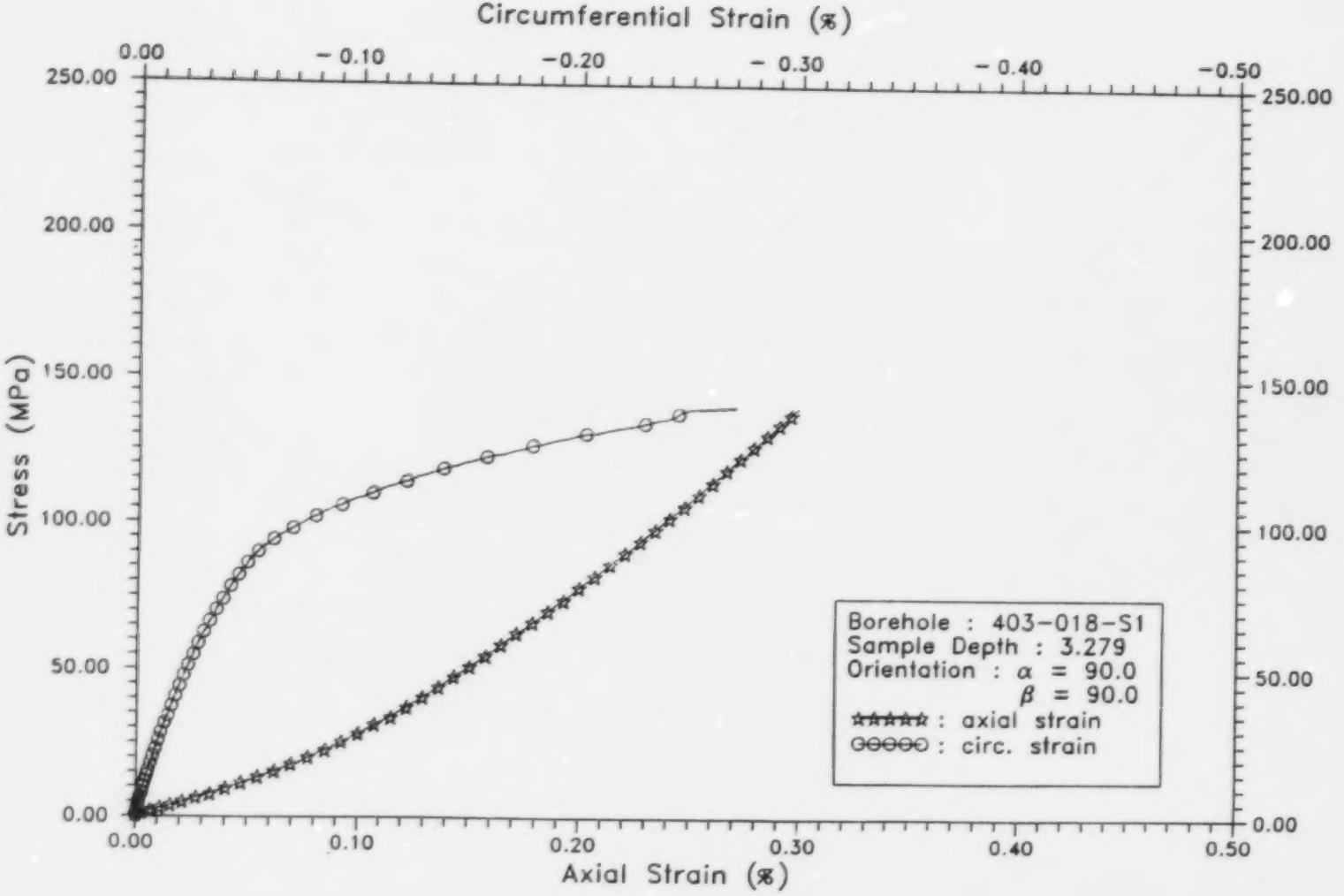

Fig. A25: Axial and Circumferential stress/strain curves for anisotropy test specimens

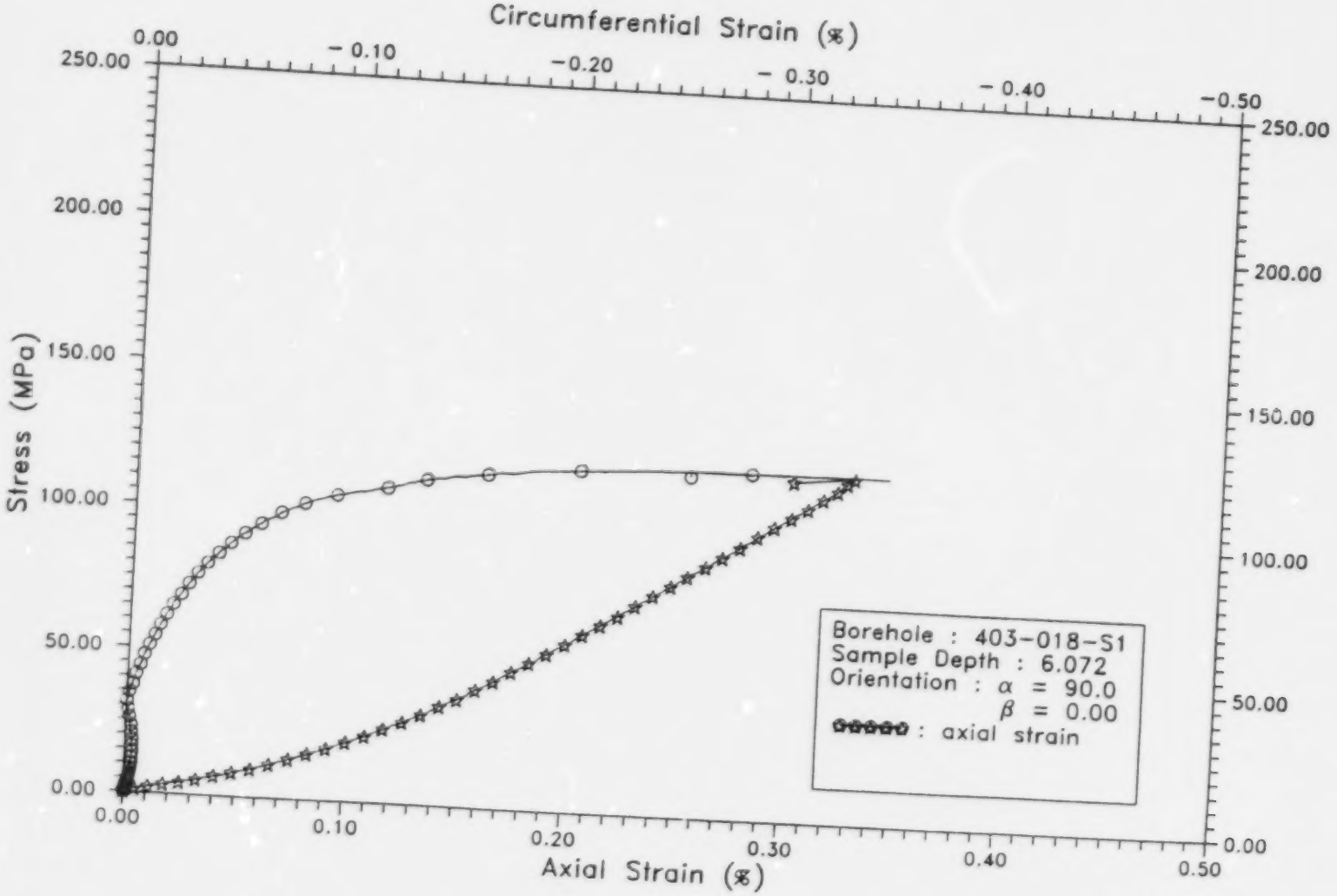

Fig. A26: Axial and Circumferential stress/strain curves for anisotropy test specimens

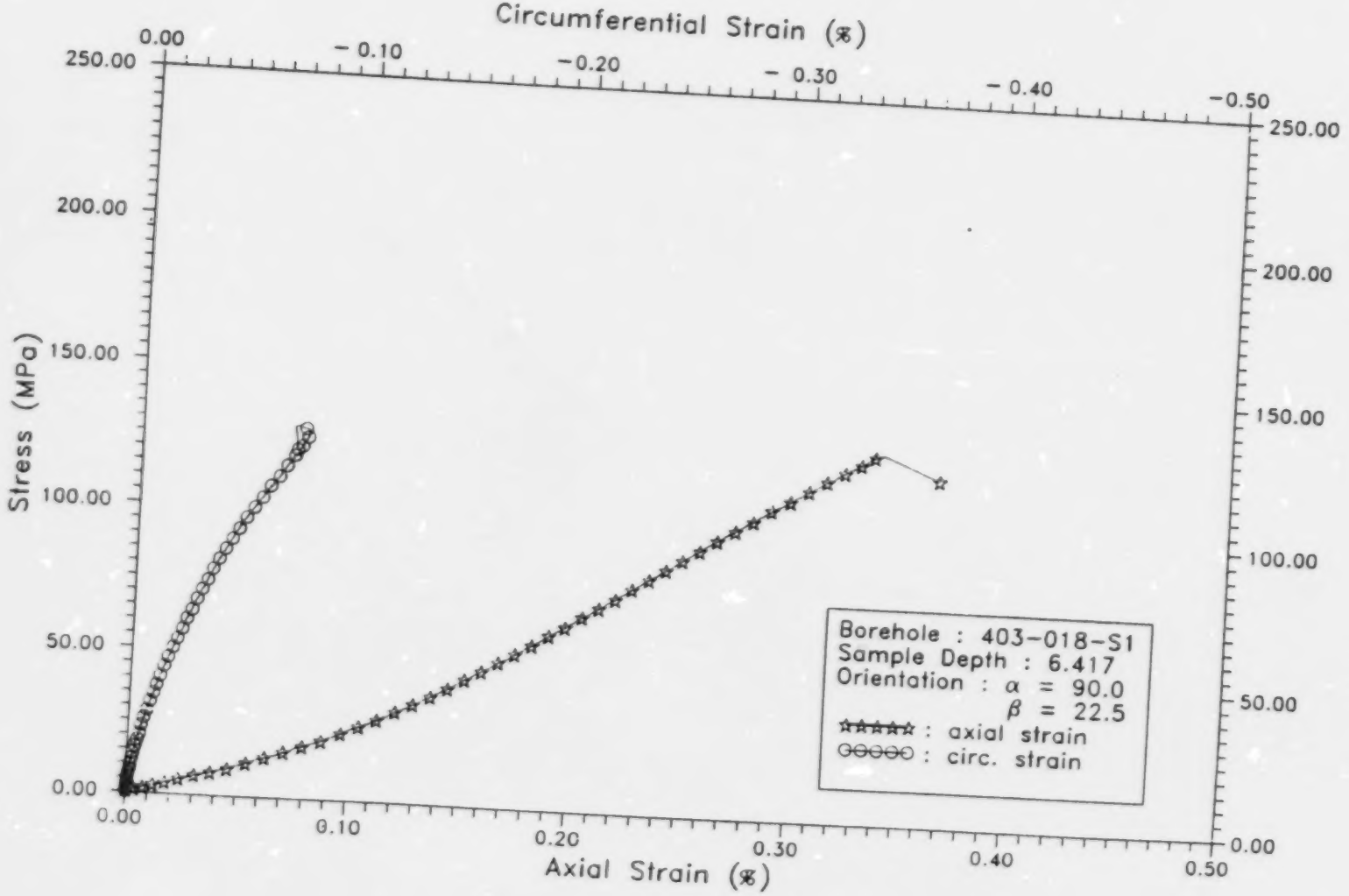

Fig. A27: Axial and Circumferential stress/strain curves for anisotropy test specimens

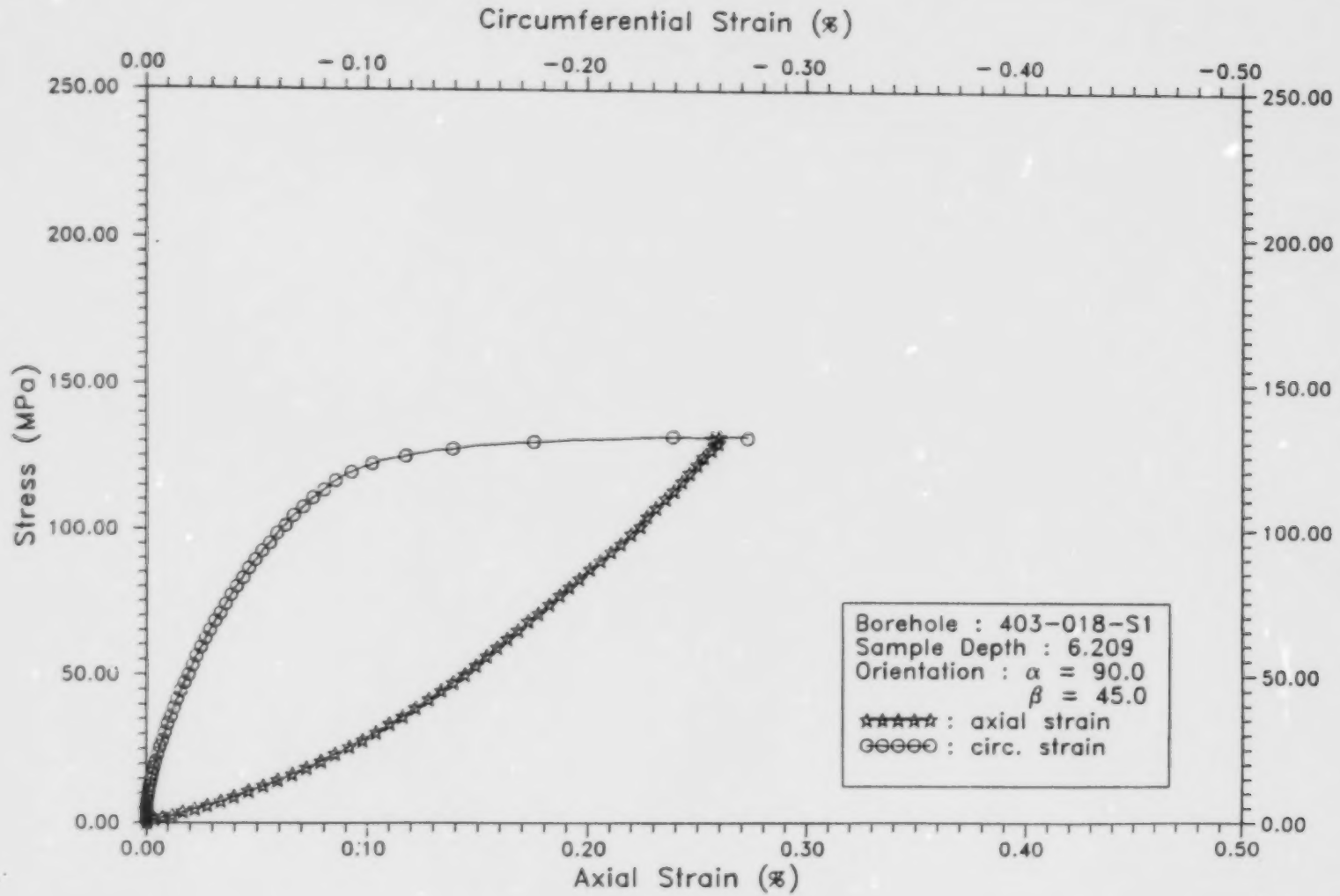

Fig. A28: Axial and Circumferential stress/strain curves for anisotropy test specimens

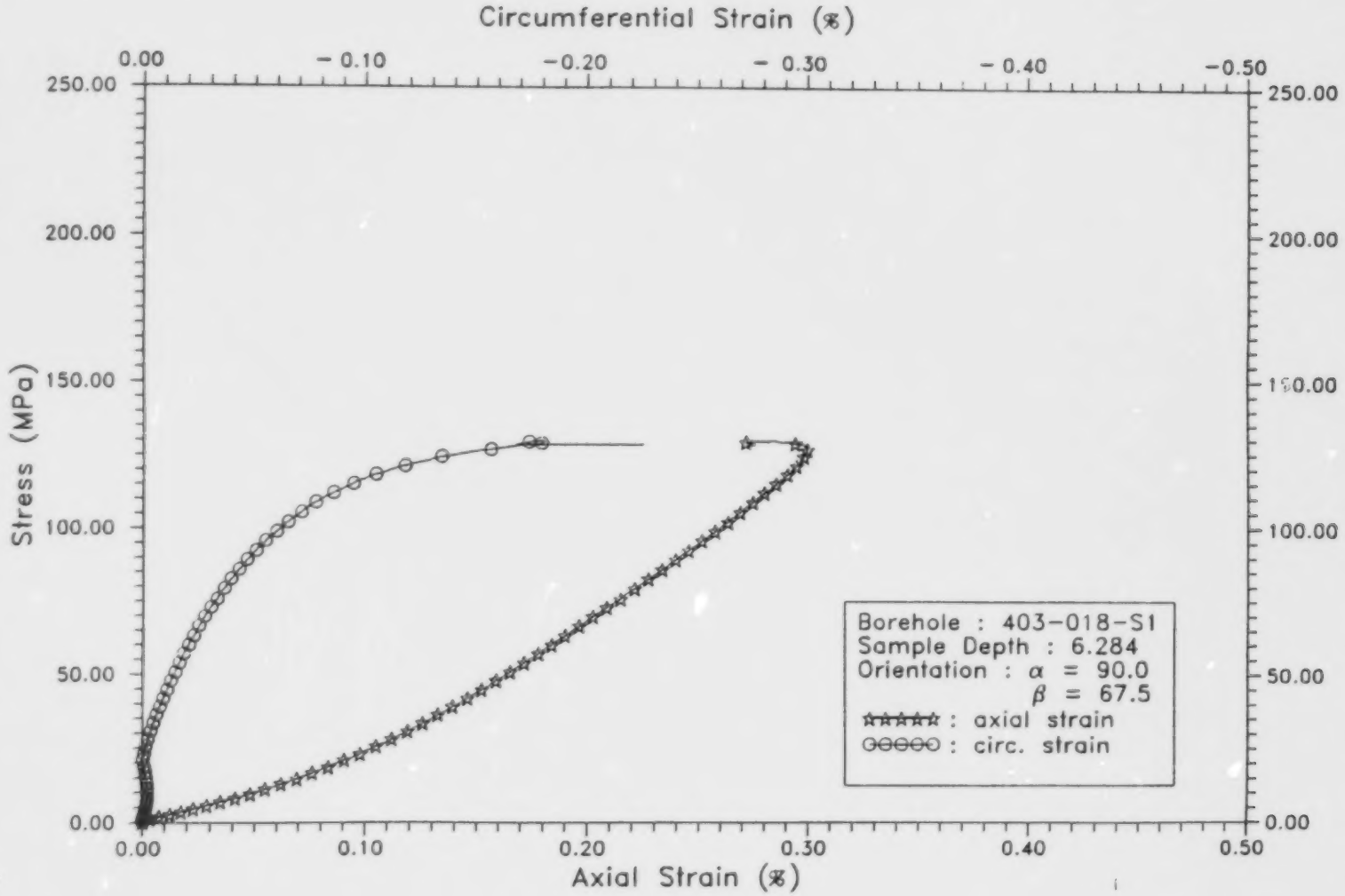

Fig. A29: Axial and Circumferential stress/strain curves for anisotropy test specimens

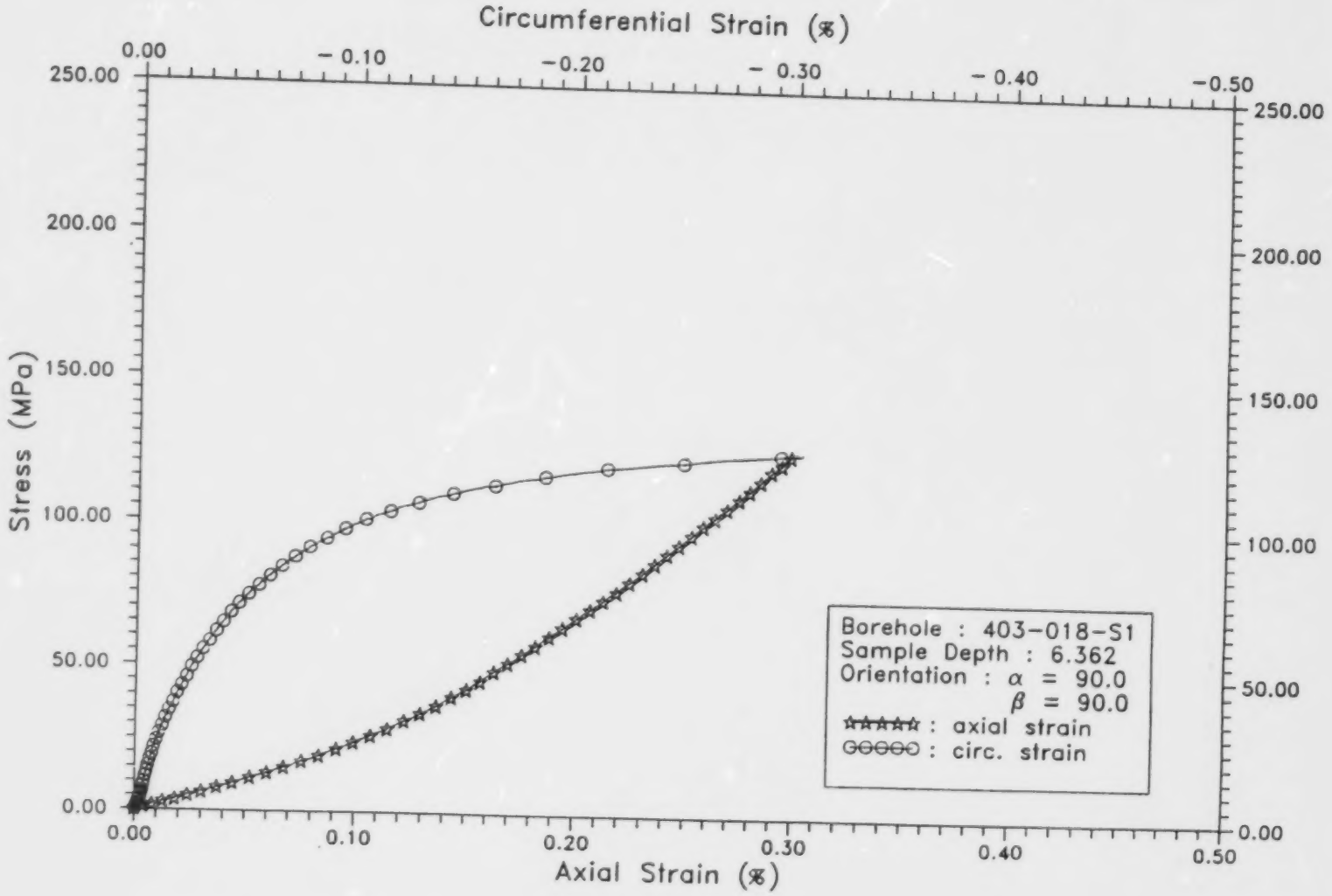

Fig. A30: Axial and Circumferential stress/strain curves for anisotropy test specimens

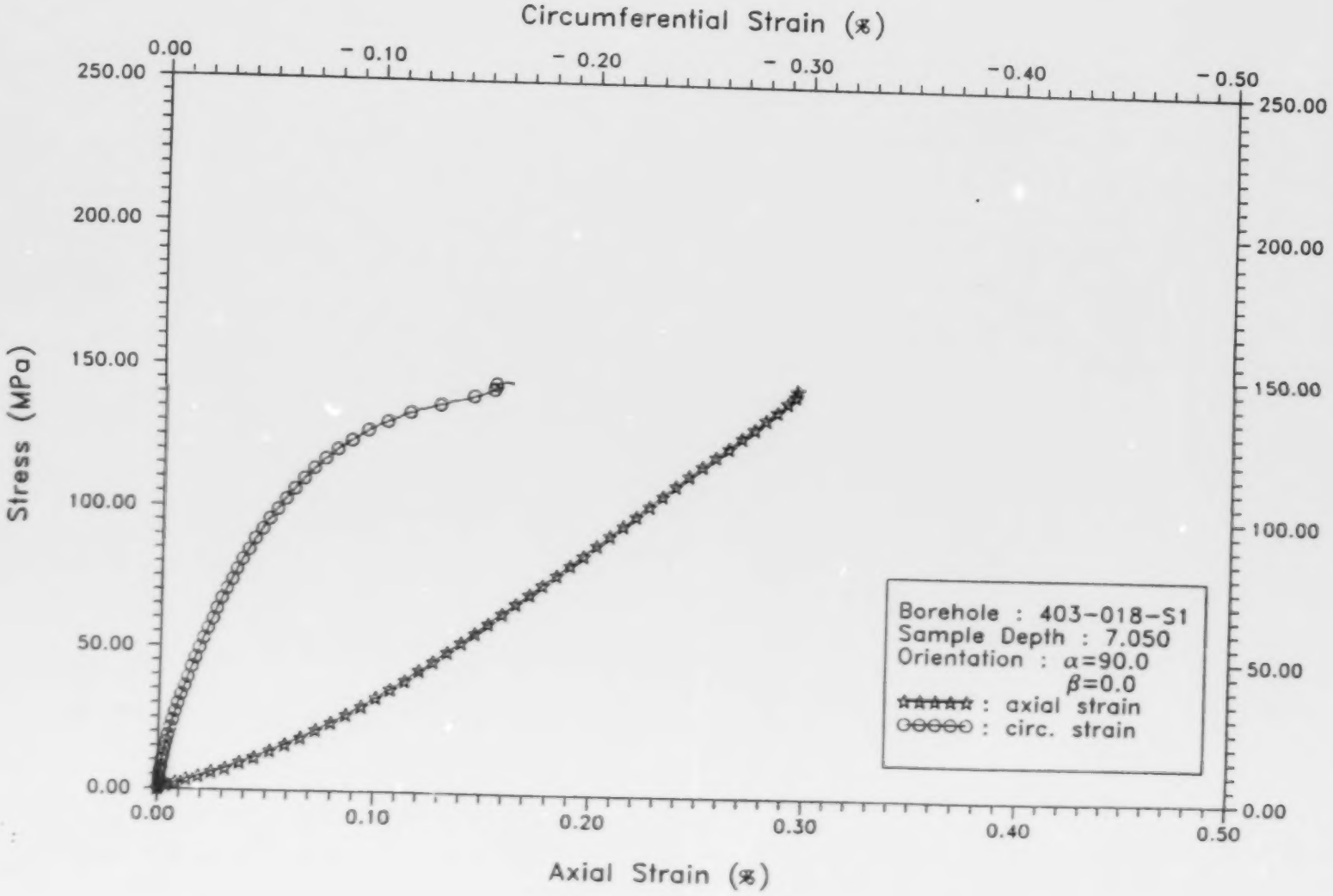

Fig. A31: Axial and circumferential stress/strain curves for anisotropy test specimens

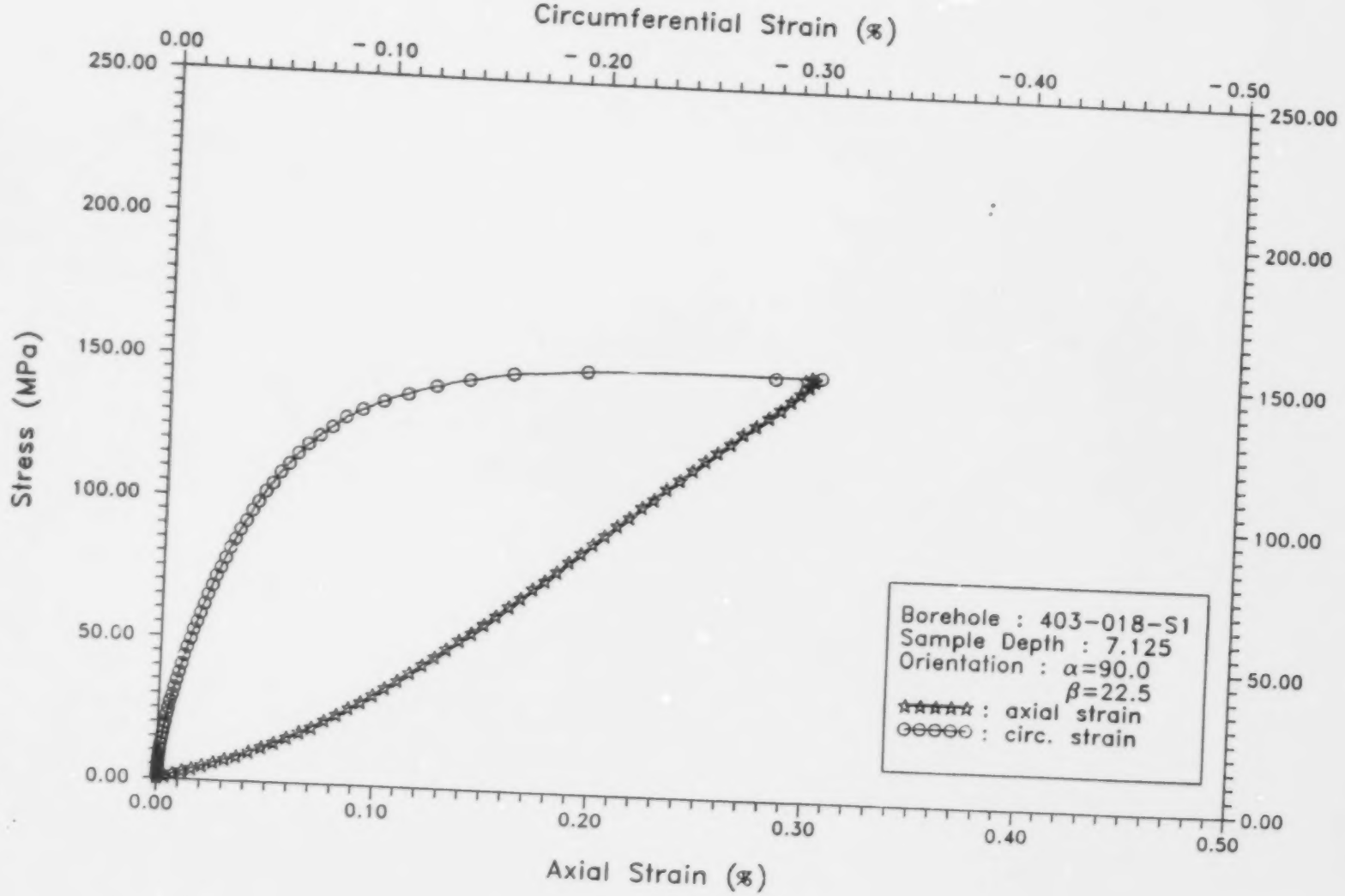

Fig. A32: Axial and circumferential stress/strain curves for anisotropy test specimens

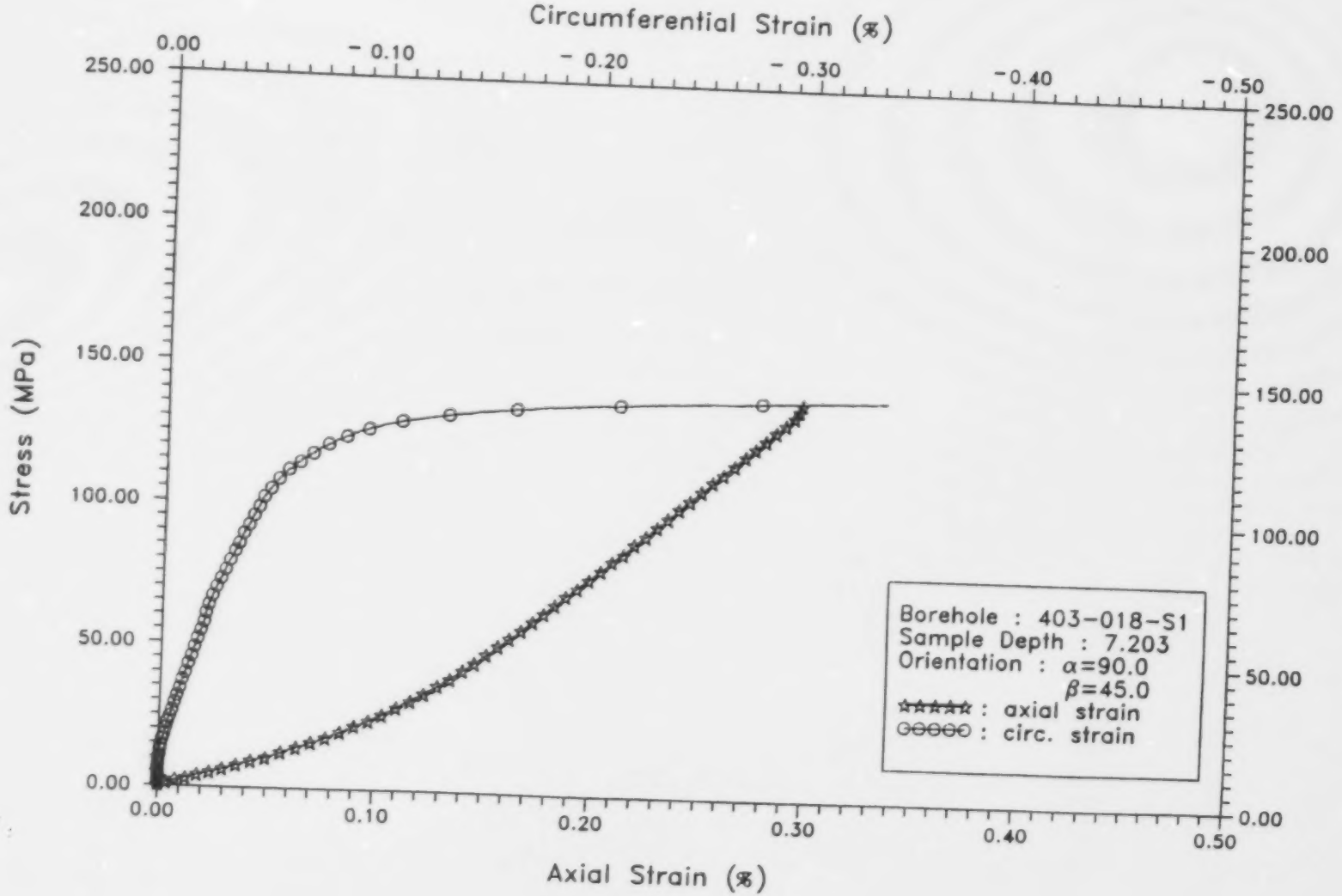

Fig. A33: Axial and circumferential stress/strain curves for anisotropy test specimens

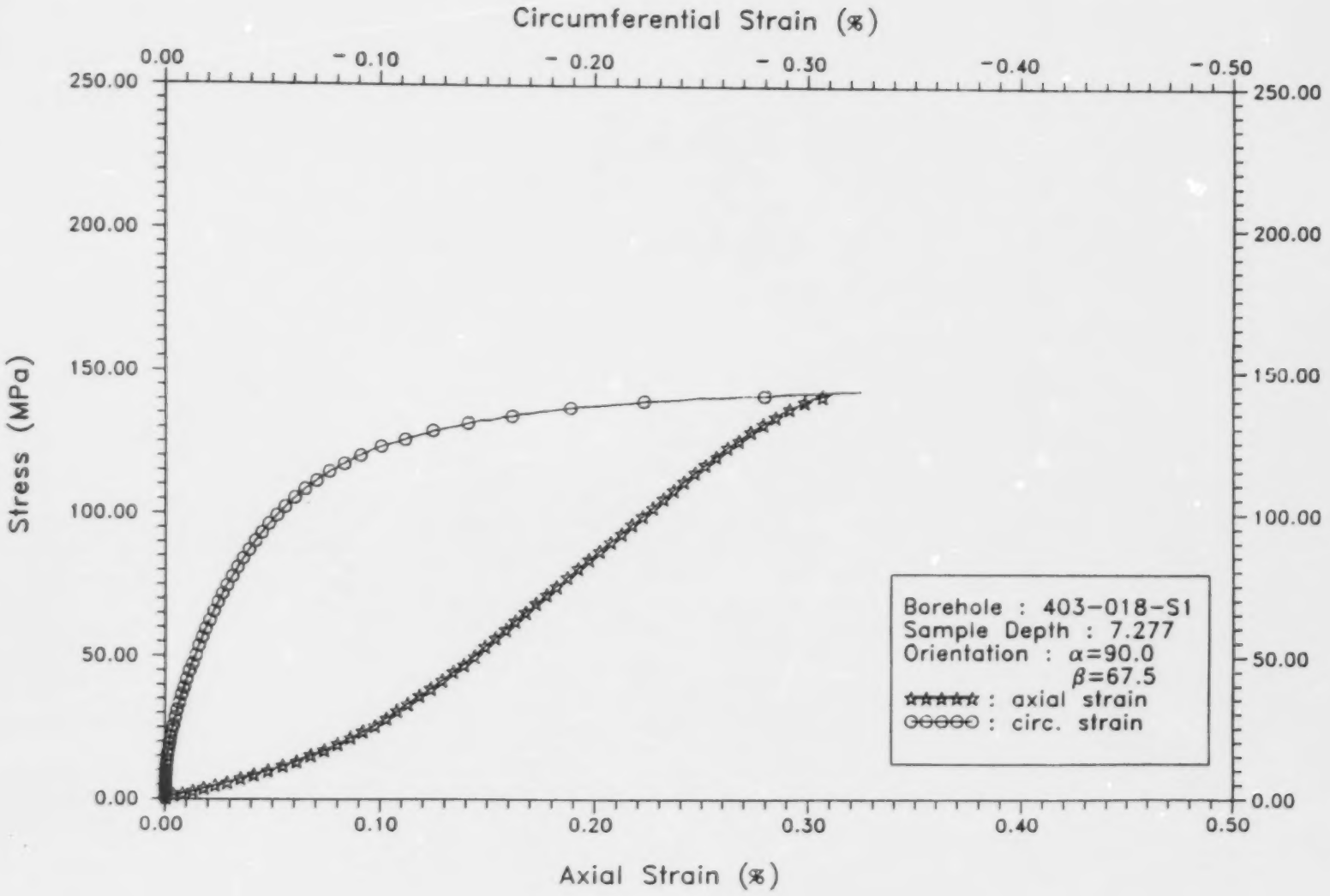

Fig. A34: Axial and circumferential stress/strain curves for anisotropy test specimens

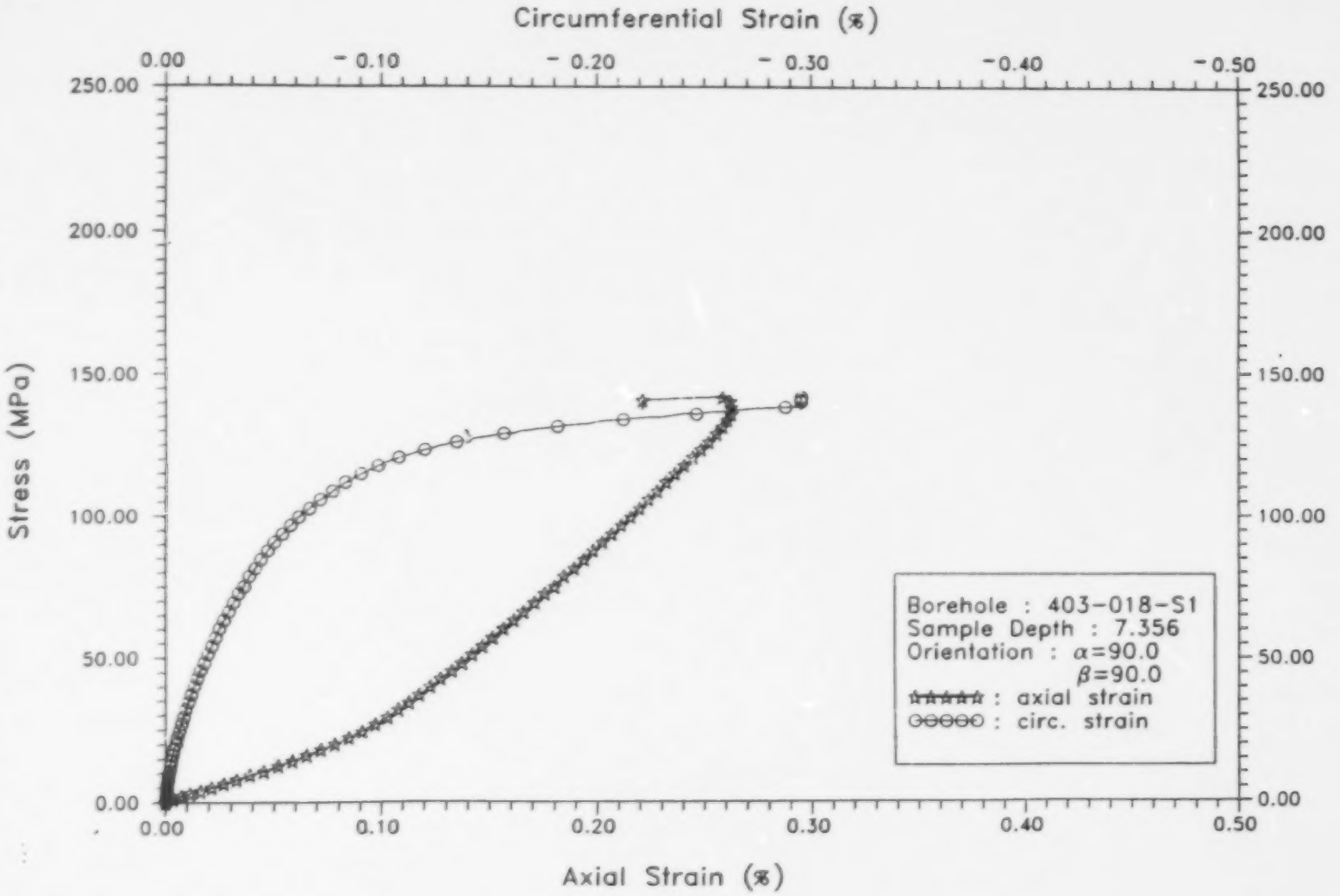

Fig. A35: Axial and circumferential stress/strain curves for anisotropy test specimens

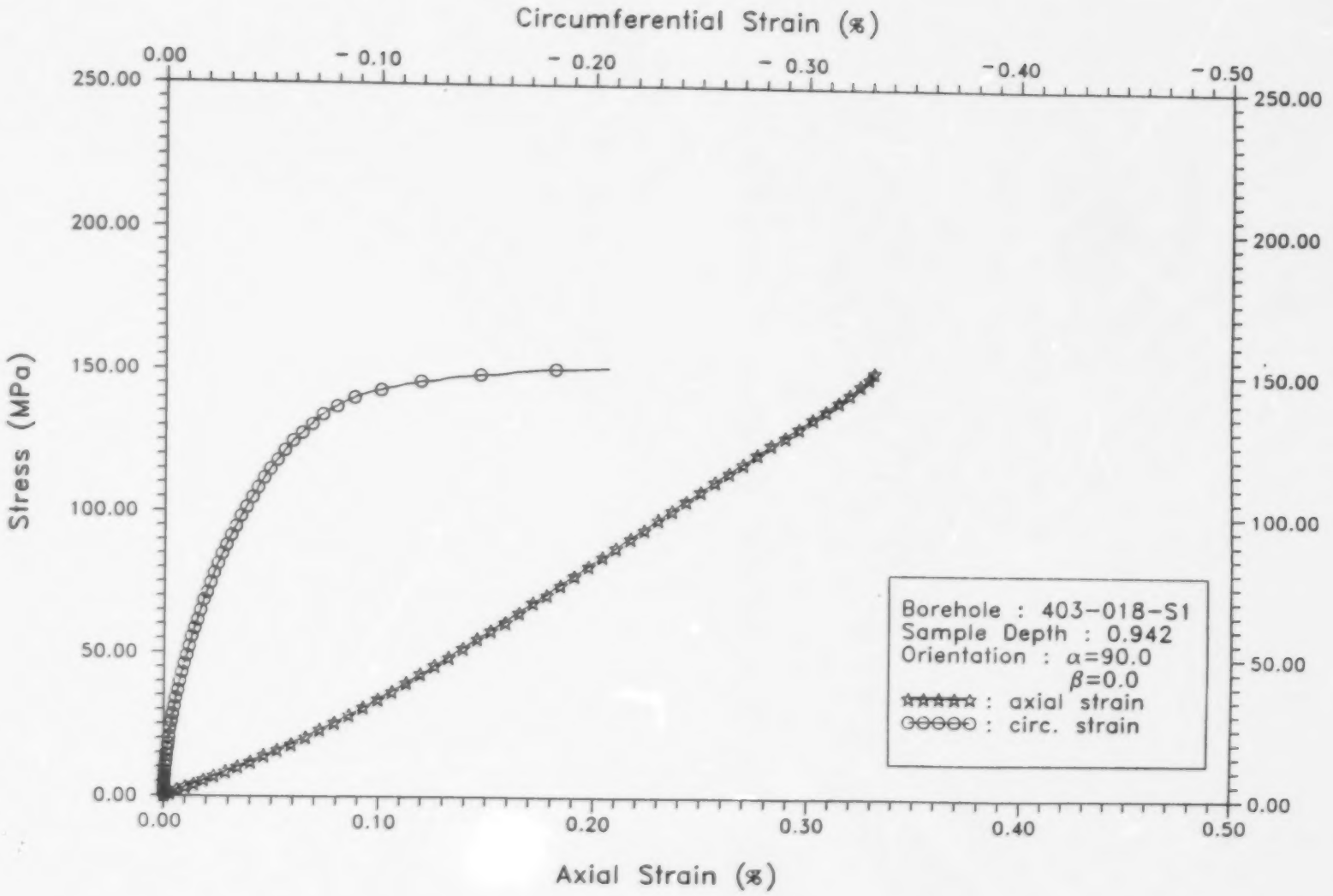

Fig. A36: Axial and circumferential stress/strain curves for anisotropy test specimens

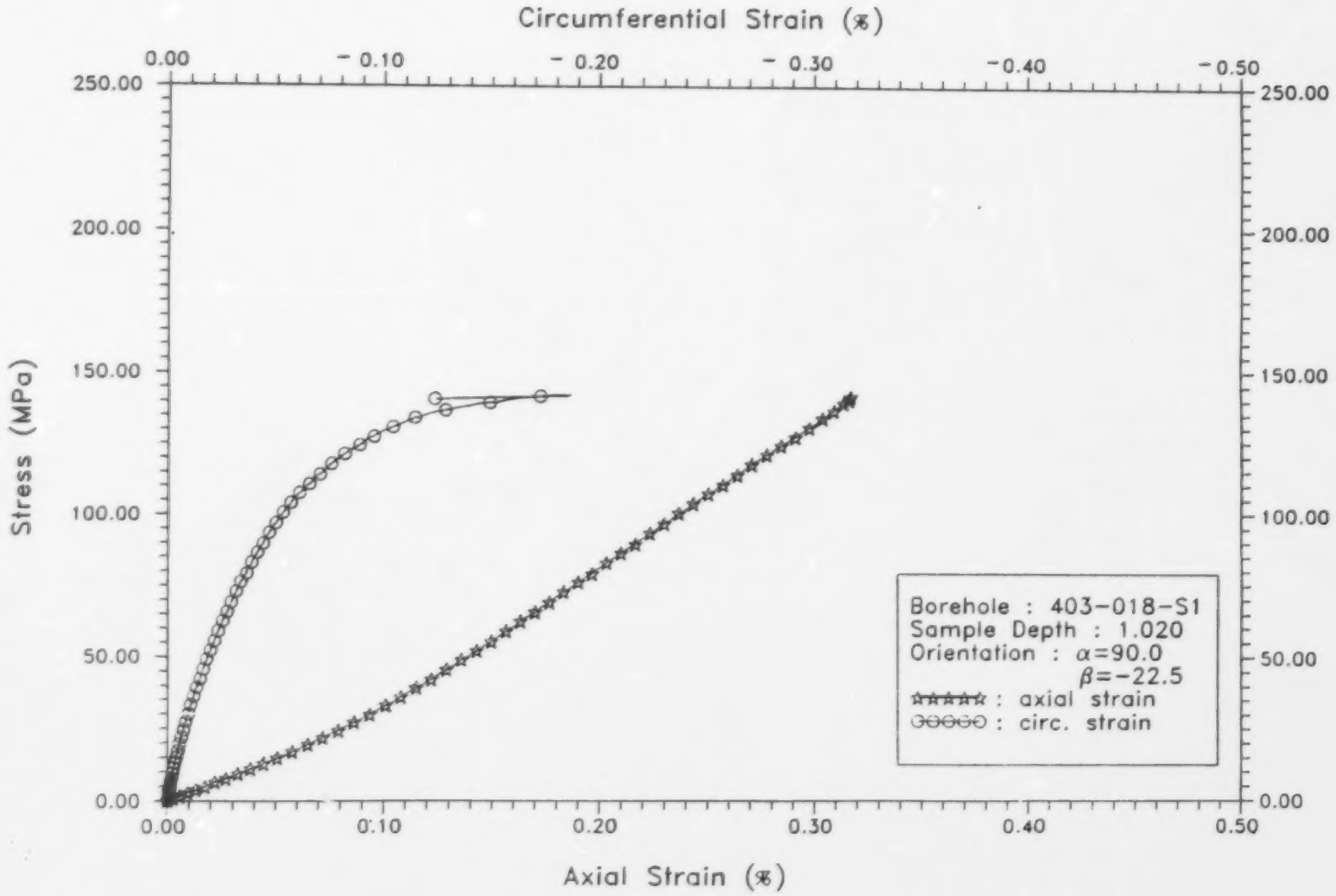

Fig. A37: Axial and circumferential stress/strain curves for anisotropy test specimens

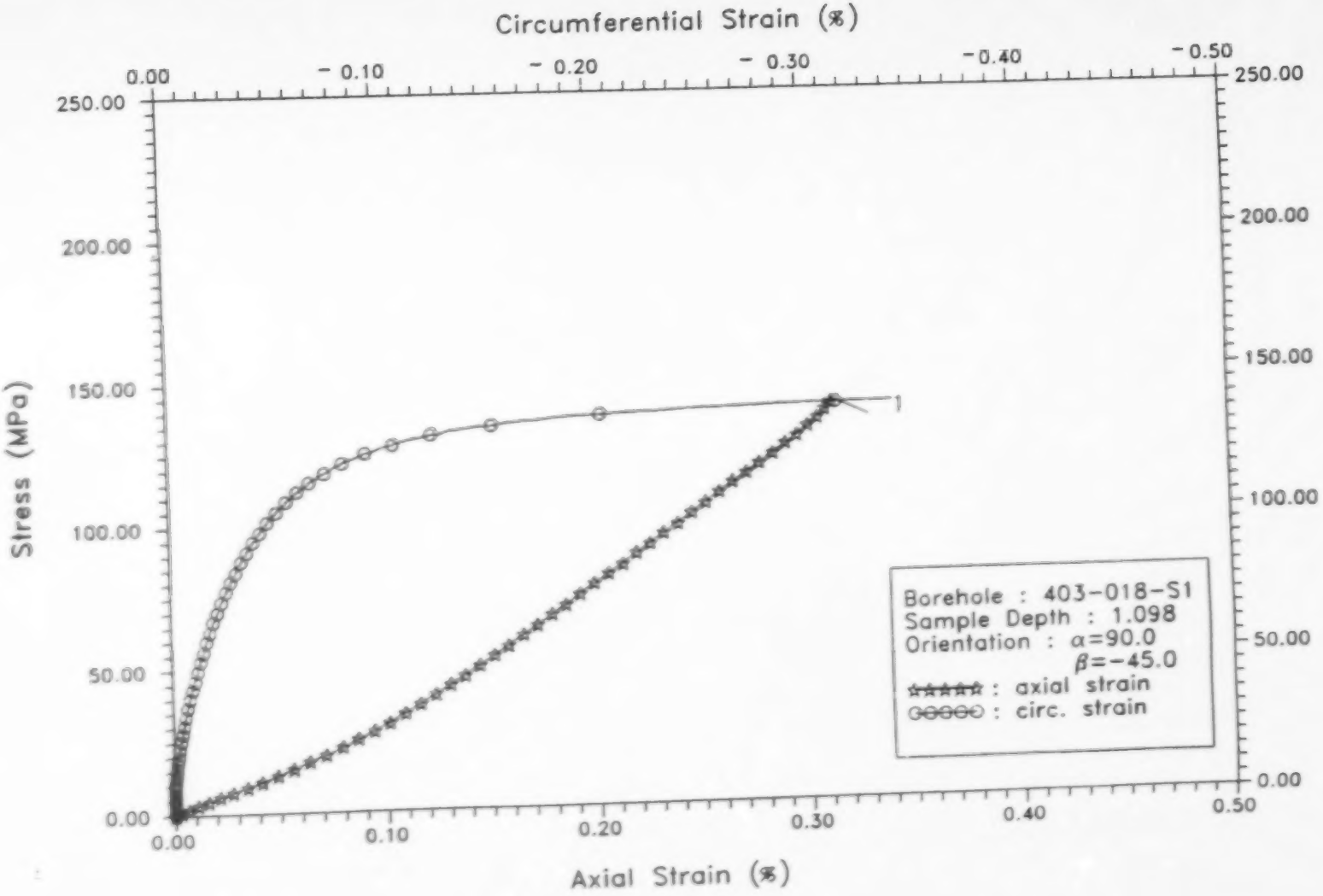

Fig. A39: Axial and circumferential stress/strain curves for anisotropy test specimens

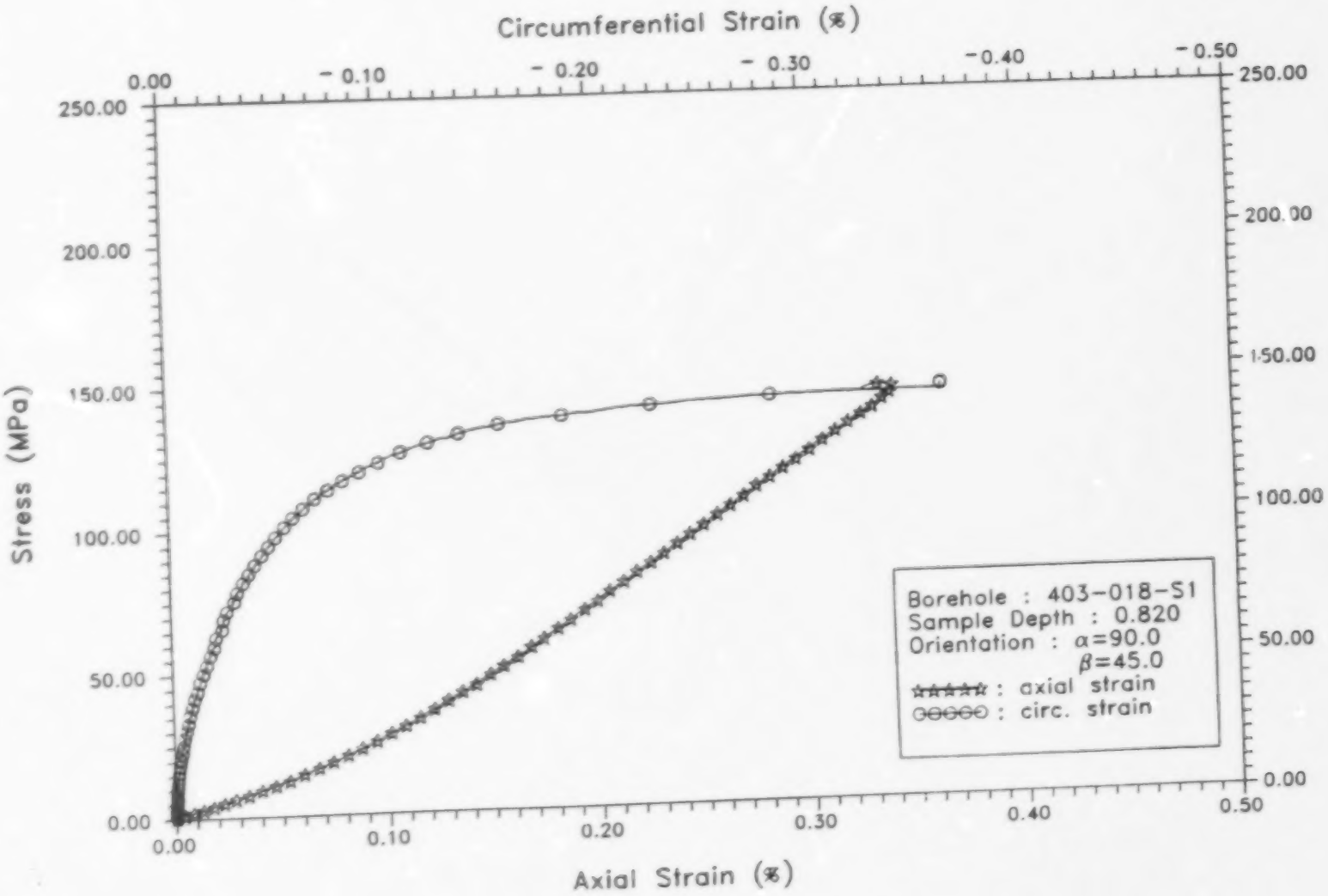

Fig. A40: Axial and circumferential stress/strain curves for anisotropy test specimens

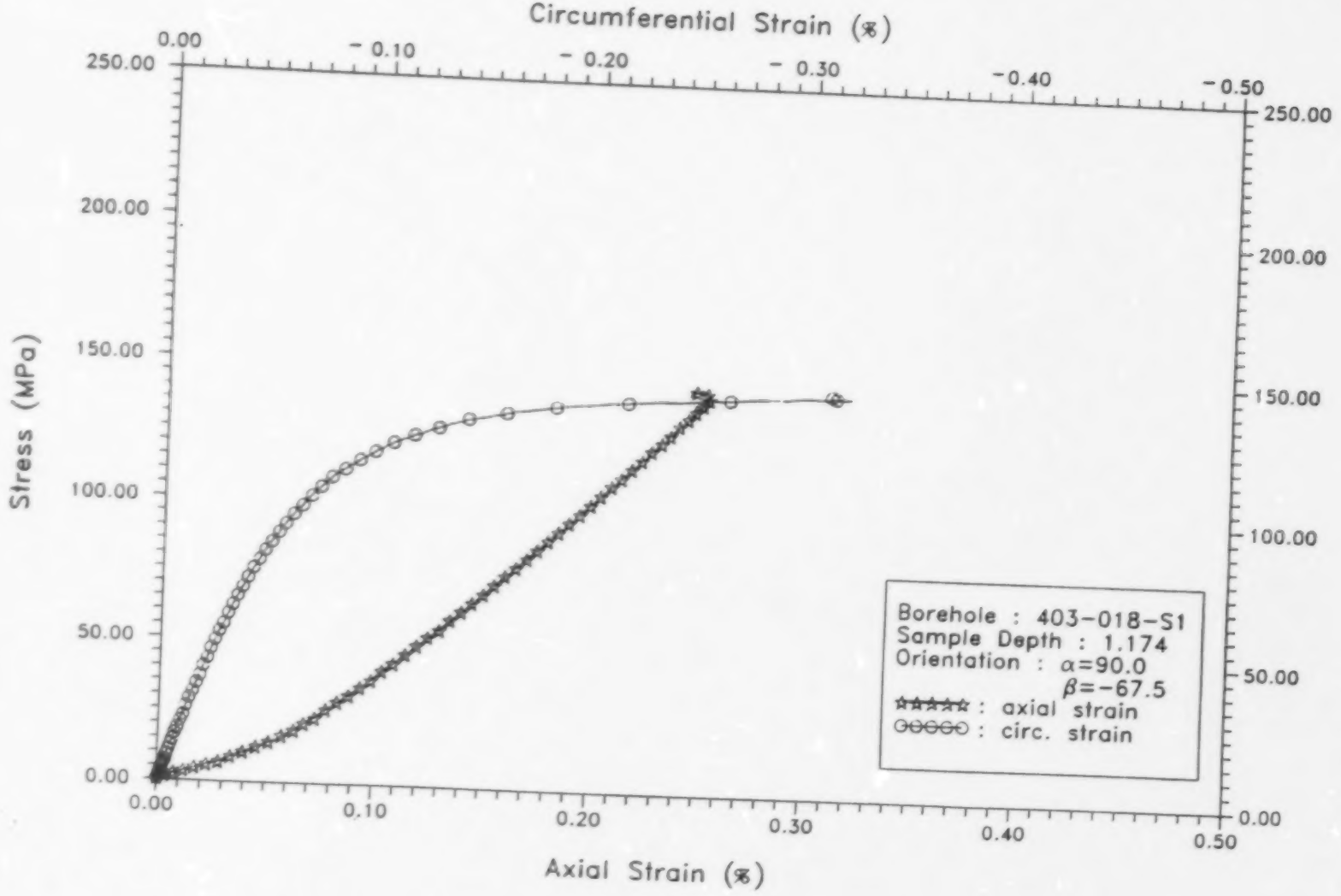

Fig. A41: Axial and circumferential stress/strain curves for anisotropy test specimens

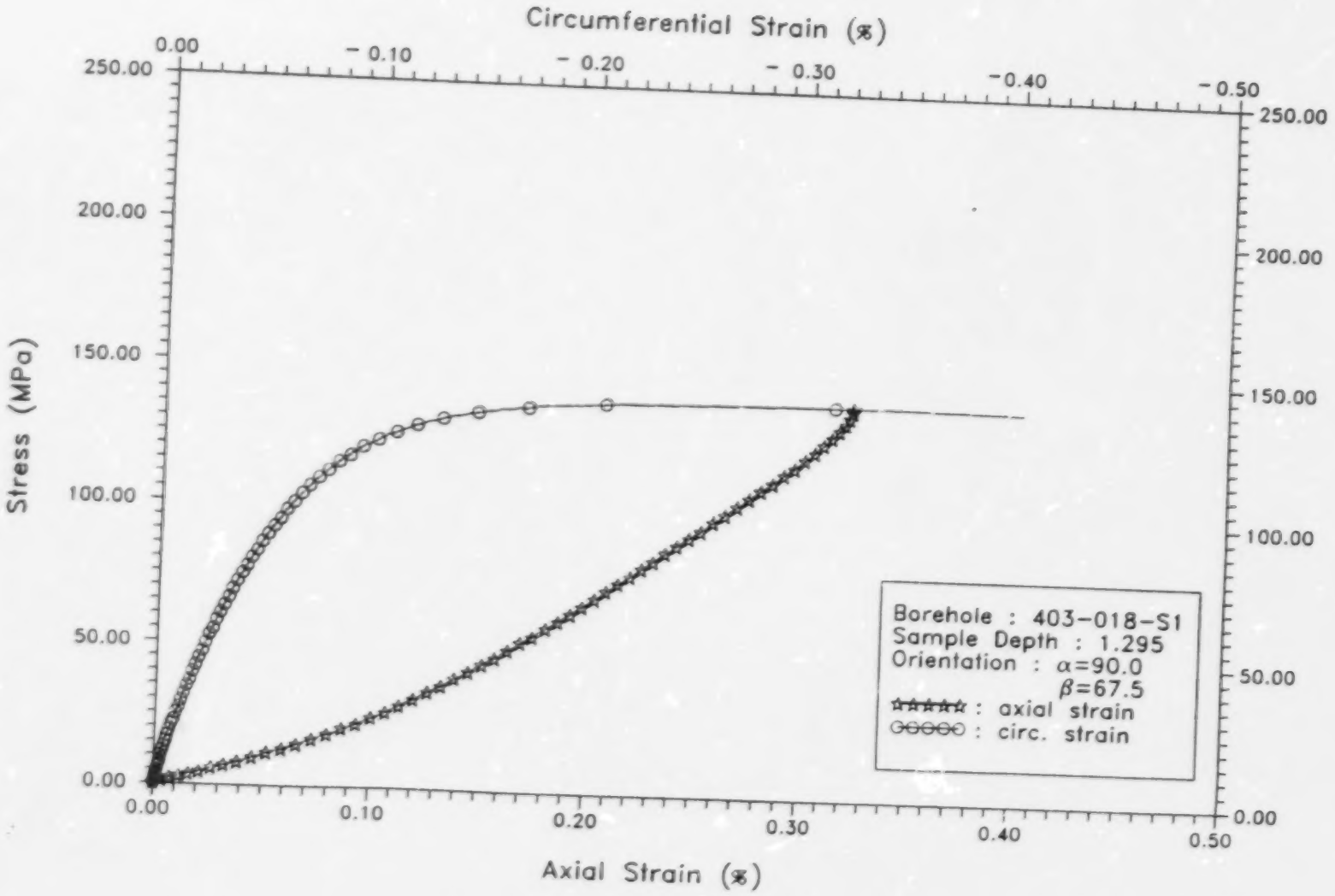

Fig. A42: Axial and circumferential stress/strain curves for anisotropy test specimens

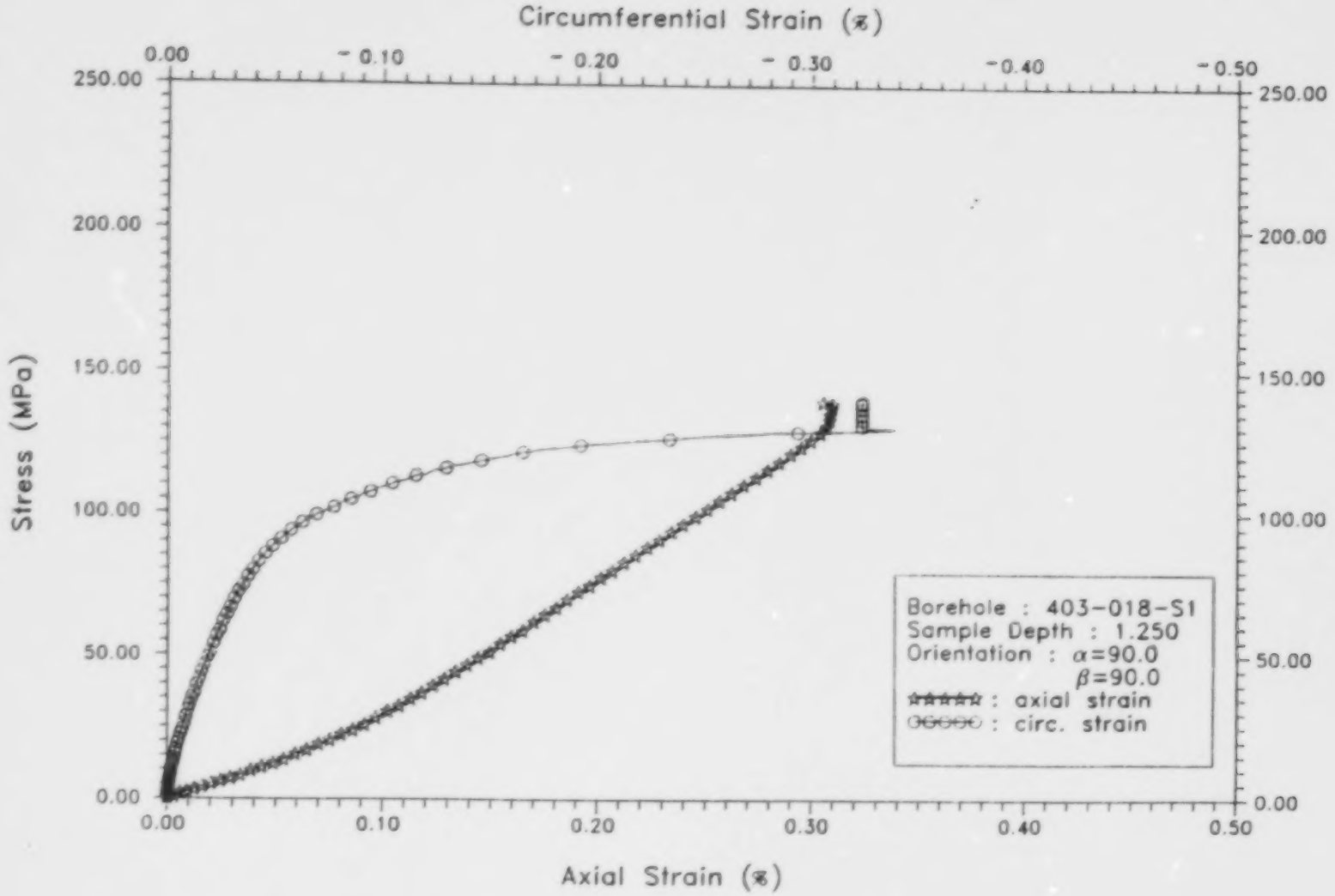

Fig. A43: Axial and circumferential stress/strain curves for anisotropy test specimens

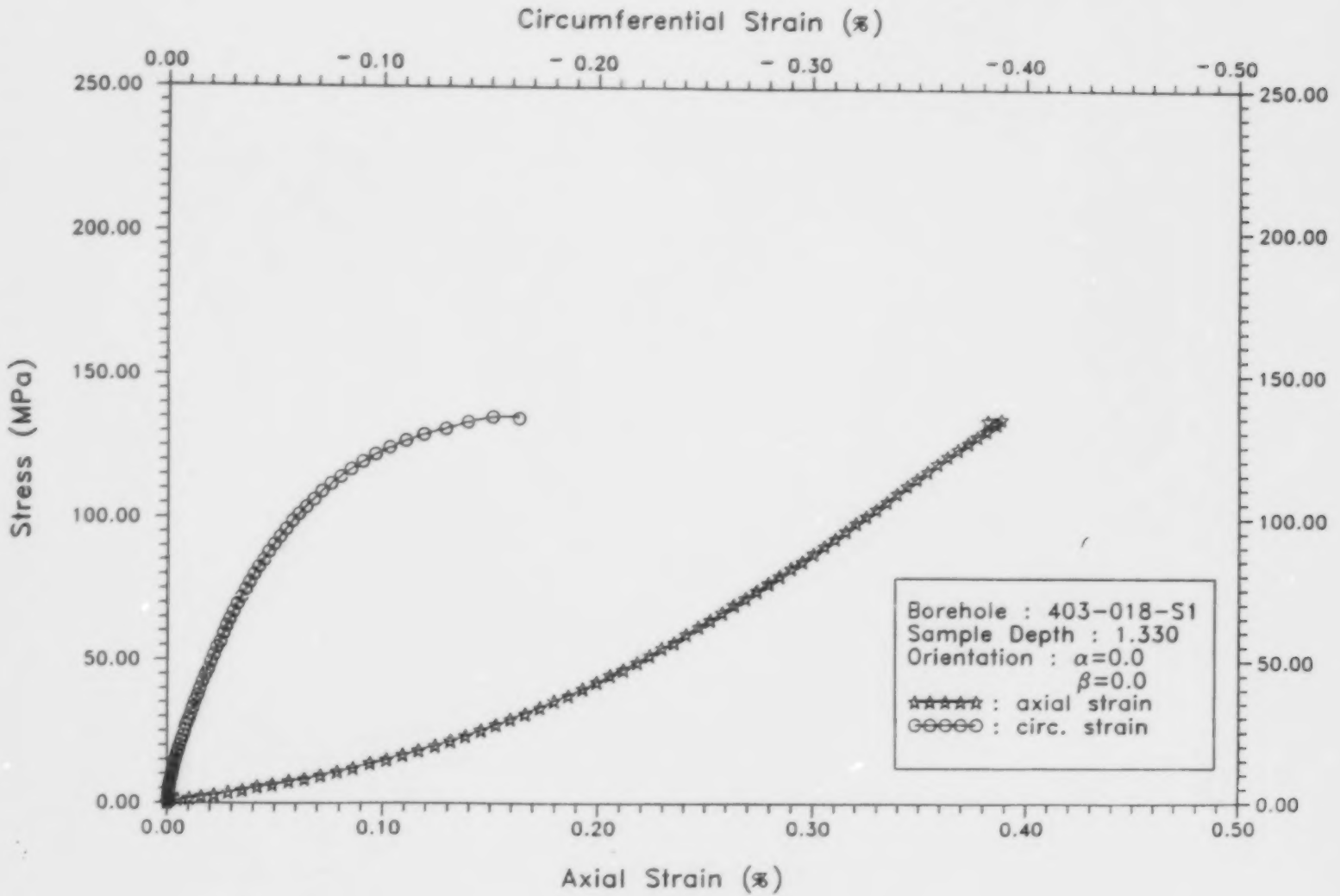

Fig. A44: Axial and circumferential stress/strain curves for anisotropy test specimens

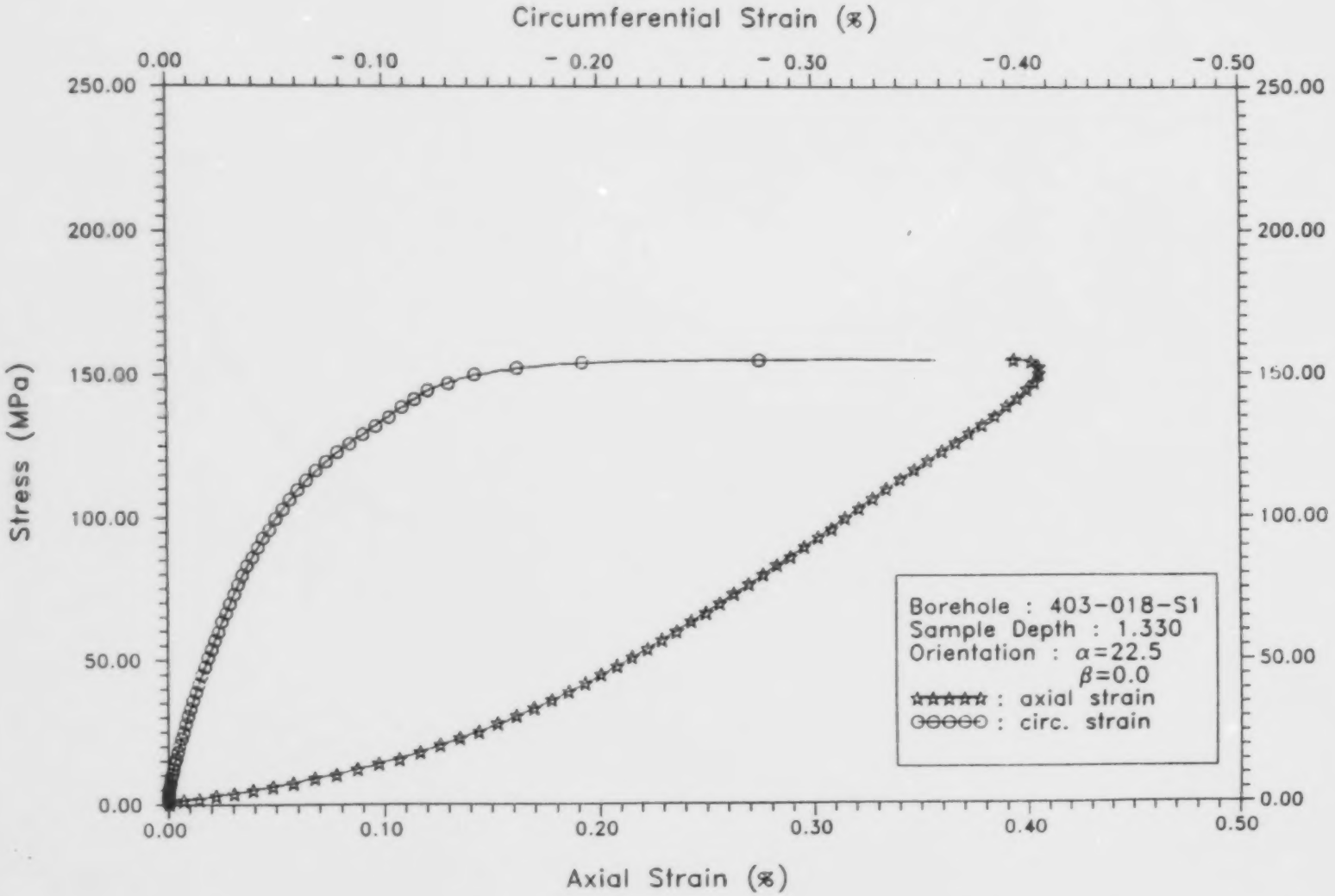

Fig. A45: Axial and circumferential stress/strain curves for anisotropy test specimens

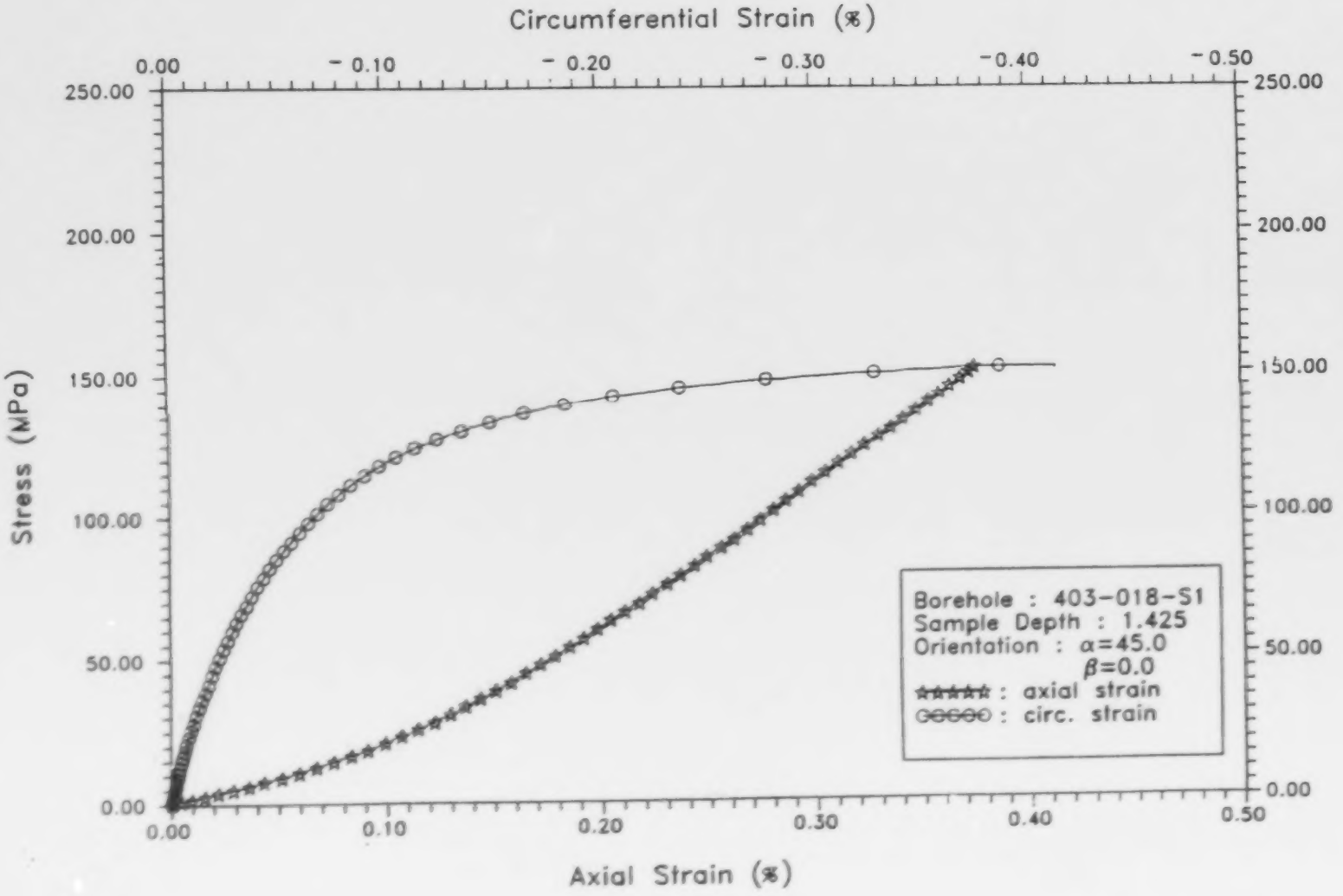

Fig. A46: Axial and circumferential stress/strain curves for anisotropy test specimens

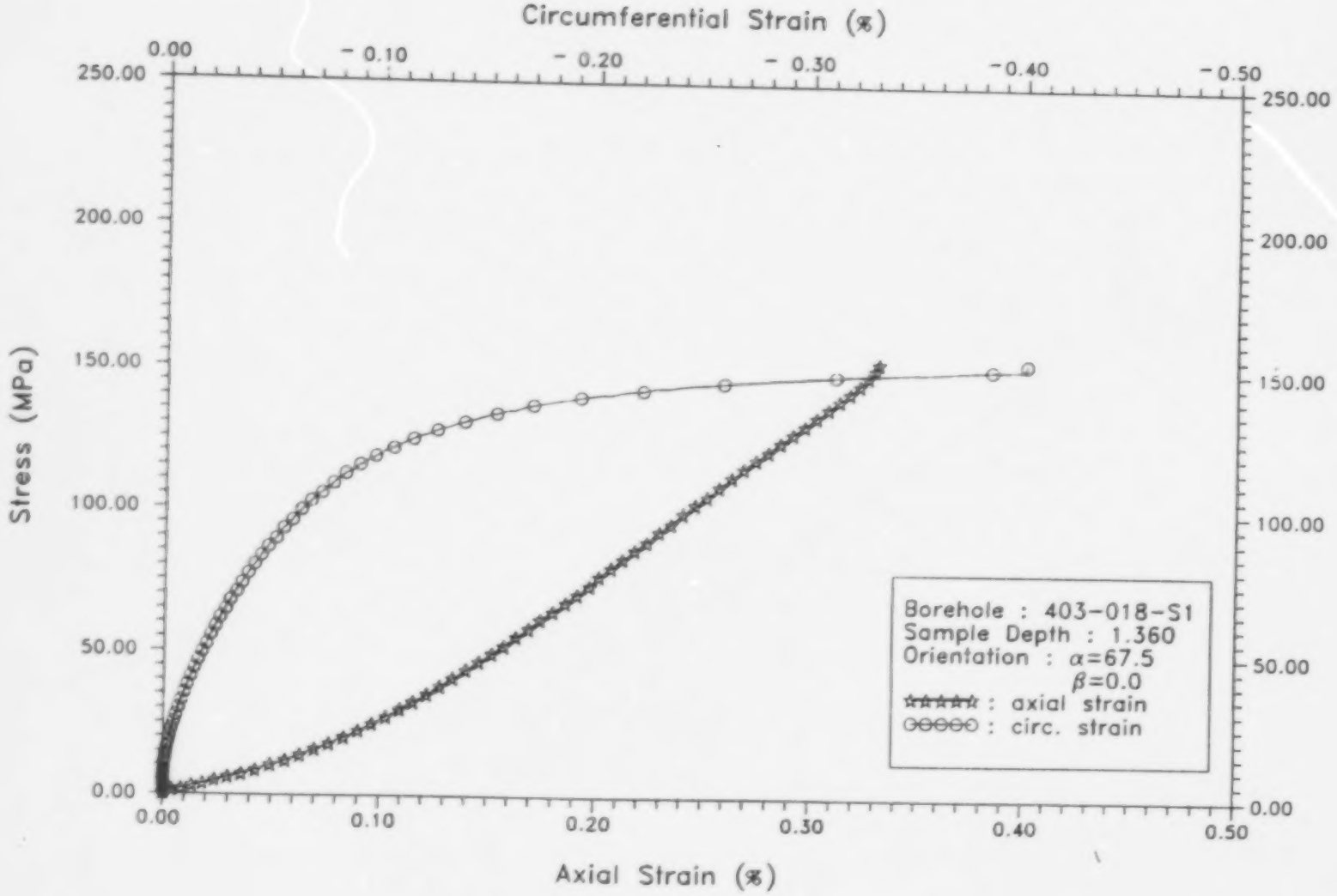

Fig. A47: Axial and circumferential stress/strain curves for anisotropy test specimens

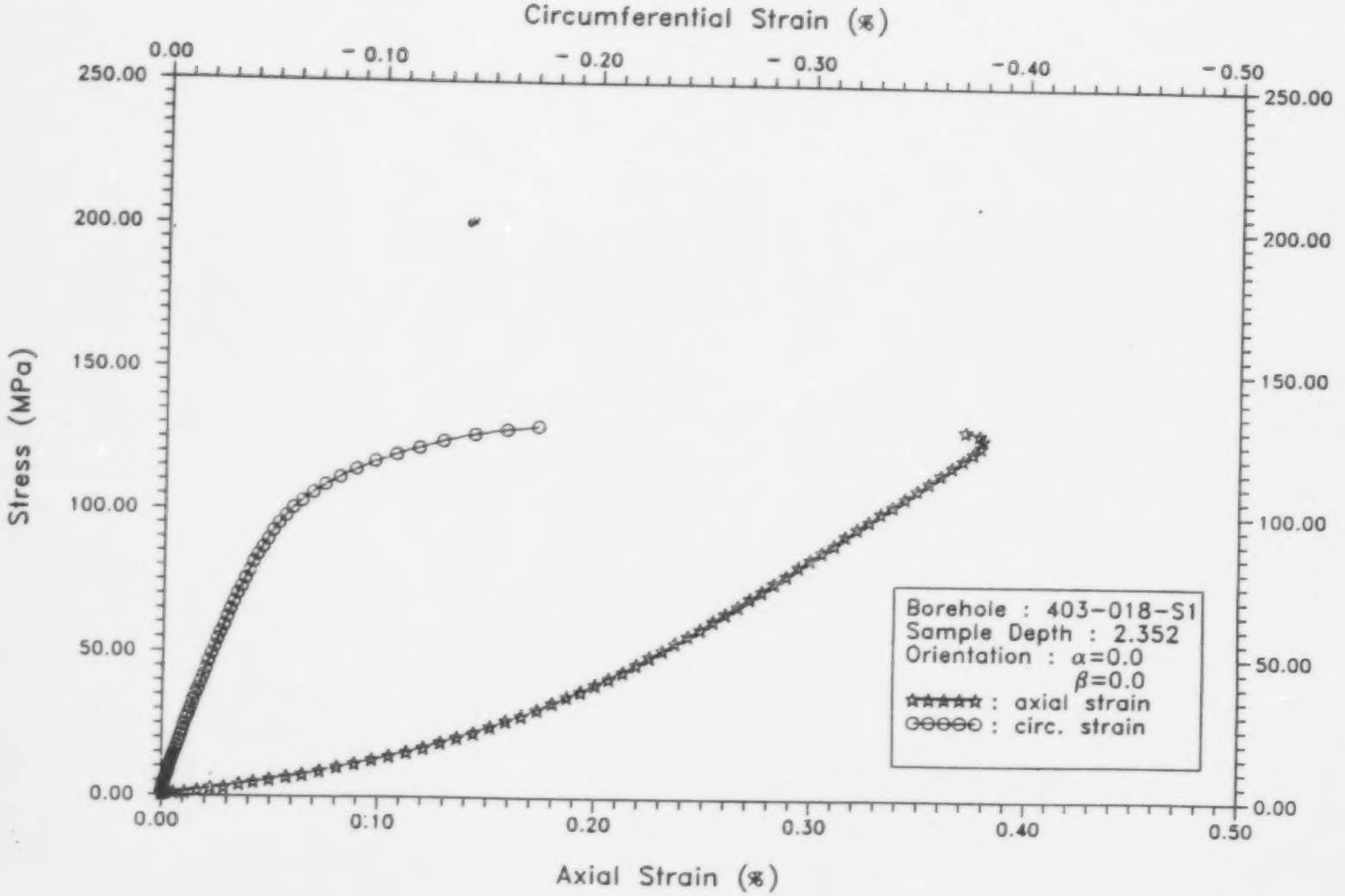

Fig. A48: Axial and circumferential stress/strain curves for anisotropy test specimens

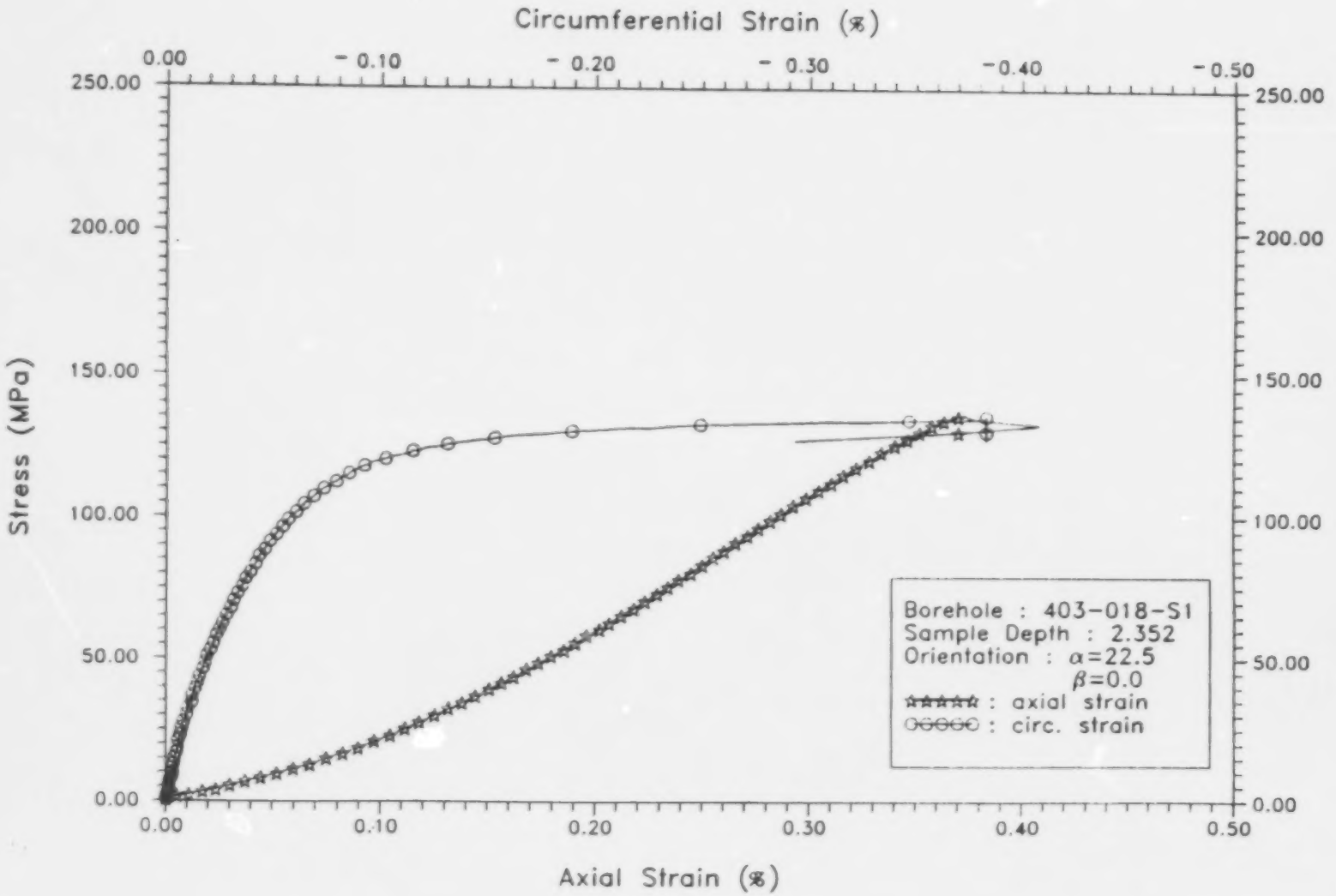

Fig. A49: Axial and circumferential stress/strain curves for anisotropy test specimens

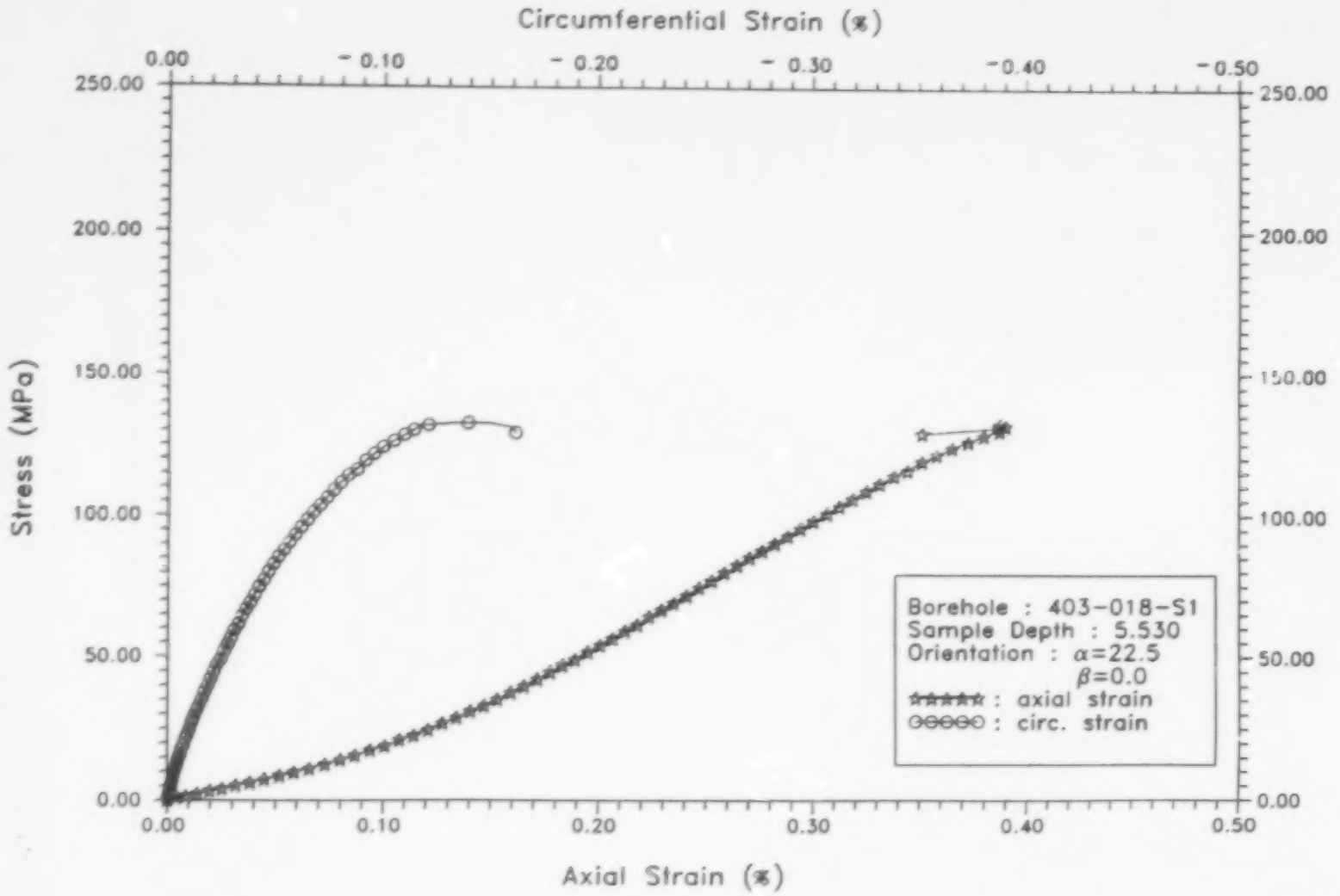

Fig. A50: Axial and circumferential stress/strain curves for anisotropy test specimens

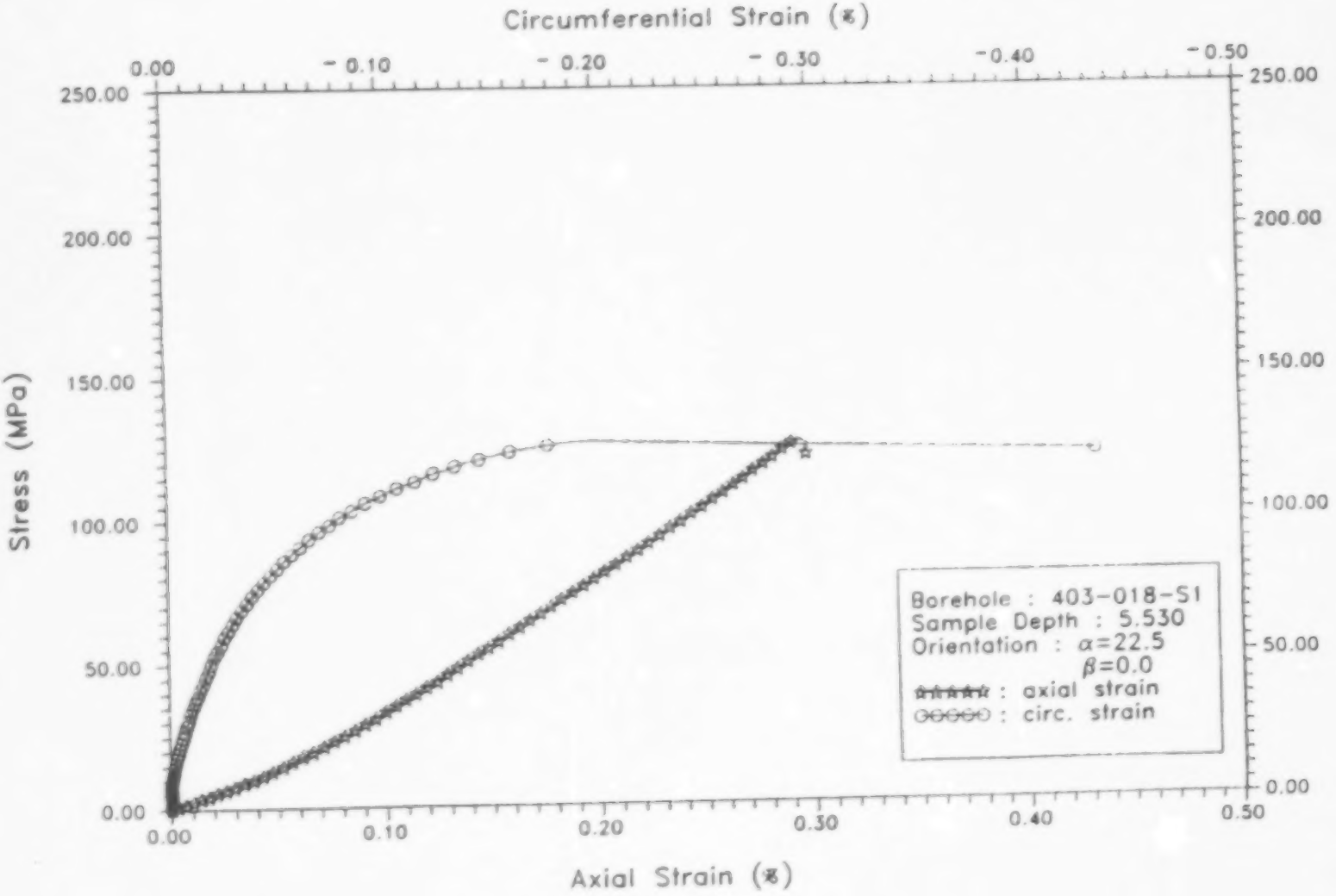

Fig. A51: Axial and circumferential stress/strain curves for anisotropy test specimens

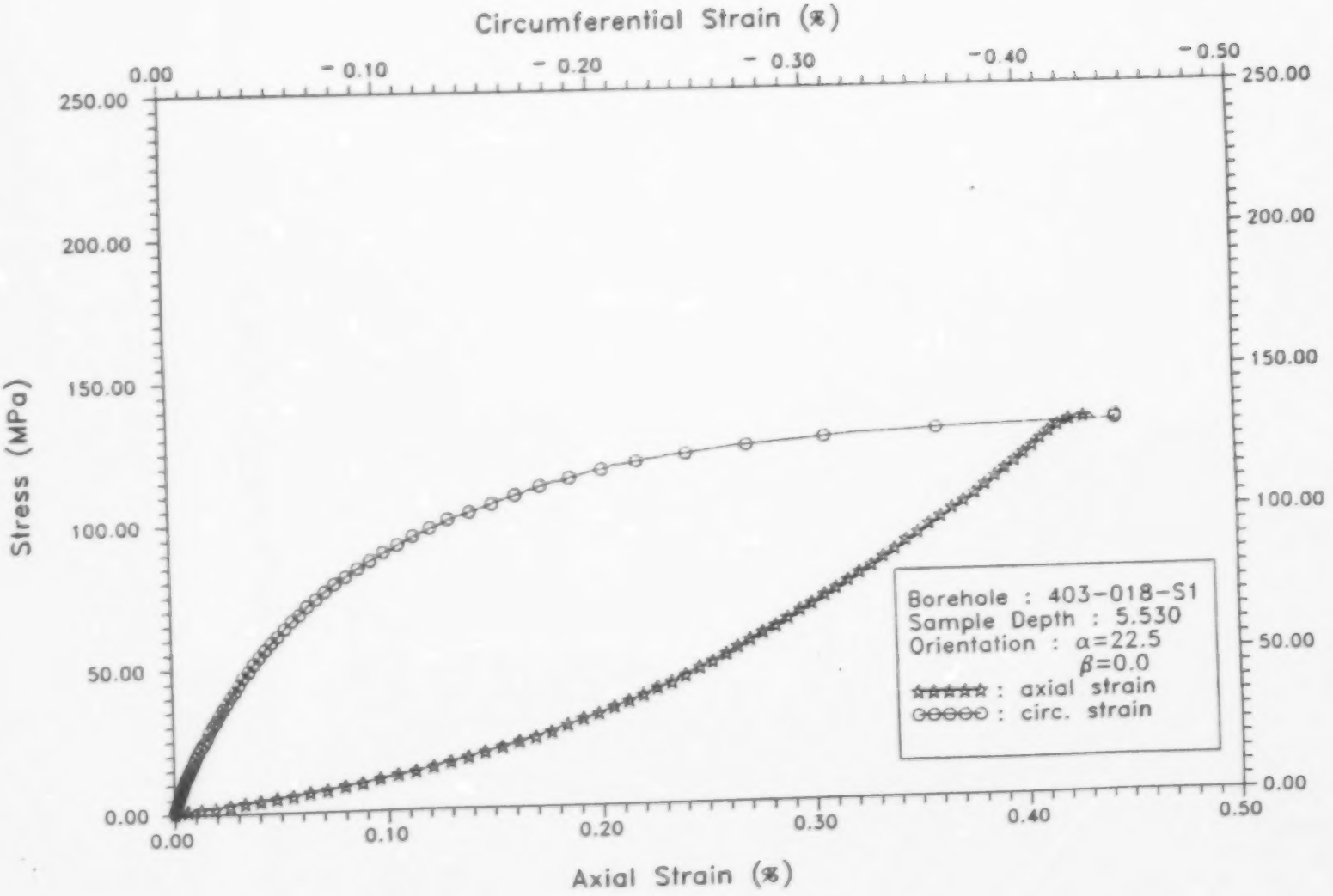

Fig. A52: Axial and circumferential stress/strain curves for anisotropy test specimens

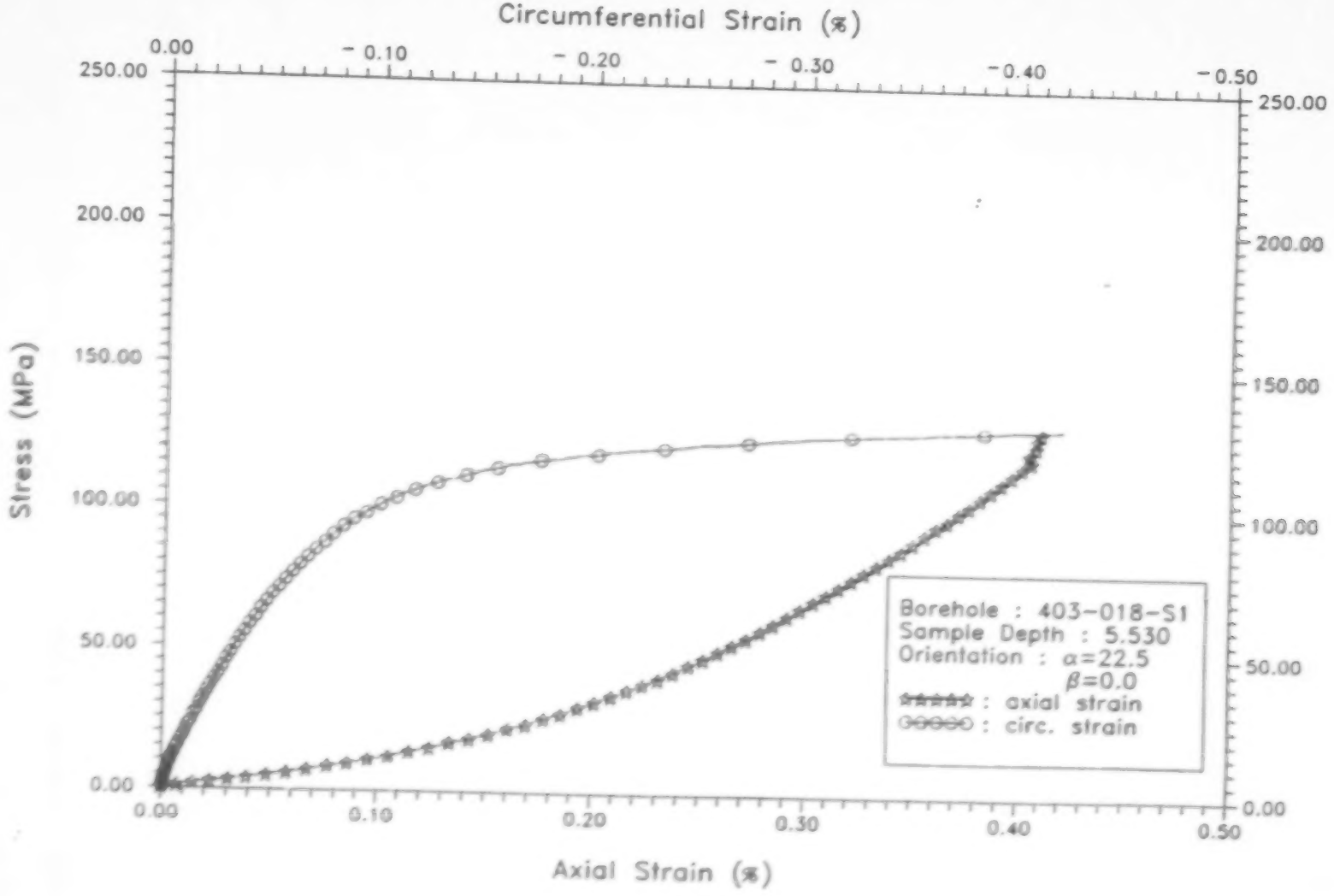

Fig. A53: Axial and circumferential stress/strain curves for anisotropy test specimens

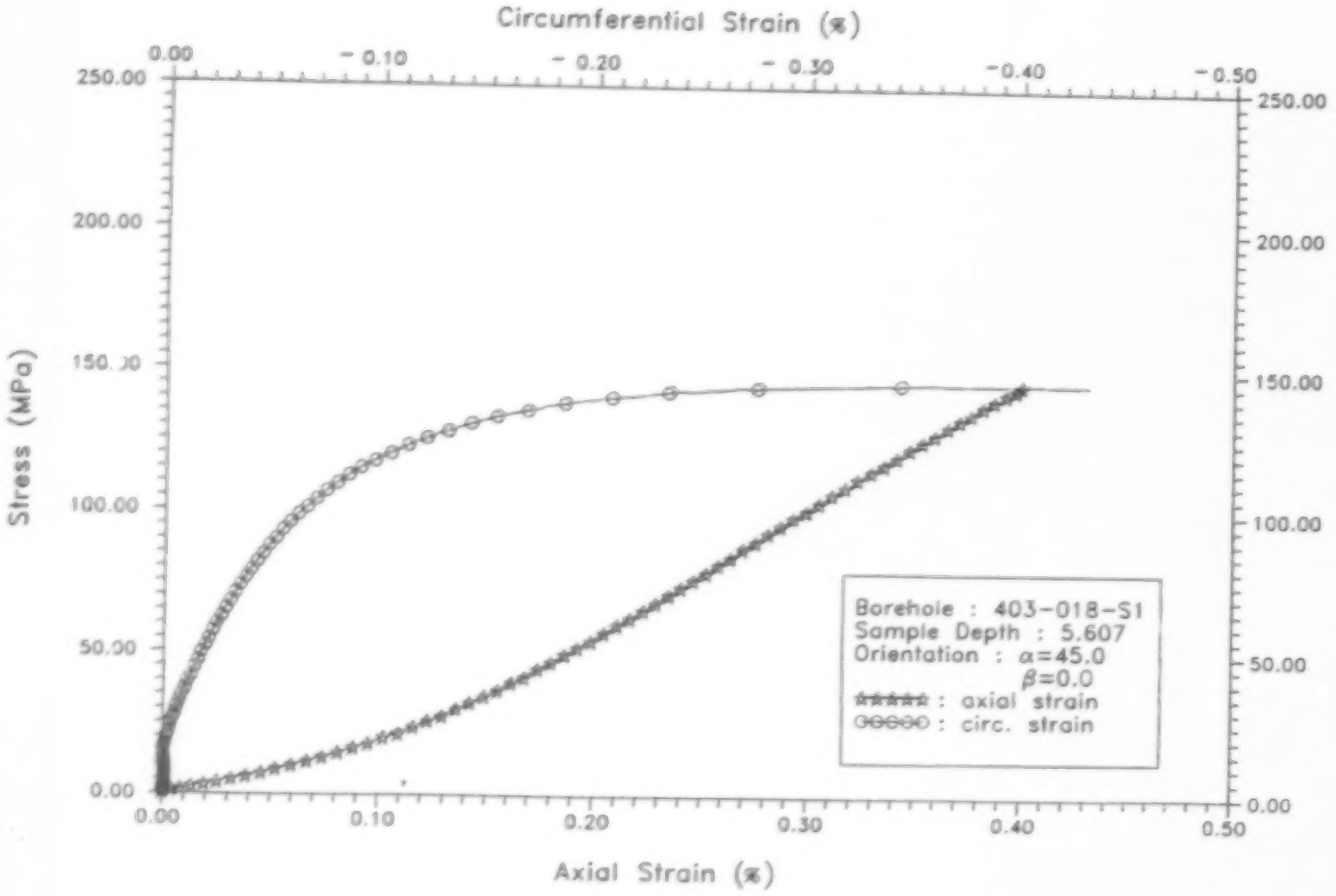

Fig. A54: Axial and circumferential stress/strain curves for anisotropy test specimens

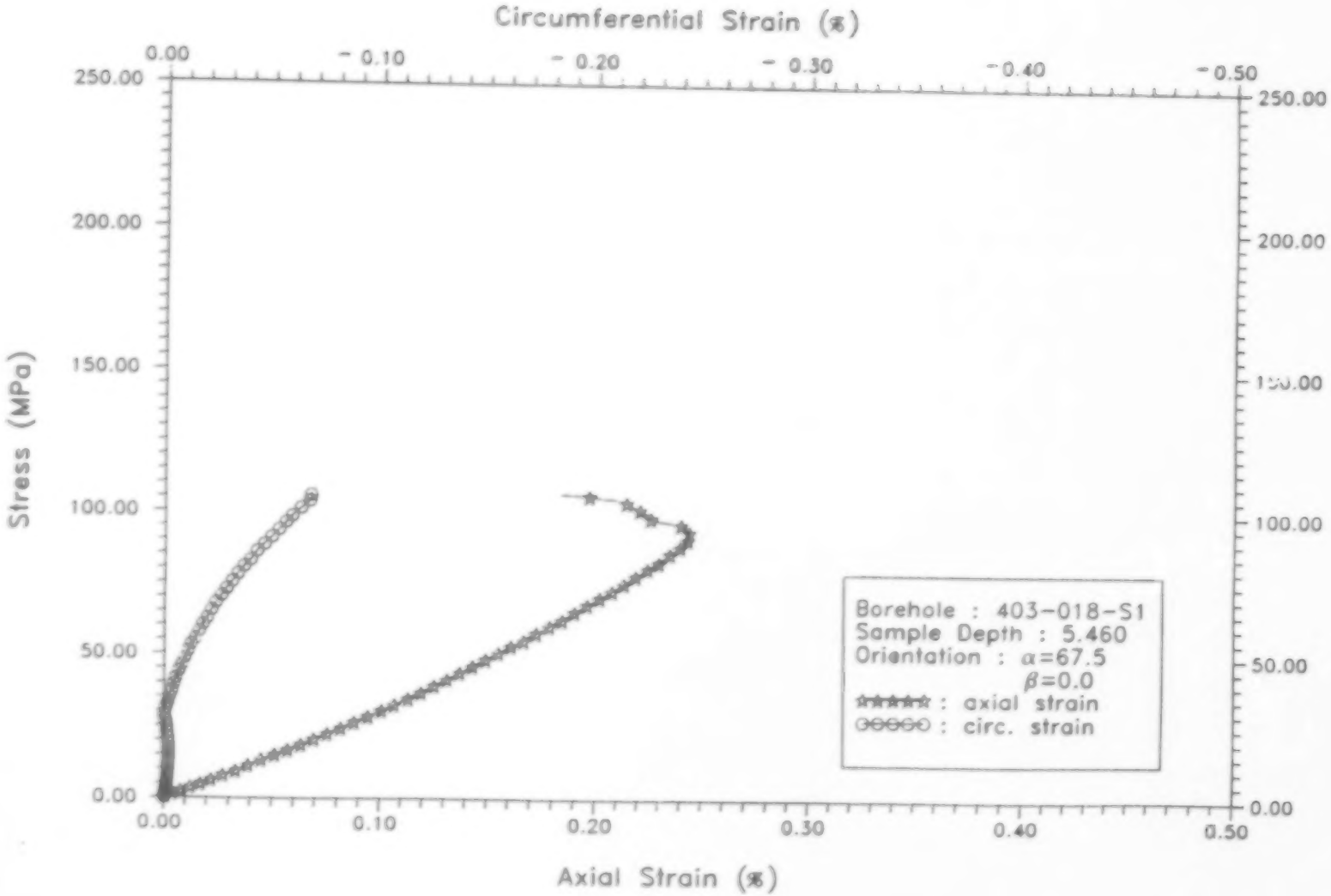

Fig. A55: Axial and circumferential stress/strain curves for anisotropy test specimens

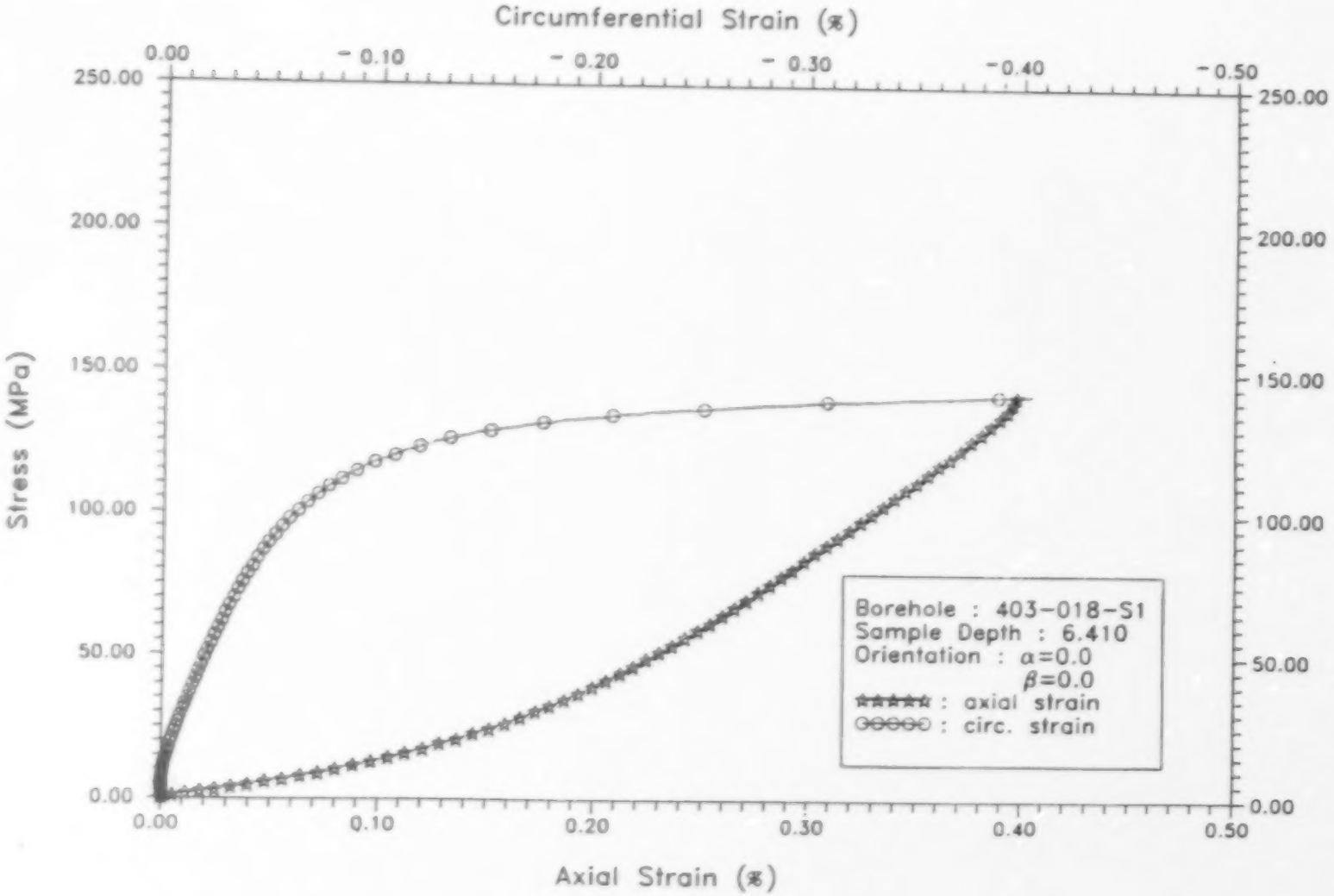

Fig. A56: Axial and circumferential stress/strain curves for anisotropy test specimens

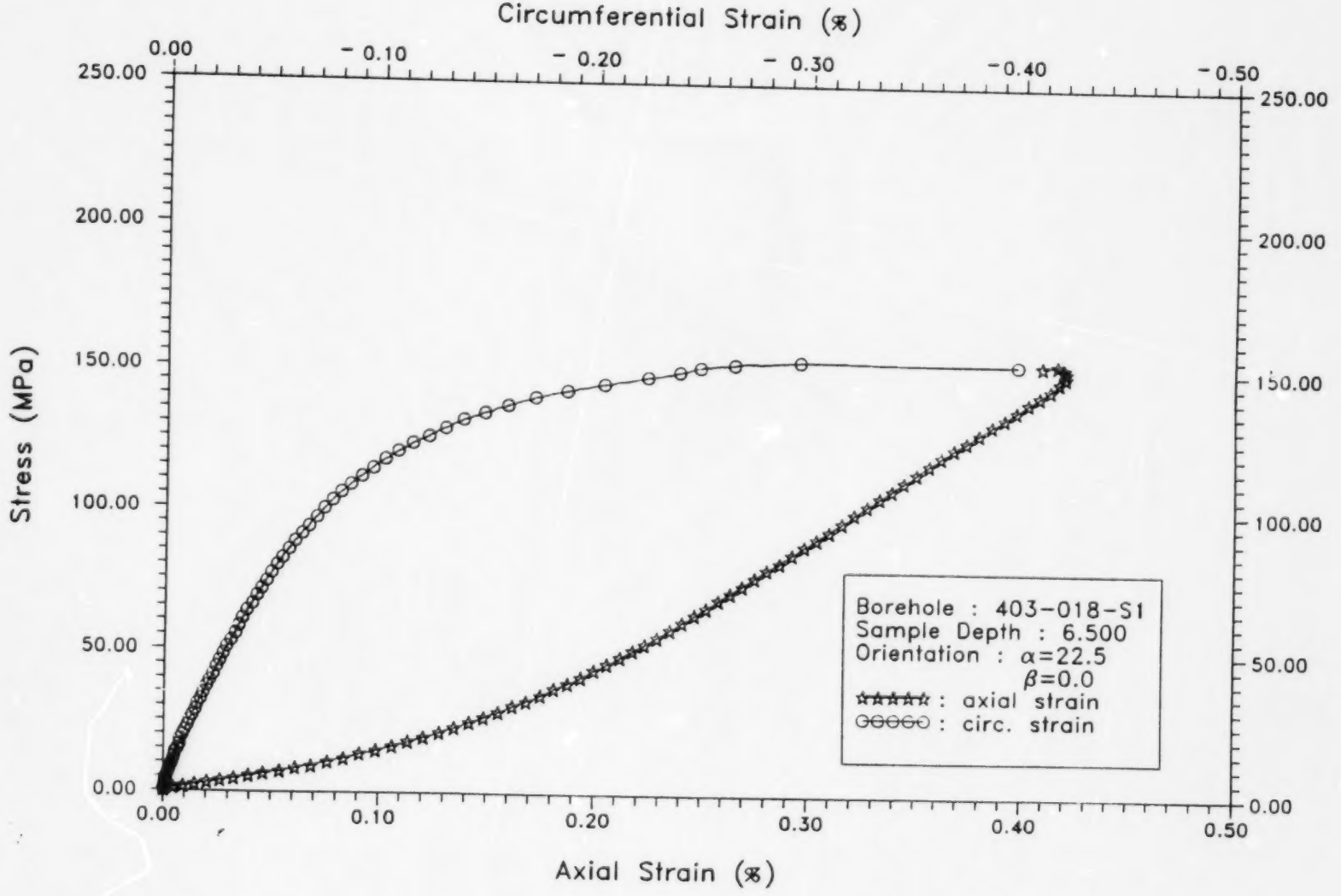

Fig. A57: Axial and circumferential stress/strain curves for anisotropy test specimens

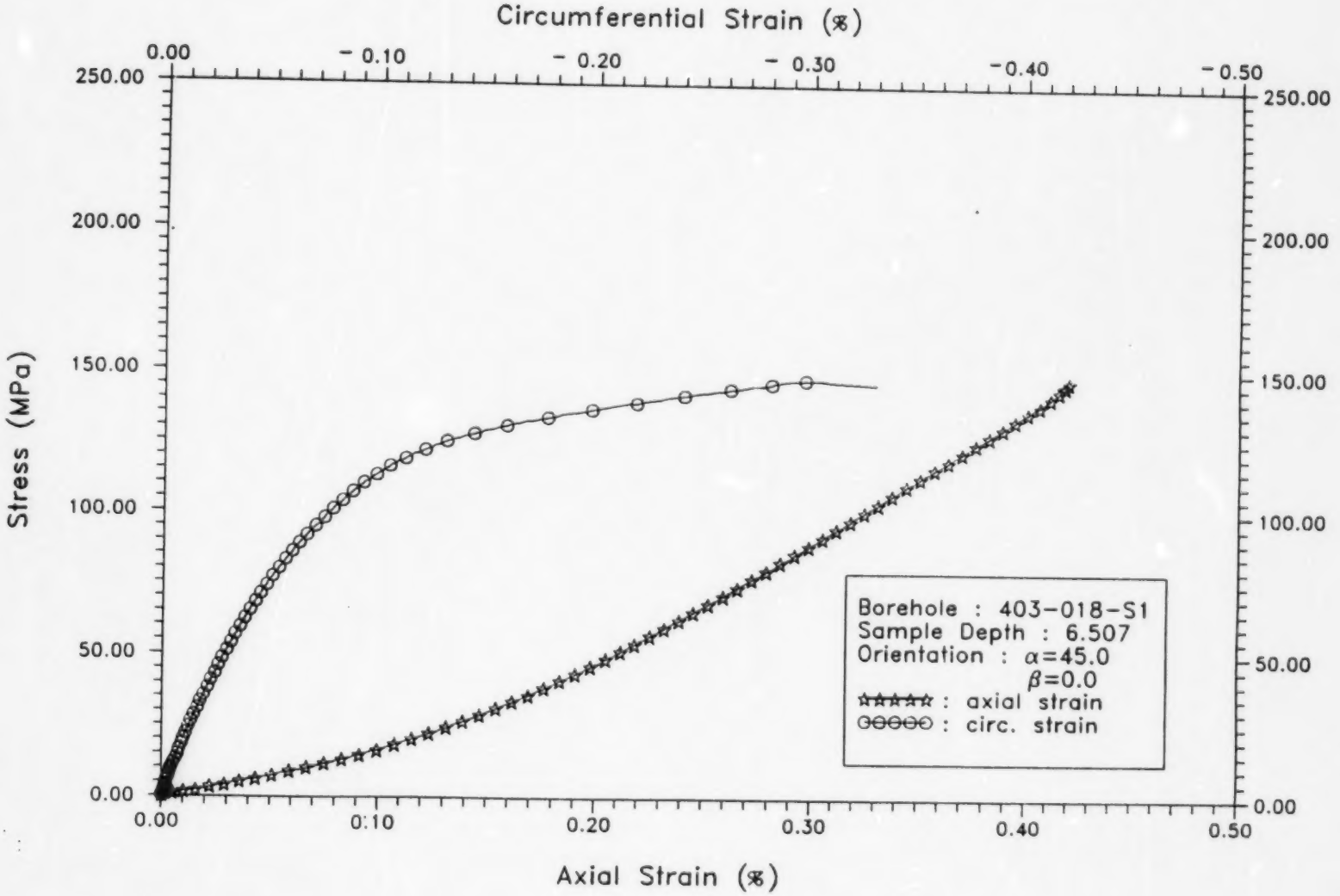

Fig. A58: Axial and circumferential stress/strain curves for anisotropy test specimens

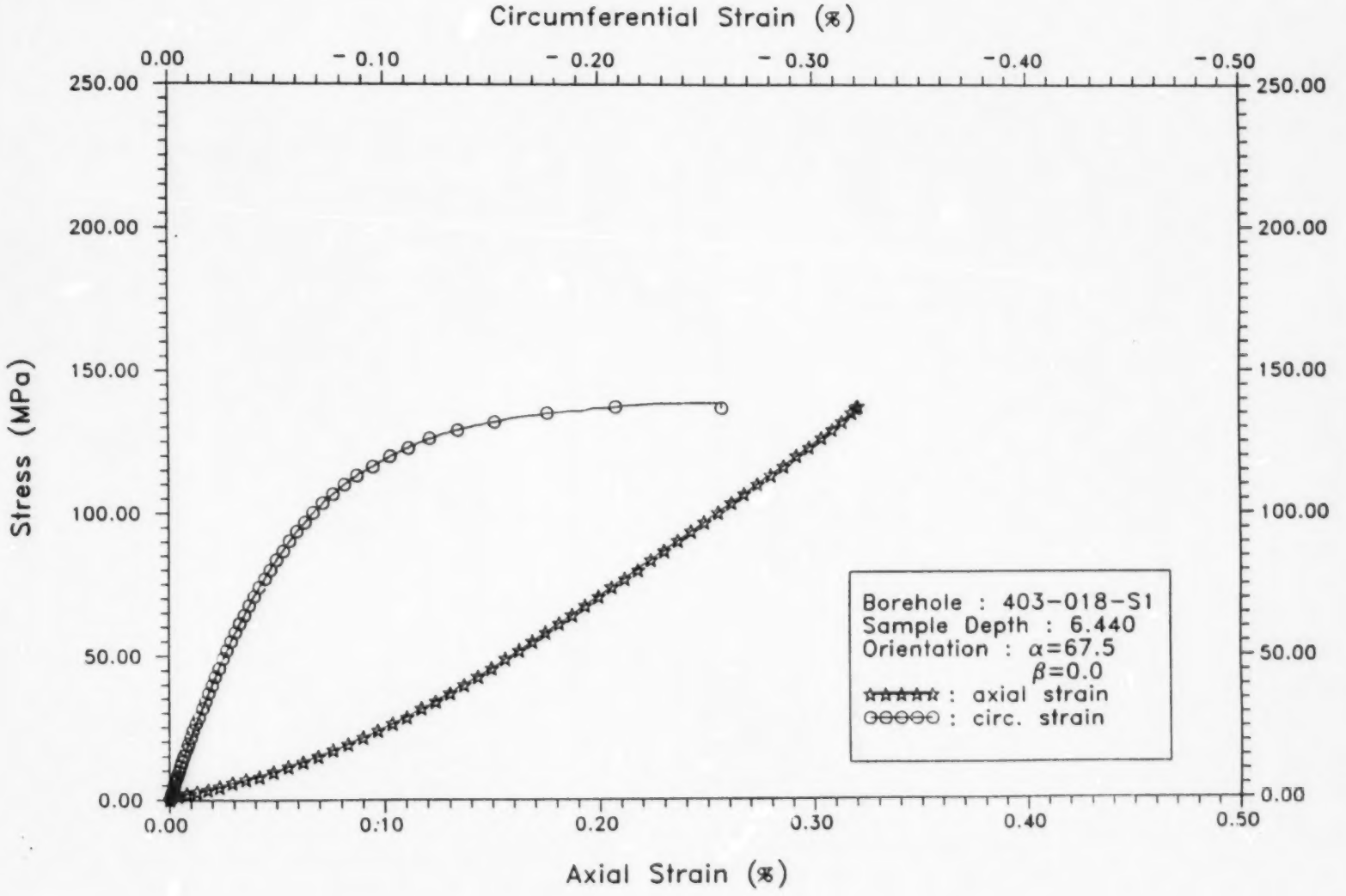

Fig. A59: Axial and circumferential stress/strain curves for anisotropy test specimens

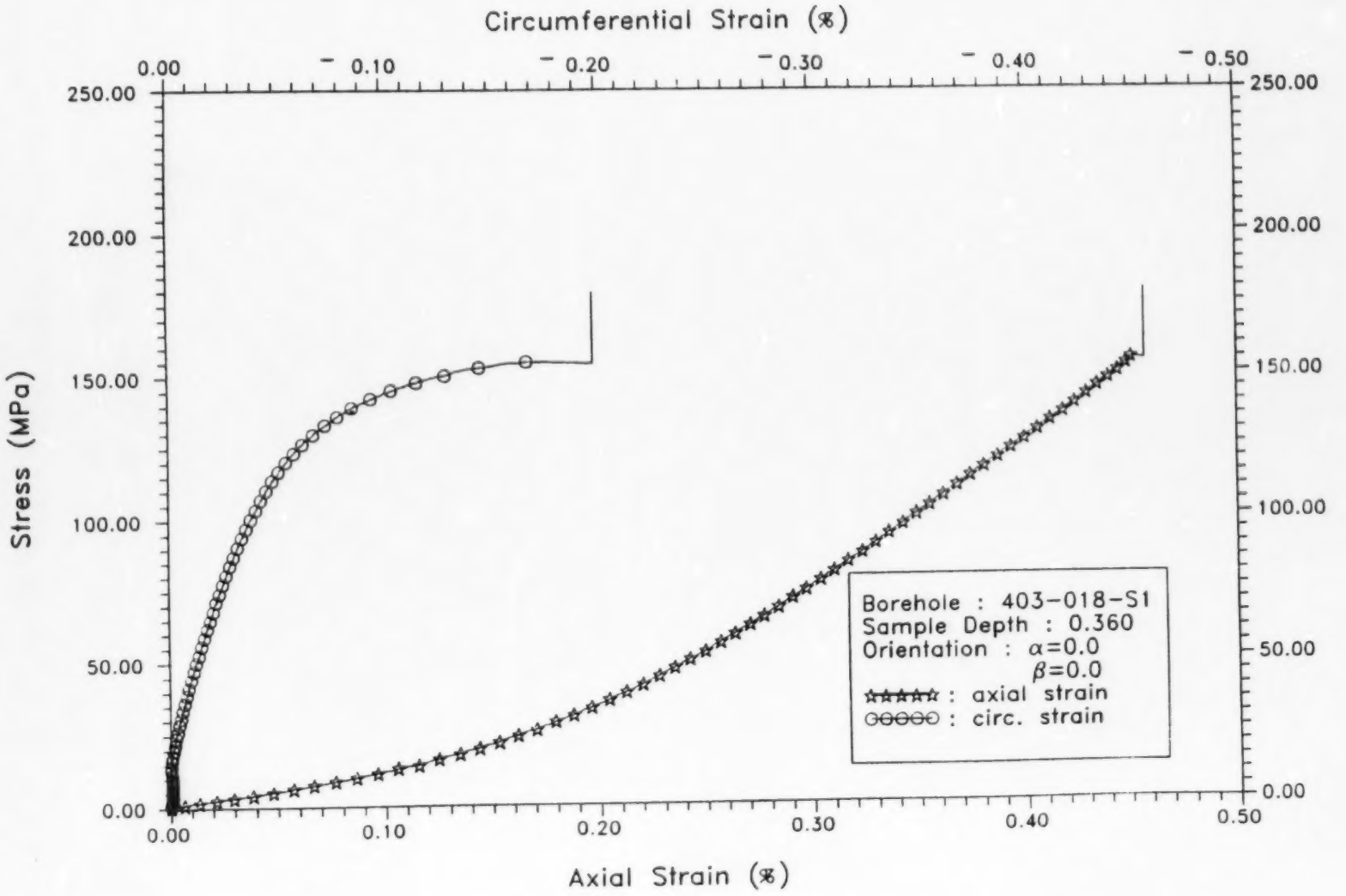

Fig. A60: Axial and circumferential stress/strain curves for anisotropy test specimens

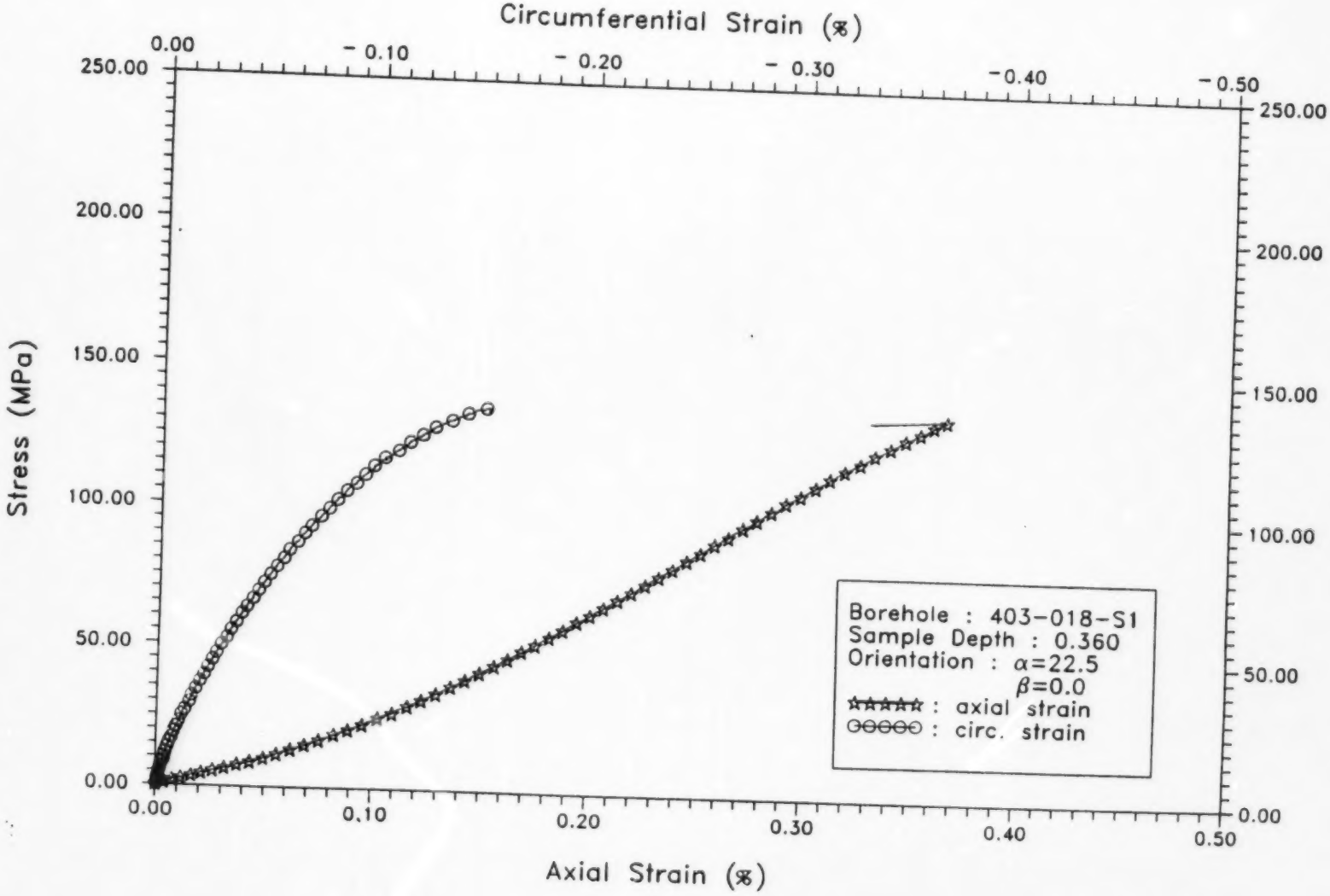

Fig. A61: Axial and circumferential stress/strain curves for anisotropy test specimens

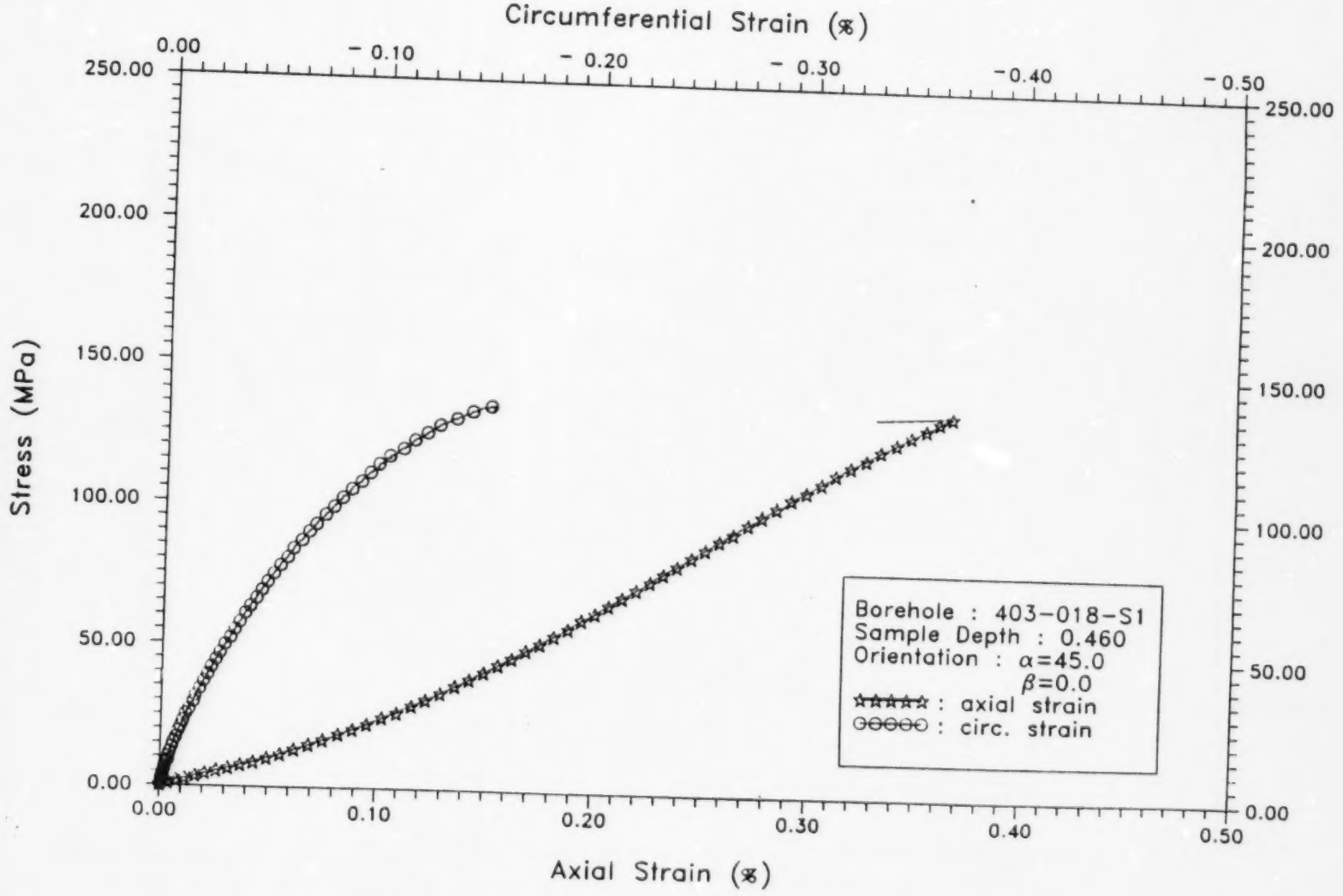

Fig. A62: Axial and circumferential stress/strain curves for anisotropy test specimens

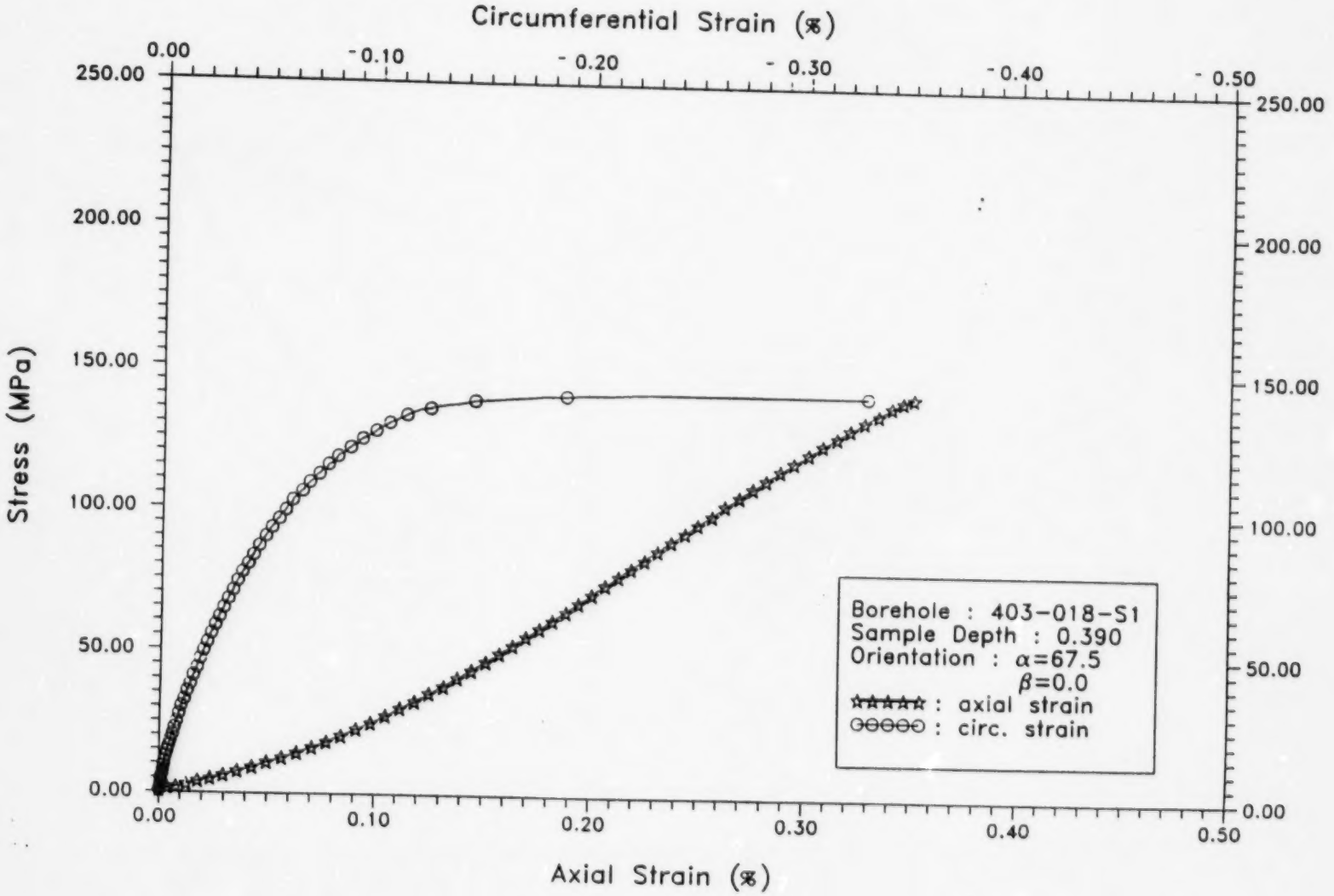

Fig. A63: Axial and circumferential stress/strain curves for anisotropy test specimens